TUNABLE MODE-LOCKED FIBER LASERS WITH OPTICAL FIBER GRATING DEVICES

WANG JIE

Ph.D.

The Hong Kong Polytechnic University

This programme is jointly offered by The Hong Kong Polytechnic University and Zhejiang University

2017

The Hong Kong Polytechnic University

Department of Electrical Engineering

Zhejiang University

College of Optical Science and Engineering

Tunable Mode-Locked Fiber Lasers with Optical Fiber Grating Devices

WANG Jie

A thesis submitted in partial fulfillment of the requirements for the degree of Doctor of Philosophy

September 2016

CERTIFICATE OF ORIGINALITY

I hereby declare that this thesis is my own work and that, to the best of my knowledge and belief, it reproduces no material previously published or written, nor material that has been accepted for the award of any other degree or diploma, except where due acknowledgement has been made in the text.

______________________________ (Signed)

WANG Jie (Name of student)

Abstract

Mode-locked ultrafast fiber lasers have grown tremendously over the past decade because of their appealing application prospects in widespread fields, such as fiber-optic telecommunications, biomedical research, and spectroscopy. Recently, tunable mode-locked fiber lasers have attracted particular attention with the emerging of broadband absorbers made in carbon nanomaterials, like carbon nanotubes (CNTs) and graphene, as well as the development of wavelength tuning technologies. In this dissertation, tunable mode-locking technologies based on optical fiber grating devices have been investigated.

First of all, a special LPG filter is developed for a widely tunable mode-locked fiber laser. By sandwiching a phase-shifted LPG (PSLPG) between two LPGs of different periods, a W-shaped spectral filter was experimentally fabricated. Through adjusting the temperature of the W-shaped filter, the emission wavelength of the mode-locked laser was tuned in a range covering both C and L bands. Because of its properly designed broad pass-band, the technology enables shorter pulses free of extra grating dispersion. Moreover, the spectral shaping effect of the PSLPG was investigated to effectively suppress the Kelly sidebands.

Apart from thermally spectrum-tunable LPG devices, an optofluidic tunable mode-locked fiber laser is demonstrated based on the refractive index (RI) sensitivity of LPG. Ultrafine wavelength tuning was enabled by integrating a PSLPG into a home-made microfluidic chip. By accurately adjusting the RI of fluid, the emission wavelength of the mode-locked laser was tuned continuously. Experimentally, stable bound solitons with different pulse separations were observed. Such a grating-integrated optofluidic device offers a promising platform to develop novel ultrafast fiber lasers for scientific and industrial applications.

Besides, a high-energy soliton fiber laser is demonstrated by using a CFBG pair. The CFBG pair with overall group velocity dispersion (GVD) of ~5 ps/nm/km was used to increase the net cavity anomalous dispersion. Stable high-energy mode-locked solitons with the typical pulse duration of 8.05 ps were obtained. The maximum pulse energy of 0.21 nJ, which is higher than the limit of conventional soliton area theorem, was achieved without soliton splitting. Numerical simulations using the split-step Fourier method (SSFM) revealed that the soliton-splitting threshold was improved by the CFBGs.

Moreover, tunable vector and scalar solitons have been demonstrated via incorporating a CFBG in a non-polarization-maintaining (PM) and a PM fiber laser oscillator, respectively. The CFBG was firmly mounted on the central line of a cantilever and acted as an all-fiber tunable filter. In the non-PM fiber oscillator, L-band tunable vector solitons were obtained by using a CFBG centered at the wavelength of around 1610 nm and a Bismuth-based Erbium-doped fiber. Through adjusting the cantilever, the wavelength of the vector solitons was tuned continuously, meanwhile the polarization-locked state sustained. Numerical simulations revealed that the FWM sidebands were correlated with the cavity birefringence. In the PM fiber oscillator, stable scalar solitons with a 99.5% degree of polarization (DOP) were obtained. By adjusting the CFBGs around 1530 and 1560 nm, the laser wavelength was tuned continuously in the C band, while the laser output maintained its polarization stably.

List of Publications

Journal papers:

1. **Jie Wang**, A. Ping Zhang, Yonghang. Shen, Hwa-yaw. Tam, and P. K. A. Wai, "Widely tunable mode-locked fiber laser using carbon nanotube and LPG W-shaped filter," *Optics Letters*, 40, 4329–4332, 2015.
2. **Jie Wang**, Zheng-Yong Liu, Shaorui Gao, A. Ping Zhang, Yong-Hang Shen, and Hwa-Yaw Tam, "Fiber-Optic Anemometer Based on Bragg Grating Inscribed in Metal-Filled Microstructured Optical Fiber," *Journal of Lightwave Technology*, 14, 4884–4889,2016.
3. **Jie Wang**, Yaxi Yan, A. Ping Zhang, Bo Wu, Yonghang Shen, Hwa-yaw Tam, "Tunable scalar solitons from a polarization-maintaining mode-locked fiber laser using carbon nanotube and chirped fiber Bragg grating," *Optics Express*, 24, 22387–22394, 2016.
4. **Jie Wang**, Mian Yao, Chengzhi Hu, A. Ping Zhang, Yonghang Shen, Hwa-yaw Tam, "Optofluidic tunable mode-locked fiber laser using long-period grating integrated microfluidic chip," *Optics Letters*, 42, 1117–1120, 2015.
5. Tao Qi, Yongmin Jun, Limin Xiao, **Jie Wang**, Shilin Xiao, Chao Lu, Hwa-yaw Tam, Anna C. Peacock, "Programmable long-period grating in a liquid core optical fiber," *Optics Letters*, 41, 4763–4766, 2016.

6. Nan Guo, Liang Wang, **Jie Wang**, Chao Jin, Hwa-yaw Tam, A. Ping Zhang, Chao Lu, "Bi-directional Brillouin optical time domain analyzer system for long range distributed sensing," *Sensors*, 16, 2156, 2016.

Conference papers:

1. **Jie Wang**, Shaorui Gao, Zhengyong Liu, A. Ping Zhang, Yonghang Shen, and Hwa-yaw. Tam, "Fiber optic anemometer based on metal infiltrated microstructured optical fiber inscribed with Bragg grating," the 24th *International Conference on Optical Fibre Sensors*, Curitiba, Brazil, 2015.
2. **Jie Wang** and A. Ping Zhang, "Grating Fabrication and Metal Filling in Six-Hole Microstructured Optical Fiber," *BGPP. BM2D.6*, Barcelona, Spain, 2014.
3. **Jie Wang**, A. Ping Zhang, Yonghang Shen, Hwa-yaw Tam, and P. K. A. Wai, "Wavelength-Tunable Mode-Locked Erbium Fiber Laser Based on Phase-Shifted Long-Period Gratings," *Asia Communications and Photonics Conference*, Hong Kong, 2015.
4. Nan Guo, Liang Wang, **Jie Wang**, Chao Jin, Hwa-yaw Tam, A. Ping Zhang, and Chao Lu, "Distributed Sensing using Bi-Directional BOTDA System," *Asia Communications and Photonics Conference*, Hong Kong, 2015.
5. Kwong Shing Tsang, **Jie Wang**, Li Jin *et al.*, "1.8 um High-Order

Microring Resonator Mode-locked Laser Using a Carbon Nanotube" *OECC/PS*, Niigata, Japan, 2016.

6. Yaxi Yan, **Jie Wang**, A Ping Zhang, Yonghang Shen, Hwayaw Tam, Tunable L-band Mode-Locked Bi-EDF Fiber Laser Based on Chirped Fiber Bragg Grating, *Photonics and Fiber Technology Conference,* Sydney, Australia, 2016.

Acknowledgements

I am grateful to all the people who had supported me during my Ph.D period.

First and foremost, I would like to express my sincere gratitude to my chief supervisor, Dr. A. Ping Zhang, for guiding me to a wonderful academic world of optical fibers and gratings. His broad knowledge, deeply academic insight, passion and enthusiasm for research, will benefit me for a long term. I appreciate all his contributions of efforts, time and fund in the experiments and journal writings.

I would like to thank Prof. Yonghang Shen, my chief supervisor at Zhejiang University, who encouraged and supported me to pursue my joint Ph.D. degree at PolyU. His guidance and assistance on my research help me a lot.

I also would like to thank Prof. Hwa-yaw Tam, my co-supervisor, who provided me first-class experimental facilities for fiber grating research. His kind guidance and advice inspired me to overcome the difficulties in my research.

I wish to thank Prof. Chao Lu for his kind support and help during my study at PolyU. I warmly thank Mr. Jimmy Tang and Miss. Hui Long, who helped me a lot in preparing CNT samples. I am thankful to Dr. Shaorui

Gao, Dr. Zhengyong Liu, Miss. Yaxi Yan, Mr. Mian Yao, Dr. Mingjie Yin, Dr. Ravi Bhushan, Mr. Nan Guo and Mr. Chengzhi Hu, who gave me much assistance in my experiments. Many thanks also go to my dear group mates, Dr. Lin Htein, Mr. Xin Cheng, Mr. Jushuai Wu, Dr. Bin Zhou, Mr. Elwin Ho, Dr. Liang Wang, Mr. Julien Bonefacino and Dr. Vincent Tse, for their productive discussions and suggestions.

I would like to acknowledge Dr. Dick Chung and Dr. Michael Liu, for their kindly assistance with the technical problems. I also wish to thank all my colleagues and friends at PolyU. It is my great honor to spend so wonderful three years with them in Hong Kong!

This dissertation is dedicated to my parents and my dearest friends. I deeply appreciate their great love, understanding, encouragement. They are always accompanying with me!

Table of Contents

Pages

Table of Figures

List of Acronyms

Acronyms	Description
ANDi	All-normal dispersion
Al	Aluminum
AC	Autocorrelation
$CaCl_2$	Calcium Chloride
CNT	Carbon Nanotube
CFBG	Chirped fiber bragg grating
PVA	Polyvinyl alcohol
CW	Continuous wave
DI	De-ionized
DOP	Degree of polarization
DOS	Density of states
DMD	Digital-micromirror device
Er	Erbium
EDF	Erbium-doped fiber
Ge	Germanium
GLE	Ginzburg-Landau equation
GVD	Group velocity dispersion
LPG	Long-period grating

MoS_2	Molybdenum disulfide
Nd	Neodymium
NOLM	Nonlinear optical loop mirror
NALM	Nonlinear amplifying loop mirror
NPR	Nonlinear polarization rotation
NLSE	Nonlinear Schrödinger equation
PBS	Polarization beam splitter
PC	Polarization controller
PMMA	Polymethyl methacrylate
PM	Polarization-maintaining
PDMS	Polydimethyl siloxane
RF	Radio frequency
SA	Saturable absorber
SPM	Self-phase modulation
SESAM	Semiconductor saturable absorber mirror
SNR	Signal-to-noise ratio
SMF	Single-mode fiber
SWCNT	Single-walled carbon nanotube
SDS	Sodium dodecyl sulfate
TBP	Time-bandwidth product
Tm	Thulium

TMM	Transfer matrix method
TBF	Tunable band-pass filter
WS_2	Tungsten disulfide
WDM	Wavelength-division multiplexer
Yb	Ytterbium

Chapter 1.

Overview

1.1 Background

Ultrafast lasers have attracted tremendous attention owing to their ultrashort pulse duration, high pulse repetition rate, broad optical spectrum and intense peak power that enable widespread applications, including analysis of chemical dynamics, high-capacity optical telecommunication systems, optical frequency metrology and nonlinear frequency conversion [1]–[6]. In particular, mode locking technique has been recognized as a superb approach to build ultrafast lasers due to its unique capability in generation of ultrashort optical pulses, structural compactness, and low cost. The first mode-locked laser was demonstrated by De Maria *et al.*, six years after the invention of the first laser [7]. In the early days, most mode-locked lasers mainly consisted of solid-state free-space optical components [8]–[14]. Even though the developments of solid-state mode-locked lasers are advancing, they have suffered from unsatisfactory beam quality, complicated cooling systems and costly maintenance.

A promising solution to the above limitations is to use optical fiber technology. The cylindrical waveguide geometry of optical fiber offers fiber lasers unprecedented advantages, such as tight confinement of laser radiation, excellent heat dissipation, and relatively high single-pass gain [15]–[17]. Particularly, the booming of the optical telecommunication in 1990s laid the groundwork for rapid developments of mode-locked fiber lasers. Moreover, coexistence of significant optical nonlinearity and dispersion in optical fibers turns mode-locked fiber lasers into a versatile platform for investigating various optical nonlinear phenomena, such as optical solitons [18]–[20], supercontinuum generation [21], [22] and other extraordinary optical wave evolutions [23]–[25].

Optical solitons, as particle-like nonlinear localized waves based on the balanced interaction between dispersion and nonlinearity, have attracted everlasting attention in the past decades owing to their theoretical values and attractive applications in the optical communication and signal processing systems [26]–[29]. In the early stages, most of soliton research works were conducted in the context of passive optical fibers. Lately, research interests have been shifted to solitons generation in mode-locked fiber lasers. Diverse soliton phenomena have been observed by optimizing the properties of optical fibers (e.g. dispersion, nonlinearity and birefringence), including conservative and dissipative solitons [20], [30]–[34], similaritons [24], [35], [36], Raman solitons [37], [38] and various vector solitons [39]–[44].

A key aspect of developing soliton mode-locked fiber lasers is the exploitation of efficient saturable absorbers (SAs). Various SAs have been demonstrated, mainly including nonlinear optical/amplifying loop mirror (NO/ALM) [18], [45], [46], nonlinear polarization rotation (NPR) [47]–[49] and semiconductor saturable absorber mirrors (SESAM) [19], [50]. Recently, the field of mode-locked fiber laser has been tremendously revolutionized by the emerging nanomaterials, including carbon nanotube (CNT), graphene and analogous 2D materials [51]–[56]. Their unique electrical and optical properties produce excellent saturable absorption with ultrafast response time and broadband operation range.

The first CNT-based SA for mode locking was demonstrated in 2003 [57], and subsequently was explosively adopted by numerous researchers because of its simple configuration and low-cost fabrication. CNT-SAs are particularly advantageous for use in fiber lasers because of their all-fiber and alignment-free integration, which are difficult to achieve by using free-space SESAMs [53], [58]–[61]. Because the electronic bandgap of CNT depends on its diameter and chirality, broadband SAs can be easily prepared by mixing CNTs with a broad diameter distribution [62]. Consequently, a single CNT-SA enables mode locking covering all the major wavelengths from 1 to 2 μm, which is undoubtedly a key advantage of CNT-SAs over SESAMs [63]–[65]. Thus, emission wavelengths of mode-locked fiber lasers have been flexibly tuned over a wide spectral ranges by using tunable band-pass filters (TBFs) [62], [66]–[69]. Apart from CNT, graphene [70], graphene oxide [71], [72], molybdenum disulfide (MoS_2) [73], [74], tungsten disulfide (WS_2) [56], [75], and other low-dimensional materials [76], [77], have lately been intensively investigated for demonstrating mode-locked fiber lasers.

1.2 Development of Mode-Locked Fiber Lasers

Fiber lasers have drawn extensive attention due to their flexibility, simplicity, durability, since the availability of low-loss silica fiber in 1970s. Nowadays, all-fiber laser systems can be quickly constructed by using convenient fiber fusion splicing methods. Moreover, many kinds of rare-earth-ion-doped fibers have been developed as the gain medium in fiber lasers or amplifiers, including erbium (Er), neodymium (Nd), and ytterbium (Yb) doped fibers. Among them, Er and Yb fiber lasers dominate in the commercial market, which emit at 1.55 and 1 μm, respectively.

To obtain ultrashort optical pulses in fiber lasers, various mode locking technologies have been exploited for generation of shorter and shorter pulses. Generally, the mode locking technique is categorized into active and passive regimes. However, actively mode-locked fiber lasers have the drawbacks of broad pulse duration, low peak power, and requiring expensive modulators. Therefore, much attention has been paid to passively mode-locked fiber lasers.

1.2.1 Conventional Mode Locking Technologies

The terminology “mode locking” describes the locking state of multiple longitudinal modes inside a laser cavity. In general, the resonant condition of lasing ensures that light is emitted at multiple discrete frequencies, which are known as modes. By synchronizing an external modulation signal with the roundtrip time of the laser, the phases of different modes could be locked, and thus pulsed radiation could be produced. The history of mode-locked laser is a progression of understanding of the mode-locking mechanism, and of exploiting better methods to generate shorter pulses. Over the past decades, the field of the mode-locked laser is blossoming with explosive increase of outstanding results of scientific research and commercial products.

To apply a synchronous modulation to the in-cavity optical field, there exist two main ways: active and passive mode locking. In this dissertation, the passive mode locking technique is employed because of its generation of ultrashort pulse and simple configuration. Passive mode locker encompasses two categories: artificial SA based on nonlinear optical interference and real SA based on the material’s nonlinear absorption. Its operation principle can be explained as shown in Figure 1.1. When an initial pulse enters into an SA with intensity dependent optical absorption, the intense part will pass through with higher transmissivity while the weak one with higher absorption. Consequently, the circulating pulse will be shortened once and once till a stable one is formed in the laser cavity.

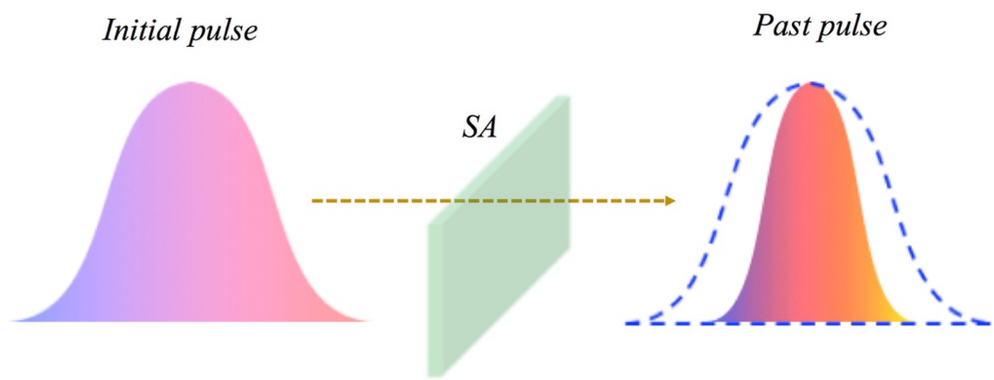

Figure 1.1 Scheme of pulse shortening through the SA.

1) Nonlinear polarization rotation (NPR)

In the NPR mode locking, an artificial saturable absorption effect is realized based on the nonlinear birefringence of single-mode optical fibers. Hoffer *et al*. firstly exploited the effect as a self-sustaining mechanism to obtain mode-locked fiber lasers [47]. Afterwards, this technique was broadly adopted and optimized to produce shorter and shorter pulses.

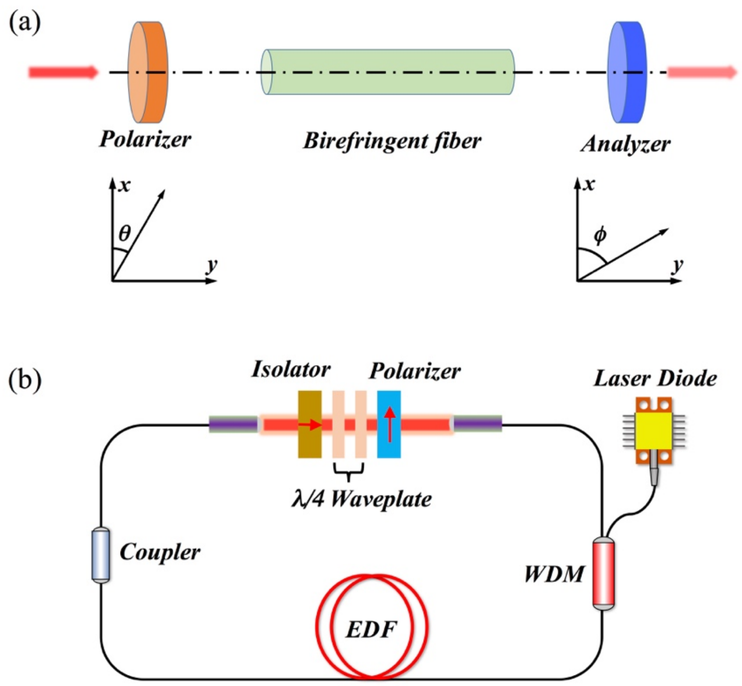

Figure 1.2 (a) Schematic of nonlinear polarization interference in NPR, and (b) configuration of a typical NPR mode-locked fiber laser.

The working mechanism of the NPR mode locking is illustrated in **Figure 1.2**(a), where a section of birefringent optical fiber is placed between a polarizer and analyzer. After the polarizer, an optical wave with arbitrary polarization state is changed into a linearly polarized one. Because of the fiber birefringence, the optical wave then evolves to be elliptically polarized. As the birefringence experienced by the optical wave is intensity dependent due to the Kerr nonlinearity, the transmission of the optical wave passing through the analyzer will evolve with respect to the optical intensity. With appropriate orientations of the polarizer and analyzer, an artificial SA can be achieved with this structure. As the Kerr nonlinear effect exhibits an ultrafast response time, ultrashort mode-locked pulses can be generated by using the NPR technique.

Figure 1.2(b) depicts a typical configuration of the NPR mode-locked fiber laser. Similar laser structures but with different fiber lengths, birefringence and dispersion have been demonstrated [78], [79]. However, the nature of polarization dependence and use of free-space elements leads to the NPR mode-locked fiber lasers environmentally unstable.

2) Nonlinear optical loop mirror (NOLM)

Apart from the NPR technique, nonlinear fiber loop mirror has been of much interest that is also based on the nonlinear Kerr effect of single-mode fibers. Generally, there exist two kinds of nonlinear loop mirror as shown in **Figure 1.3**, nonlinear optical loop mirror (NOLM, in **Figure 1.3**(a)), and nonlinear amplifying loop mirror (NALM, **Figure 1.3**(b)). In both devices, a Sagnac fiber interferometer is constructed by splicing together two output ports of a fiber coupler. Due to the nonlinear effects of optical fiber lasers, the two counter-propagating optical pulses with unequal intensities will experience different phase shifts. Assume that the dispersion is ignored, the transmission of the NOLM is described as [45]

$$\begin{aligned} |E_{out}|^2 = {} & |E_{in}|^2\big(1-2\alpha(1-\alpha)\big) \\ & \cdot\{1+cos[(1-2\alpha)|E_{in}|^2 2\pi n_2 L/\lambda]\} \end{aligned} \tag{1.2.1}$$

Where α is the splitting ratio of the fiber coupler, n_2 represents the nonlinear refractive index, L is the fiber loop length, λ is the operating wavelength, E_{in} is the input optical field, and E_{out} is the output field. However, the transmission of the NOLM does not monotonically increase along with the intensity, and drops back to the minimum value if the experienced phase shift is greater than π, which forms a clamping effect on the obtained pulse energy.

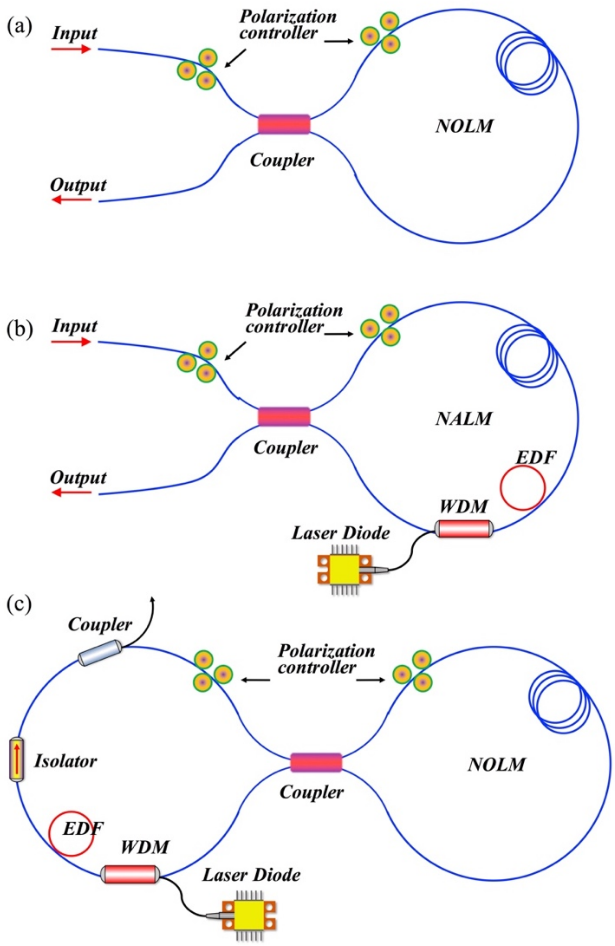

Figure 1.3 Configuration of (a) NOLM, (b) NALM and (c) a typical NOLM mode-locked fiber laser.

A typical configuration of the NOLM mode-locked fiber laser is plotted in **Figure 1.3**(c), which consists of two unbalanced fiber loops and is known as “figure of eight”. This mode locking technique has been widely exploited for building all-fiber mode-locked fiber lasers with various cavity lengths, active fibers (e.g. Yb- and Tm-doped fibers), and dispersion maps [80]–[83]. In addition, all-polarization-maintaining (PM) mode-locked fiber lasers can be realized by building the NOLM or NALM-like cavities with PM fibers and components, which emits environmentally stable ultrashort pulses. However, the non-monotonic intensity-dependent transmission of this SA may introduce the “power clamp” effect, which limits the maximum peak power of the emitted pulses.

3) Semiconductor saturable absorber mirror (SESAM)

Since many efforts have been paid to develop various real SAs (e.g. a dye or ion-doped crystal), the most efficient one is semiconductor saturable absorber mirror (SESAM), which is based on a specially-designed semiconductor structure. A typical SESAM mainly consists of a Bragg mirror on a semiconductor wafer as shown in **Figure 1.4**(a). When the incident photons are absorbed, electron-hole pairs will be generated in the SA. However, the light absorption will be saturated owing to the limited number of available electron-hole pairs. After a short time (i.e. response time), the excited electron-hole pairs will recombine and be able to absorb photons again. The essential parameters of an SESAM including the recovery time, modulation depth, operation bandwidth, saturation intensity and non-saturable loss, determines its mode locking performance.

(a)

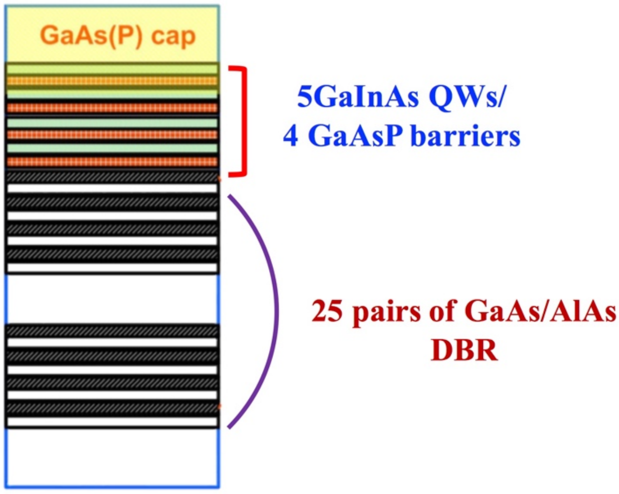

(b)

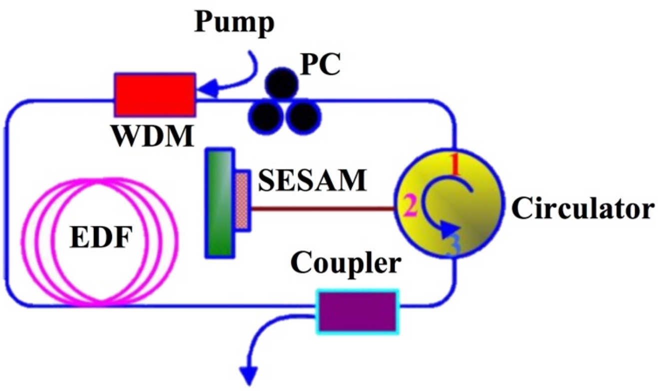

Figure 1.4 (a) Schematic diagram of the SESAM structure and (b) a typical configuration of an SESAM mode-locked fiber laser [84].

Figure 1.4(b) shows a typical configuration of an SESAM mode-locked fiber laser, which has been broadly studied by numerous researchers [39], [40], [84]–[86]. Even though appreciable success has been achieved with SESAMs, their fabrication of using the MBE growth and requiring complicated post-treatments results in a high price. Moreover, the narrow operation bandwidth restricts their potential applications in wide spectral ranges. Consequently, there exists a strong demand of seeking alternatives with a faster response time, broader operation range and lower cost.

1.2.2 Carbon Nanomaterials

Recently, carbon nanomaterials have attracted much attention in the field of ultrafast photonics. In particular, CNT and graphene have emerged as important absorbers in ultrafast fiber lasers owing to their excellent electrical and optical properties. Single-layer graphene is a flat monolayer of carbon atoms regularly arranged into a 2-D honeycomb lattice (**Figure 1.5**(a)). While single-walled CNT (SWCNT) is regarded as the 1-D rolled graphene forming a seamless cylinder (**Figure 1.5**(b)). As shown in **Figure 1.5**(c), the energy-momentum relation of graphene is linear at low energy near the six corners of the two-dimensional hexagonal Brillouin zone, enabling ultra-broadband mode locking based on the Pauli blocking effect. By contrast, the electronic properties of CNT depend on its diameter and chirality (that is, the twist angle along the tube axis). The typical electronic density of states (DOS) of a semiconducting CNT is plotted in **Figure 1.5**(d), consisting of a series of intrinsic van Hove singularities owing to its one-dimensional electronic band structure. As a consequence, saturable absorption of the CNT depends on strong depletion of electrons in the valence band and full occupation of the conduction band.

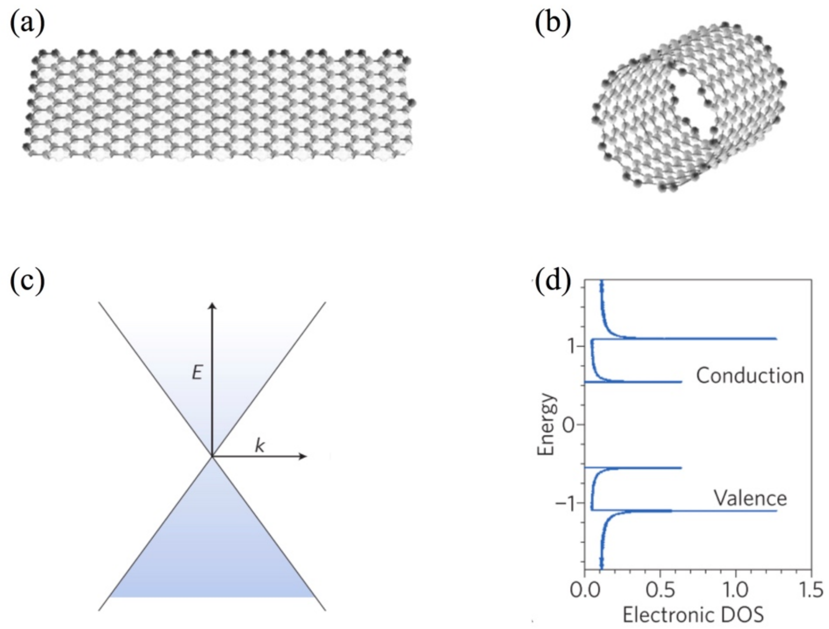

Figure 1.5 Schematic diagram of (a) Graphene and (b) CNT; (c) energy-momentum relation of graphene and (d) electronic density of states (DOS) of a semiconducting CNT [52].

To easily integrate these carbon nanomaterials into fiber lasers, free-standing SA films have been prepared with polymeric materials because of their excellent thermal property and radiation stability [53]. As shown in **Table 1.1**, the performance of CNT is comparable to that of graphene in serving as SAs for mode-locked fiber lasers. However, in comparison with graphene, it requires less efforts to disperse CNTs in polymeric films. Consequently, much attention has been paid to develop various CNT and polymer composites, providing efficient SAs for mode-locked fiber lasers operating at wavelengths from 1 to 2 μm [59], [87]–[90]. Previous reports indicate that CNT-based SAs perform well in terms of ultrafast recovery time, easy preparation, and low cost. Additionally, their operation bandwidth could be broadened by mixing CNTs with different diameters, facilitating widely tunable mode-locked fiber lasers. In this dissertation, CNT and Polyvinyl alcohol (PVA) films have been own-fabricated and used to develop various tunable mode-locked fiber lasers because of good transparency of PVA in near-infrared.

Table 1.1 A comparison table of laser parameters using various carbon nano-materials as SAs.

Nano-material	**Laser parameters**				**Ref.**
	λ (nm)	τ	f (MHz)	P (mW)	
Carbon nanotube	1557	354 fs	41.3	4.5	[91]
	1518-1565	2.39 ps	15	0.36	[62]
Graphene	1565	756 fs	1.79	2	[54]
	1570-1600	40-140 ps	1.5	3.5	[92]
Graphene Oxide (GO)	1559.3	587 fs	15.95	2.5	[93]
Reduced GO	1559 nm	390 fs	58	1.68	[72]

1.3 Motivations and Objectives of Research

In the past decades, intensive efforts have been paid to research of the mode-locked fiber lasers, producing many excellent commercial products and creating a large amount of business values. Thus far, mode-locked fiber lasers operate over a wideband spectral range (from visible to infrared spectral bands) based on various rare-earth-ion doped fibers. Nevertheless, most of them operate at discrete wavelengths, whose spectra are not adjustable to fit in some practical applications. Instead of grouping multiple different mode-locked fiber lasers, it is more attractive to develop tunable ones in terms of flexibility, structural compactness and cost-effectiveness. There are two key aspects to obtain a widely tunable mode-locked fiber laser: one is to develop an SA with a broad operation range, and another is to search for a tunable spectral filter for flexible wavelength tuning.

As efficient SAs, CNT-polymer films have been demonstrated to own many advantages, including ultrafast response time, suitable modulation depth and broadband absorption range. Moreover, CNT and light interaction can be enabled by sandwiching these films between two fiber connectors, which has exhibited good thermal stability and long-term durability. Thus, it will be of great interest to exploit such an SA in tunable mode-locked fiber lasers.

On the other hand, much attention has been paid to developing suitable tunable band-pass filters (TBFs) to spectrally tune mode-locked fiber lasers. However, the all-fiber structures of mode-locked lasers could be broken by commercially available TBFs, which comprise of free-space optical components. To address this problem, all-fiber birefringence filters have been demonstrated by utilizing the cavity birefringence and polarization dependent loss of fiber components. Nevertheless, it is challenging to practically repeat and quantify their performance, which is typically sensitive to environmental perturbations. However, the above issues can be addressed by fiber gratings owing to their inherent advantages, including all-fiber format, low insertion loss and potentially low cost. Moreover, their effects on mode-locked pulses can be optimized by flexibly tailoring their tractable physical parameters, including refractive index modulation, grating length, period, and structural profile. To the best of our knowledge, however, there are not many research works on fiber gratings in tunable mode-locked fiber lasers, and particularly less on exploiting long-period gratings (LPGs) for wavelength tuning. Therefore, it is important to comprehensively study the effects of fiber gratings on mode-locked pulses, including spectral tuning and shaping effects, pulse stretching and birefringence effect.

Therefore, the main objective of this research is to develop tunable mode-locked fiber lasers by using the CNT-PVA absorber and fiber gratings.

Experimentally, CNT-PVA absorbers and fiber gratings (i.e. LPGs and chirped fiber Bragg gratings (CFBGs)) will be own-fabricated and optimized for use in tunable mode-locked fiber lasers. Theoretically, soliton pulse formation and propagation in fiber lasers will be numerically investigated. In particular, a special LPG filter will be applied for widely tunable mode-locked fiber lasers. Additionally, a novel LPG-integrated optofluidic device will be demonstrated for generation of tunable bound solitons based on the advanced microfluidic chip technology. Eventually, dramatic attention will be paid to tunable vector and scalar solitons from a non-PM and PM mode-locked fiber laser, respectively.

1.4 Outline of Thesis

The chapters of my dissertation are organized as follows:

Chapter 1: Overview of mode-locked fiber lasers. In this chapter, the background and development of mode-locked fiber lasers are introduced. Several typical mode locking technologies are also reviewed. Additionally, the objective of our research is included. Finally, the outline of the thesis is presented.

Chapter 2: Fundamentals of tunable mode-locked fiber lasers. In this chapter, the theoretical backgrounds on pulse propagation in a fiber laser are reviewed, including fiber dispersion, Kerr nonlinearity, and amplification. On the other hand, the potential roles of fiber gratings in mode-locked fiber lasers are also discussed. Finally, the preparation of SWCNT-PVA films used in our research is described.

Chapter 3: Widely tunable mode-locked fiber lasers using LPGs. In this chapter, a widely tunable mode-locked fiber laser is obtained based on a novel LPG filter, whose spectrum covers C and L bands. The fabrication of LPG and procedure of thermal adjusting are also described. Additionally, the corresponding temporal and spectral properties of the obtained pulses are characterized.

Chapter 4: Optofluidic tunable mode-locked fiber lasers. In this chapter, an optofluidic tunable mode-locked fiber laser is presented based on a novel LPG-integrated microfluidic device. The preparation and characterization of this optofluidic chip are described at length. Afterwards, experimental results of the proposed mode-locked fiber are discussed, including optical spectra and temporal traces. Moreover, the observed bound solitons are analyzed.

Chapter 5: High-energy soliton fiber lasers using a CFBG Pair. In this chapter, a high-energy mode-locked fiber laser is presented based on a CFBG pair. Firstly, the CFBG inscription with a Talbot interferometer is discussed. Later, the emitted solitons without soliton-splitting are characterized. Finally, the reason of higher soliton-splitting threshold is theoretically analyzed.

Chapter 6: Tunable vector and scalar solitons based on CFBGs. In the chapter, generation of tunable vector and scalar solitons by using CFBGs are reported. The experimental setup of adjusting the CFBG is described. On one hand, vector solitons produced from a non-PM fiber oscillator are measured with the polarization-resolved technique. In addition, numerical simulations are conducted on the birefringence's effect on the spectra of vector solitons. On the other hand, scalar solitons generated from a PM fiber laser cavity are characterized in terms of spectrum, pulse trace and polarization stability.

Chapter 7: Conclusions and future outlook. In this chapter, all the research results are summarized and the relevant suggestions are offered for future work and developments.

Chapter 2.

Fundamentals of Tunable Mode-Locked Fiber Lasers

2.1 Introduction

In a mode-locked fiber laser, the propagation of an optical pulse not only depends on the dispersion and nonlinearity of optical fibers, but also relies on the laser gain and cavity loss, which interact mutually to produce various solitons. To provide a prerequisite for the soliton formation, an initial optical pulse can be effectively created by using the mode locking technique. Thus, the final solitons formed in a mode-locked fiber laser are determined by both the cavity parameters and the SA. As a result, it is important to investigate the pulse propagation in the fiber laser and characterize the used SA, in order to analyze and optimize the emitted solitons.

On the other hand, as the key components, fiber gratings are employed here to obtain tunable mode-locked fiber lasers. Even though they have been extensively studied in optical telecommunications and fiber sensors, there are few reports on applying them in mode-locked fiber lasers, to the best of our knowledge. It is of much interest to investigate their effects on the mode-locked fiber lasers, including wavelength tuning, spectral filtering and pulse stretching.

In this chapter, the pulse propagation in a fiber laser will be discussed, including the effects of dispersion, Kerr nonlinearity and laser gain. And the Ginzburg-Landau equation that governs the soliton formation will be given. Bedsides, the roles of fiber gratings in the mode-locked fiber lasers will be discussed. At last, the preparation of SWCNT-PVA SAs used in our research will be described.

2.2 Soliton Formation in a Fiber Laser

2.2.1 Nonlinear Schrödinger Equation

1) Fiber dispersion

In general, the refractive index (RI) experienced by an optical pulse in an optical fiber is frequency dependent, which is called as chromatic dispersion. As a result, the fiber dispersion plays a critical role on the propagation of short pulses. Normally, an optical pulse consists of a number of frequency modes in frequency domain. And different frequency modes travel at different speeds owing to the dispersion. Consequently, the optical pulse will be broadened while propagating in optical fibers.

Fundamentally, the frequency-dependent RI can be well approximated by the Sellmeier equation at frequencies far from the material resonances:

$$n^2(\omega) = 1 + \sum_{j=1}^{m} \frac{B_j {\omega_j}^2}{{\omega_j}^2 - \omega^2}, \tag{2.2.1}$$

where ω_j is the resonance frequency and B_j is the resonant strength at the j^{th} order. The sum term in Eq. (2.2.1) includes all resonance frequencies in the range of interest.

With Taylor expansion near the frequency ω_0, the mode-propagation constant β can be mathematically derived as

$$\begin{aligned} \beta(\omega) &= n(\omega)\frac{\omega}{c} \\ &= \beta_0 + \beta_1(\omega - \omega_0) + \frac{1}{2}\beta_2(\omega - \omega_0)^2 + \cdots \end{aligned} \tag{2.2.2}$$

$$\beta_m = \left(\frac{d^m\beta}{d\omega^m}\right)_{\omega=\omega_0} \quad (m = 0,1,2,\dots) \tag{2.2.3}$$

The parameters β_1 and β_2 depend on the RI n and its derivatives by the relations

$$\beta_1 = \frac{1}{v_g} = \frac{n_g}{c} = \frac{1}{c}\left(n + \omega\frac{dn}{d\omega}\right), \tag{2.2.4}$$

$$\beta_2 = \frac{1}{c}\left(2\frac{dn}{d\omega} + \omega\frac{d^2n}{d\omega^2}\right), \tag{2.2.5}$$

where n_g is the group RI and v_g is the group velocity at which the envelope of the optical pulse moves. The parameter β_2 represents the group velocity dispersion (GVD) parameter.

Figure 2.1 shows the GVD parameter β_2 as a function of wavelength in the fused silica [94]. In this figure, β_2 vanishes at ~1.27 μm, which is referred to as the zero-dispersion wavelength, λ_D. For wavelengths $\lambda < \lambda_D$, the medium exhibits normal dispersion as $\beta_2 > 0$, where the higher frequency components of the optical pulse travel slower than the lower frequency ones. By contrast, the medium shows anomalous dispersion as $\beta_2 < 0$ at wavelengths $\lambda > \lambda_D$, where the higher frequency parts travel faster than the lower frequency ones.

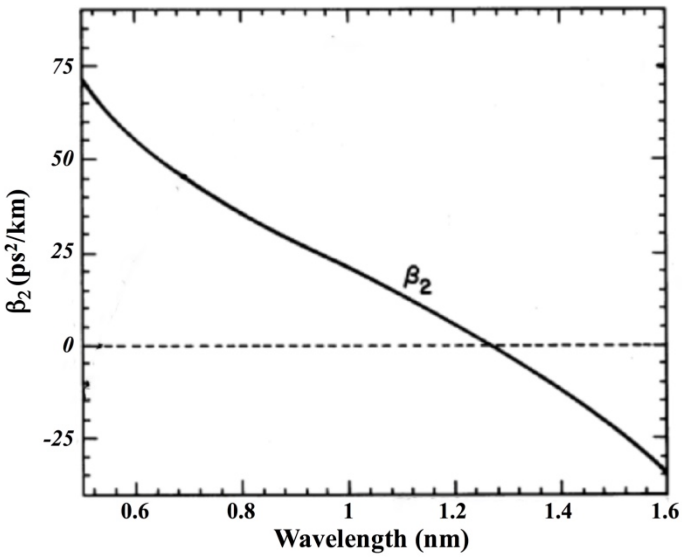

Figure 2.1 GVD of fused silica as a function of wavelength (After Ref. [94]).

2) Kerr nonlinearity

Apart from the dispersion, the RI of an optical fiber depends on the intensity of the optical pulse. As a consequence, an optical pulse with an intense peak power will experience spectral broadening due to the self-phase modulation (SPM) arising from the Kerr nonlinearity [94].

Most of the nonlinear effects in optical fibers, including the Kerr effect, stimulated Raman and Brillouin scattering, are related to the nonlinear RI that can be written as:

$$n(\omega, |E|^2) = n(\omega) + n_2|E|^2, \tag{2.2.6}$$

where $n(\omega)$ is the linear part presented by Eq.(2.2.1), $|E|^2$ is the intensity of optical pulse, and n_2 represents the nonlinear-index coefficient.

Even though n_2 in optical fibers is relatively small and typically in the range of $2.2{\sim}3.4\times10^{-20}$ m^2W^{-1} [94], the nonlinear effect experienced by the pulse is still strong because of tight modal confinement and long interaction length. Consequently, the self-induced phase shift experienced by an optical field can be expressed as:

$$\phi = nk_0L = (n + n_2|E|^2)k_0L, \tag{2.2.7}$$

where $k_0 = 2\pi/\lambda$, and L is the fiber length. The intensity-dependent nonlinear phase shift is correlated with the spectral broadening and thus formation of optical solitons in the anomalous-dispersion regime of fibers.

3) Nonlinear Schrödinger equation

Here, the Nonlinear Schrödinger equation (NLSE) that governs the nonlinear optical pulse propagation in optical fibers is derived as:

$$\frac{\partial E}{\partial z} + \beta_1\frac{\partial E}{\partial t} = i\frac{\beta_2}{2}\frac{\partial^2 E}{\partial t^2} - i\gamma|E|^2E, \tag{2.2.8}$$

Theoretically, the fundamental soliton solution can be derived from the NLSE by assuming the balance between the GVD and SPM terms. Based on the inverse scattering method [94], the analytical solution of the fundamental soliton is written as:

$$E = \sqrt{\left(\frac{\beta_2}{\alpha}\right)}\frac{1}{\tau_p} sech\left(\frac{t - {}^{z}/{}_{v_g}}{\tau_p}\right) exp\left(-i\frac{\pi z}{4z_0}\right), \qquad (2.2.9)$$

where α is the fiber loss, z_0 represents the soliton period as defined:

$$z_0 = \frac{\pi}{2}\cdot\frac{{\tau_p}^2}{|\beta_2|} \qquad (2.2.10)$$

2.2.2 Ginzburg-Landau Equation

1) Laser gain

In addition to dispersion and nonlinearity, the optical pulse also experiences laser gain and loss in the fiber laser cavity. In principle, the gain of an erbium-doped fiber amplifier (EDFA) depends on the simulated emission of upper-level ions. A classical three-level model is typically used to describe the excitation and emission of the Er^{3+} ions as illustrated in **Figure 2.2**. By pumping the ions from their ground state to the upper state, population inversion between the two levels can be formed. Thus, the incident photons will be amplified due to the simulated emission. Based on the rate equations, the gain coefficient of the EDFA is derived as $g = \sigma(N_2 - N_1)$, where σ is the emission cross-section, and N_1 and N_2 represents the atomic densities in the ground and upper states. In practice, this gain coefficient depends on multiple factors, such as doping concentration, fiber lengths and pump directions.

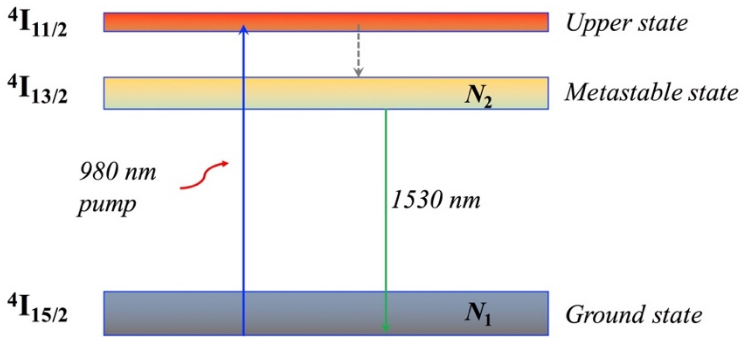

Figure 2.2 A three-level model of the Er^{3+} ions.

In general, an EDFA is characterized by its small-signal gain, gain saturation power, gain bandwidth, and the noise figure. With the assumption of homogeneous broadening, the gain coefficient of an EDFA is written as:

$$g(\omega) = \frac{g_0}{1 + (\omega - \omega_0)^2 {T_2}^2 + P/P_S}, \qquad (2.2.11)$$

where g_0 is the small signal gain, ω is the light frequency, ω_0 is the resonant frequency of the dopants, T_2 is the dipole relaxation time of the dopants, P is the light power, and P_S is the saturation power of the EDFA that depends on the pump strength.

However, the asymmetric gain and absorption spectrum are formed due to the interaction of Er^{3+} ions with silica host and other co-dopants (e.g. germania (Ge) and alumina (Al)) as shown in **Figure 2.3**. As a result, the gain bandwidth is estimated to be ~40 nm, corresponding to short pulse of

60 fs. In practice, however, the full-range gain cannot be efficiently used owing to the non-uniform gain profile, birefringence filtering, and cavity loss in fiber lasers.

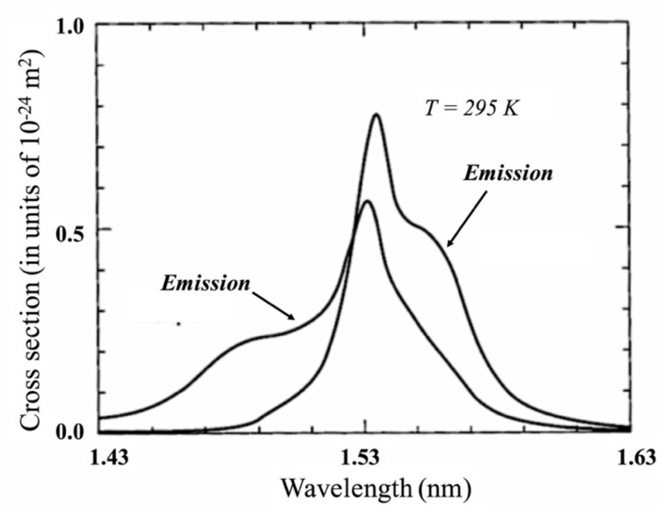

Figure 2.3 Typical absorption and emission cross sections of the EDFs (After Ref. [95]).

2) Ginzburg-Landau equations

When an optical pulse propagates in an erbium fiber laser, the laser gain must be considered. With including the laser gain into the NLSE, the Ginzburg-Landau equation (GLE) is derived,

$$\begin{aligned}\frac{\partial E}{\partial z} &= -\beta_1 \frac{\partial E}{\partial t} - \frac{i}{2}\beta_2 \frac{\partial^2 E}{\partial t^2} + i\gamma |E|^2 E \\ &+ \frac{g}{2}E + \frac{g}{2{\Omega_g}^2}\frac{\partial^2 E}{\partial t^2},\end{aligned} \tag{2.2.12}$$

where g represents the gain coefficient and Ω_g is the gain bandwidth. And the time dependence of the gain coefficient is determined by

$$g(t) = g_0 \, exp\left[-\frac{1}{E_s}\int_{-\infty}^{t}|E|^2 dt\right], \tag{2.2.13}$$

where g_0 is the small-signal gain, T_1 is the population decay time, and E_s is the saturation energy.

In reality, fiber loss α_l (~0.2 dB/km) need also be considered for long-distance propagation in fibers. Thus, the modified GLE is expressed:

$$\begin{aligned}\frac{\partial E}{\partial z} = -\beta_1\frac{\partial E}{\partial t} - \frac{i}{2}\beta_2\frac{\partial^2 E}{\partial t^2} + i\gamma|E|^2 E \\ + \frac{g-\alpha_l}{2}E + \frac{g}{2{\Omega_g}^2}\frac{\partial^2 E}{\partial t^2}\end{aligned} \tag{2.2.14}$$

2.3 Roles of Fiber Gratings in Fiber Lasers

Fiber gratings have found many important applications in widespread fields, including optical telecommunication, fiber sensor and laser systems, because of their inherent advantages, including all-fiber format, low insertion loss and potentially low cost [96]–[109]. Moreover, they can be flexibly optimized by designing their physical parameters, including RI modulation, length, period, structural profile [96], [110]. Generally, fiber gratings are categorized: long-period grating (LPG) and fiber Bragg grating (FBG) according to their grating periods. As shown in **Figure 2.4**(a), the LPG operates in a transmissive way that depends on resonant coupling between the co-propagating core and cladding modes. Its grating period is typically at the level of micrometers. And its transmission spectrum compromises a series of discrete resonant dips in a full spectral range. By introducing a π phase shift in the middle of a uniform LPG (i.e. PSLPG), a pass-band structure is formed, which can potentially be used as a band-pass filter [111]. By contrast, FBG works in a reflective mode based on the mode coupling between counter-propagating core modes (**Figure 2.4** (b)). Its period is typically hundreds of nanometers. With its period chirped along the fiber, a CFBG can own a broader reflective band.

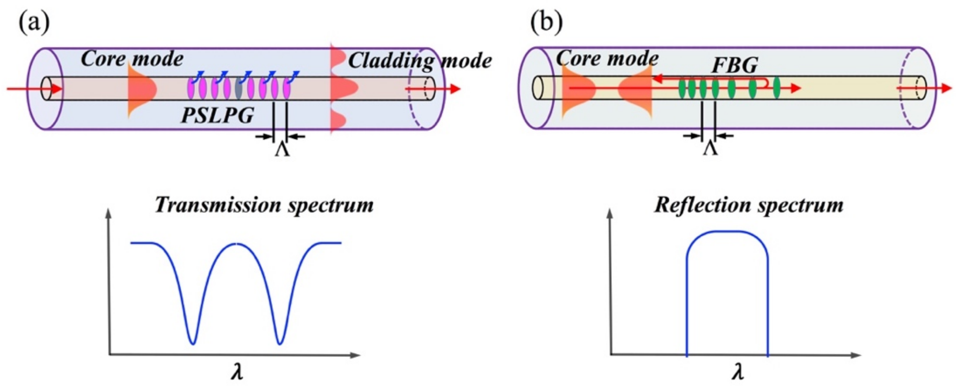

Figure 2.4 Schematic of modal coupling (top) and corresponding spectrum (bottom) of (a) PSLPG and (b) CFBG.

2.3.1 Long-Period Grating (LPG)

In the early days, LPG has been broadly employed as optical fiber sensors, such as temperature, strain, and RI sensing [112]–[114]. Besides, it has also been utilized for gain flattening of EDFA and suppressing the stimulated Raman scattering [98], [104]. Particularly, PSLPG with a pass-band spectral structure was demonstrated by O. Deparis *et al.* and served as a fiber spectral filter in an actively mode-locked fiber laser [115]. Later, PSLPG was used to build a switchable dual-wavelength mode-locked fiber laser [116].

Different from CFBG, the transmission spectrum of LPG consists of multiple discrete attenuation notches as plotted in **Figure 2.5**. Each spectral notch due to the modal coupling between co-propagating core and cladding modes occurs at the wavelength λ_R,

$$\lambda_R = \left[n_{eff}^{co}(\lambda) - n_{eff}^{cl}(\lambda)\right]\Lambda, \qquad (2.3.1)$$

where n_{eff}^{co} and n_{eff}^{cl} are the effective indices of the core and cladding mode, respectively, and Λ is the grating pitch.

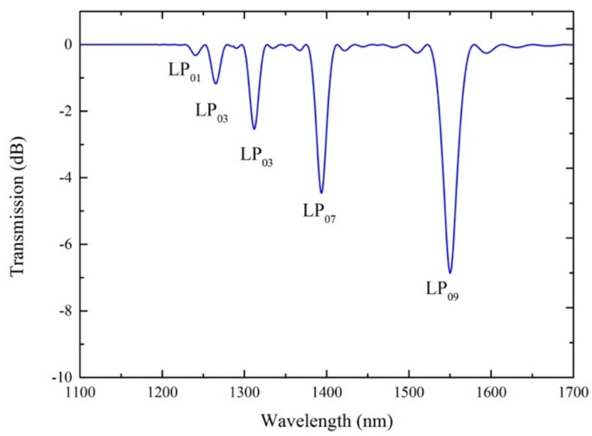

Figure 2.5 Simulated transmission spectrum of a typical LPG with length and pitch of 2 cm and 410 μm, respectively.

When a phase shift of π is introduced in the middle of LPG, the band notch at ~1.55 μm disappears and two new rejection bands appear at its both sides as shown in **Figure 2.6**. Formation of the pass-band is attributed to the converting of destructive interference to constructive interference due to the π phase shift, which can then be used for spectral filtering in mode-locked fiber lasers [111]. Moreover, spectral profile of the pass-band can be flexibly designed by changing the position or number of phase shifts.

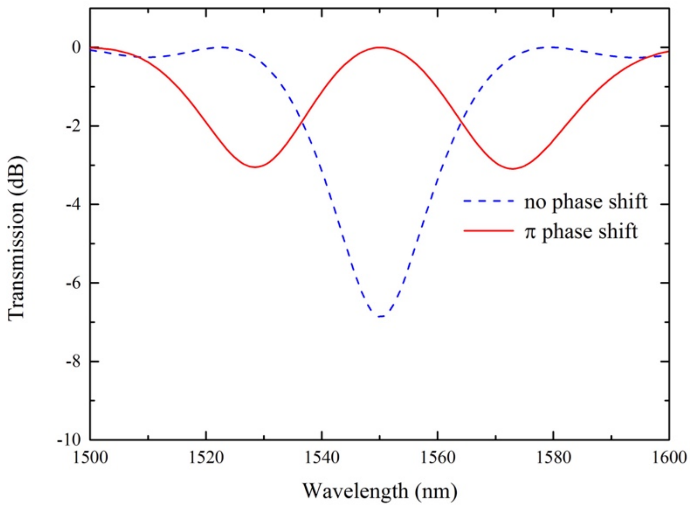

Figure 2.6 Spectral responses for LPG without phase shift and with a π phase shift at the center.

Moreover, PSLPG is spectrally sensitive to surrounding environments, including temperature, strain and RI of surrounding medium. Thus, optical spectrum of PSLPG can be tuned by adjusting these parameters, forming an all-fiber tunable spectral filter.

For instance, the temperature sensitivity of a PSLPG can be expressed as,

$$\frac{d\lambda_R}{dT} = -\frac{d\lambda}{d\left(\delta n_{eff}^{co}\right)}\left(\frac{dn_{eff}^{co}}{dT} - \frac{dn_{eff}^{cl}}{dT}\right) + \Lambda\frac{d\lambda}{d\Lambda}\frac{1}{L}\frac{dL}{dT}, \tag{2.3.2}$$

where λ_R is the central wavelength of the PSLPG, T is the temperature, n_{eff}^{co} and n_{eff}^{cl} are the effective RI values of the core and cladding modes, $\delta n_{eff} = \left(n_{eff}^{co} - n_{eff}^{cl}\right)$, L is the grating length, and Λ is the grating period. In silica fibers, the thermooptic coefficients dn_{eff}^{co}/dT and dn_{eff}^{cl}/dT of the core and cladding materials are typically ~7.8×10^{-6}/°C, while the thermal expansion coefficient dL/dT is typically 4.1×10^{-7}/°C [112]. The temperature sensitivity of LPG is thus predominantly determined by the thermooptic term in **Eq. (2.3.2)**.

In addition, PSLPG's spectrum can be shifted with respect to the RI of cladding mode. Different from core mode, the RI of cladding mode in a standard single-mode fiber (SMF) is sensitive to the surrounding medium. Normally, the induced spectrum-shift of the PSLPG with respect to the RI change of cladding mode can be deduced as,

$$\Delta\lambda_R = -\Delta n_{eff}^{cl}(\lambda)\cdot\Lambda\,, \tag{2.3.3}$$

where Δn_{eff}^{cl} is the effective RI change of cladding mode. In this dissertation, the RI response of PSLPG will also be investigated to develop optofluidic tunable mode-locked fiber lasers.

2.3.2 Chirped Fiber Bragg Gratings (CFBGs)

Generally, the central wavelength of a uniform FBG is determined by the Bragg condition as:

$$\lambda_B = 2n_{eff}\Lambda\,, \tag{2.3.4}$$

where λ_B is the Bragg wavelength, n_{eff} is the effective RI of the core mode and Λ is the period of the grating structure.

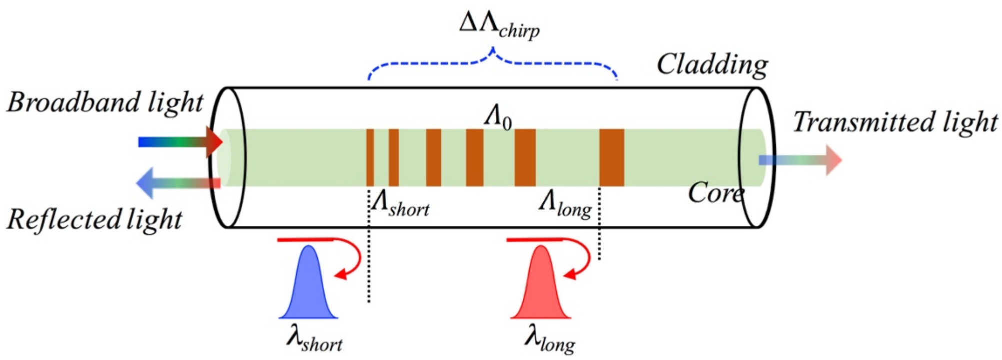

Figure 2.7 Schematic of a linearly-chirped CFBG.

When the grating period is varying monotonically along the fiber, a CFBG is formed as shown in **Figure 2.7**. The period is increased from Λ_{short} to Λ_{long} over a fiber length L_g. Therefore, a broad reflection spectrum of CFBG can be obtained with its bandwidth defined as,

$$\lambda = 2n_{eff}\left(\Lambda_{long} - \Lambda_{short}\right), \tag{2.3.5}$$

As different parts of an optical pulse at short and long wavelengths are reflected at different positions, a time delay between them is induced as:

$$\tau(\lambda) \approx \frac{(\lambda_0 - \lambda)}{\Delta\lambda_{chirp}} \frac{2L_g}{v_g}, \qquad (2.3.6)$$

where v_g refers to as the group velocity of the pulse in the CFBG.

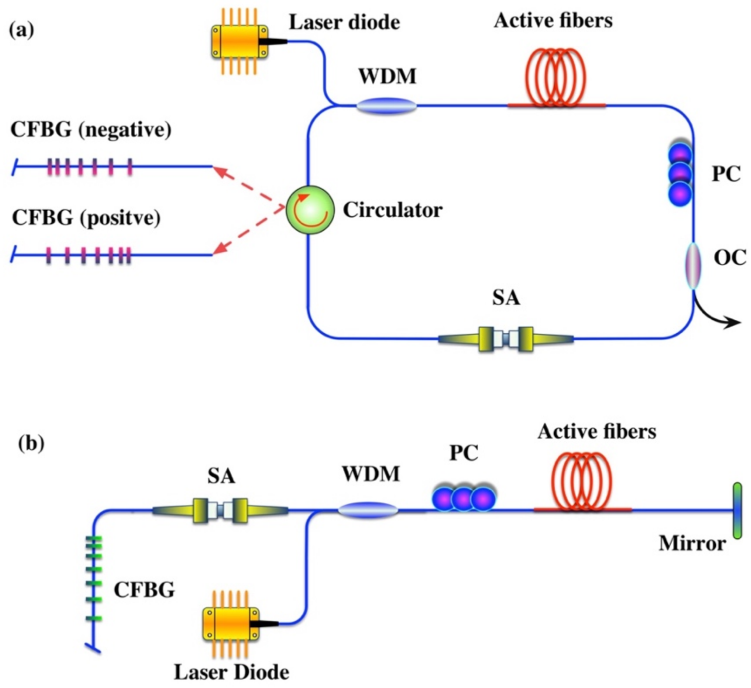

Figure 2.8 Typical configurations of mode-locked fiber lasers incorporated with CFBGs: (a) fiber ring cavity structure and (b) linear cavity structure.

Thus, CFBG can offer a broad reflection band for mode-locked fiber lasers. For instance, a multi-wavelength mode-locked fiber laser has been demonstrated by using multiple CFBGs [117]. Moreover, CFBGs have been used for dispersion management in mode-locked fiber lasers [118]–[121]. Dependent on the operation direction, CFBG can provide anomalous and normal dispersion in the mode-locked fiber lasers. Consequently, the mode-locked fiber lasers using CFBGs can emit both conventional and dissipative solitons [119]. **Figure 2.8** shows the mode-locked fiber lasers incorporated with CFBGs. In the ring cavity, CFBG is incorporated through a fiber circulator (**Figure 2.8** (a)), while it is directly spliced as a resonator mirror in the linear cavity (**Figure 2.8** (b)).

Analogous to LPG, CFBG also responses to the strain and temperature changes, which has been broadly exploited in fiber sensors. Among them, the shift of Bragg wavelength with respect to strain is expressed as,

$$\Delta\lambda_B = 2n_{eff}\Lambda\left(\left\{1-\left(\frac{n^2}{2}\right)[P_{12}-v(P_{11}+P_{12})]\right\}\varepsilon\right), \tag{2.3.7}$$

where ε is the applied strain, P_{12} and P_{11} represent the Pockel's coefficients of the stress-optic tensor, and v is the Poisson's ratio. The factor $\{(n^2/2)[P_{12}\text{-}v(P_{11}+P_{12})]\}$ has a typical value of ~0.22. Thus, the strain response of CFBG at a constant temperature is given as,

$$\frac{1}{\lambda_B}\frac{\delta\lambda_B}{\delta\varepsilon} = 0.78\times10^{-6}\mu\varepsilon^{-1} \tag{2.3.8}$$

In this dissertation, the dependence of CFBG on strain will be used to develop an all-fiber tunable filter for mode-locked fiber lasers.

2.4 Preparation of SWCNT/PVA Based SA

2.4.1 Preparation Procedure of SWCNT/PVA Films

Apart from fiber gratings, SWCNT-based SA is another key component of a well-performed tunable mode-locked fiber laser. All the SWCNT-based SAs used in our research are own-prepared. The commercial-available SWCNTs were grown by the electric arc discharge technique, with a mean diameter of ~1.5 nm. And the SWCNT/PVA films were fabricated by using the following steps as illustrated in **Figure 2.9**(a):

1) Several milligrams of SWCNT powder were poured into 10 ml 0.1% sodium dodecyl sulfate (SDS) aqueous solution which was used as a surfactant. SWCNT aqueous dispersion with saturable concentration was then obtained after 10 hours of ultrasonic agitation produced. Later, large SWCNT bundles were precipitated by centrifuging the dispersion.
2) The upper portion of the centrifuged solution was then decanted and some PVA powder was added in. It was dissolved at 90°C with ultrasonic agitation of 3 hours.
3) The resultant dispersion consisting of SWCNT and PVA was then poured into a polystyrene cell. Thin SWCNT/PVA films were adhered on the cell walls after evaporation of 1~2 days at temperature of 40°C.
4) Eventually, the solidified SWCNT/PVA film was easily peeled off the polystyrene cell with tweezers. Note that the SWCNT/PVA film on the cell wall was better than that on the bottom.

This preparation method was very easy to handle. At last, the obtained SWCNT/PVA films could be cut into many pieces for use in mode locking.

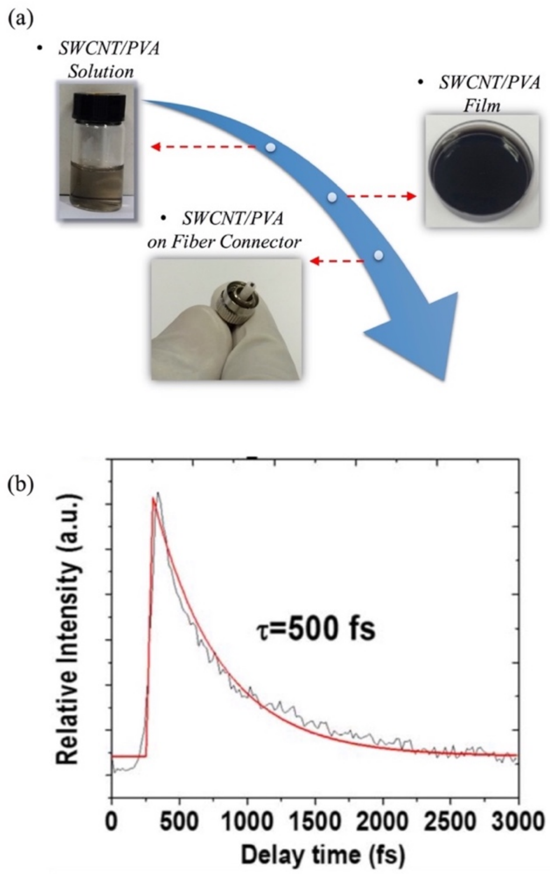

Figure 2.9 (a) Preparation procedure and (b) measured time response of the SWCNT/PVA film.

2.4.2 Characterization of SWCNT/PVA Films

Firstly, a standard time-resolved pump-probe experiment was conducted to measure the ultrafast recovery time of the SWCNT/PVA composites [122]. An ultrafast laser system from Spectra-Physics and two balanced detectors were used. The ultrafast transient absorption of the SWCNT/PVA SA is plotted in **Figure 2.9**(b), where an instantaneous rise of absorption was followed by an exponential decay with response constant of 500 fs. The result shows that the prepared SWCNT/PVA film exhibits a very short response time, which is desirable for the use in mode-locked fiber lasers. The average thickness of the SWCNT/PVA film was measured to be ~110 microns. To characterize its linear absorption, a broadband light source covering C and L bands was used together with an optical spectrum analyzer (OSA).

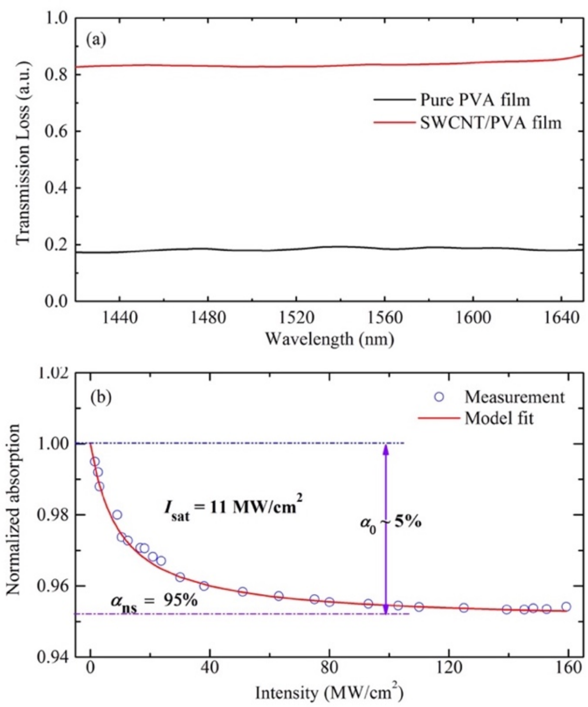

Figure 2.10 (a) Linear absorption spectrum of the SWCNT-PVA film and pure PVA film and (b) saturable absorption curve of the SWCNT-PVA SA. Measurement data (circle symbols) is well fitted with the red solid curve.

As shown in **Figure 2.10**(a), the linear loss of the SWCNT/PVA SA at 1560 nm is ~83.7% (including the absorption and connection loss). Its saturable absorption was also measured by utilizing a picosecond fiber laser, a variable attenuator together with an optical power meter. As shown in **Figure 2.10**(b), non-saturable loss α_{ns}, modulation depth α_0, and saturation intensity I_{sat} are evaluated to be 95%, 5% and 11 MW/cm^2, respectively. The experimental results are fitted based on a simple two-level model [85].

2.5 Summary

In summary, the fundamentals of tunable mode-locked fiber lasers have been discussed. Firstly, the pulse propagation in a fiber laser has been analyzed with including dispersion, Kerr nonlinearity and laser gain effects. The GLE that governs the pulse propagation has been derived. Additionally, the spectral properties of fiber gratings and their potential applications in mode-locked fiber lasers have been discussed. At last, the preparation and characterization of the SWCNT/PVA film used in our research have been described at length.

Chapter 3.

Widely Tunable Mode-Locked Fiber Lasers Using LPGs

In this chapter, a widely tunable mode-locked fiber laser based on an SWCNT/PVA absorber and an LPG W-shaped spectral filter is demonstrated. The used W-shaped filter is prepared by sandwiching a PSLPG between two different uniform LPGs. Through thermally tuning the LPG filter from 23 to 100°C, the mode-locked laser can be tuned continuously from 1597 to 1553 nm. With a shorter erbium-doped fiber, the spectral tuning range is further extended to 1531.6 nm. In addition, the spectral shaping effect of PSLPG on the mode-locked pulses is investigated. The experimental observations show that the large thermal tunability of the LPG filter offers an efficient way to obtain widely tunable ultrafast fiber lasers covering both C and L bands.

3.1 Introduction

Tunable mode-locked fiber lasers have attracted intense research interests owing to their promising applications in widespread fields, such as biomedical research, optical telecommunication and spectroscopy [1], [50], [123]. Compared to other mode-locking approaches, passive mode locker based on SA has been extensively used because of its capability of ultrashort pulse generation and compact configuration. Among different kinds of SAs, e.g. SESAM [32], [50], graphene [54], [124], graphene oxide [72], [125] and MoS_2 [74], [126], SWCNT has attracted much attention owing to its inherent advantages, including ultrashort recovery time and possibility of mass production [52], [65], [127]. Moreover, a broadband SA for wideband mode-locking could be quickly prepared by mixing SWCNTs of distributed diameters.

To obtain a tunable mode-locked fiber laser, a TBF which operates within the gain spectrum of the laser is inserted into its laser cavity. Through using commercial available TBFs, mode-locked fiber lasers with spectral tunable ranges of 40 nm (1518–1558 nm) [62] and 34 nm (1525–1559 nm) [128] have been achieved with CNT and graphene, respectively. However, the free-space coupled TBF will introduce a large insertion loss. An all-fiber solution for in-cavity filtering is based on the cavity birefringence and polarization dependent loss of fiber components. By adjusting polarization controllers (PCs), artificial birefringence filters have been used for tunable mode-locked fiber lasers [67], [68], [92]. Another all-fiber solution is to use fiber grating technology. For instance, CFBG has been employed as an in-cavity tunable filter for a graphene mode-locked fiber laser with a tuning range of 4.5 nm [129]. LPG filters have been incorporated in an actively mode-locked fiber laser [130] and an NPR mode-locked fiber laser [131], respectively.

In this dissertation, we present a widely tunable SWCNT mode-locked fiber laser based on a novel LPG-based tunable filter. Owing to the grating's spectrum-tailoring capability [132], a W-shaped spectral filter is built based on a three-LPG concatenated structure. A PSLPG is sandwiched in the center, which forms a pass-band with a 3-dB bandwidth of ~20 nm, and two uniform LPGs of different periods are used to extend the stop-bands. Because of the large thermal tunability of LPGs, the emission wavelength of the mode-locked fiber laser can be continuously tuned over a broad range.

3.2 Fabrication and Characterization of LPG Filters

The LPGs were fabricated based on an own-established point-by-point LPG inscription platform with a 248-nm excimer laser (BraggStarTM M, Coherent, Inc.) as illustrated in **Figure 3.1**. The hundred-μm-level grating structures can be formed in the fiber core based on intense UV beam spots shaped by the adjustable slit. Based on a high-precision translation stage, the grating parameters of LPG can be accurately controlled, including grating period, length, and phase shift position. In our study, photosensitive SMFs (PS1250/1500, Fibercore Ltd) were used for LPG fabrication.

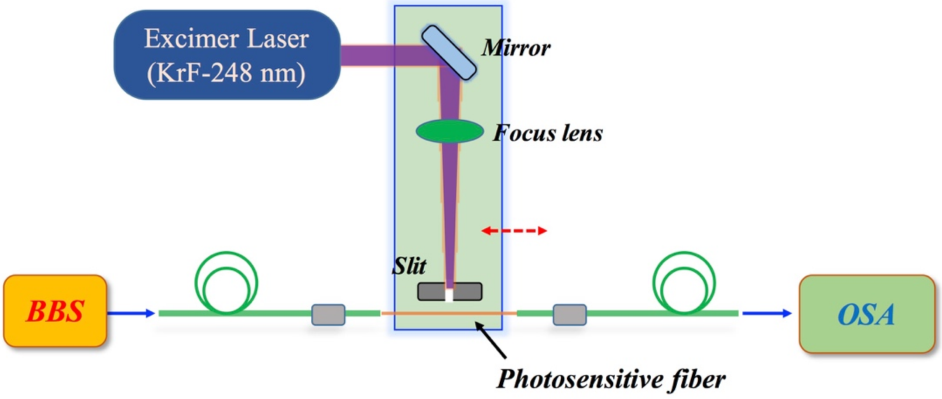

Figure 3.1 Schematic of LPG fabrication based on the point-by-point method.

As shown in **Figure 3.2**(b), the transmission spectrum of the π-phase PSLPG (i.e. LPG-2) owns a central pass-band, the grating length and pitch of which are 34.4 mm and 430 μm, respectively. When a π-phase shift is introduced in the middle of the grating, the initial spectral dip splits into two notches and forms a pass-band with a bandwidth of 20 nm. Such a broad pass-band can reduce the filtering effect on the mode-locked pulses. The two spectral notches are measured with 3-dB bandwidths of 20.8 and 26 nm, respectively. As shown in **Figure 3.2**(d), the two notches were broadened further to 37 nm and 45 nm, respectively, when two uniform LPGs (i.e. LPG-1 and LPG-3) with grating pitches of 424 and 438 μm were used. The lengths of the two LPGs are 26.28 and 25.44 mm, respectively. The OSA used in the experiment can only display wavelength up to 1650 nm. The broad bandwidths of the stop-bands at both sides prohibit lasing outside of the pass-band and ensure wideband continuous tuning operation.

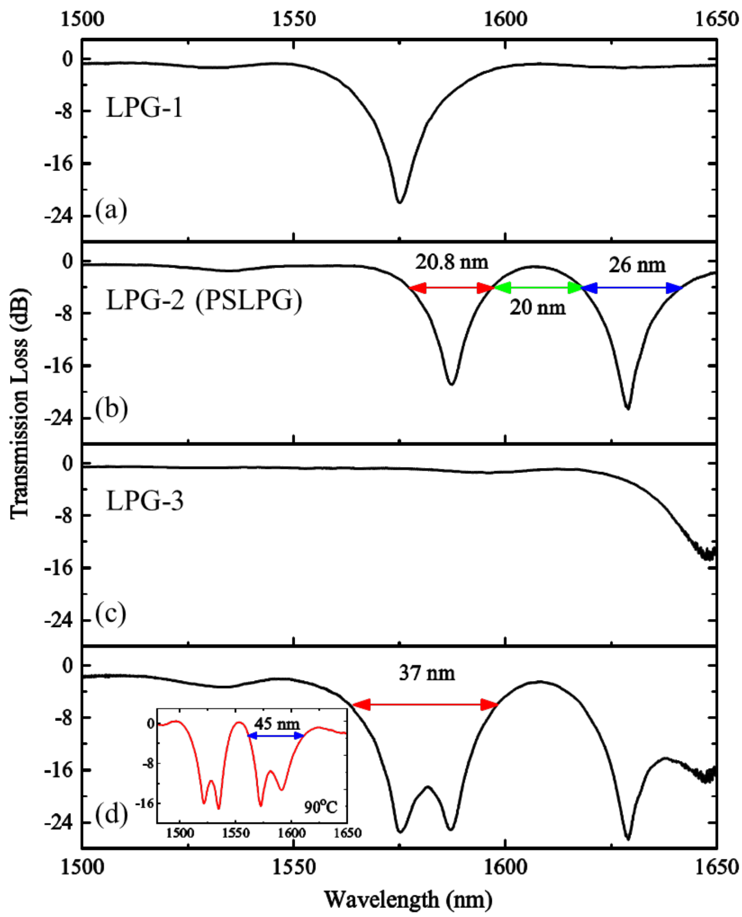

Figure 3.2 Measured spectra of (a) LPG-1, (b) LPG-2 (PSLPG), (c) LPG-3 and (d) the LPG W-shaped filter at 23°C. The corresponding transmission spectrum at 90°C is shown in the inset.

The temperature response of the W-shaped filter was characterized by using an oven. As plotted in **Figure 3.3**, the central wavelength of the pass-band decreases from 1598 to 1542 nm linearly along with temperature from 23 to 100°C. During the thermal tuning process, the spectral profile of the filter remains unchanged. The thermal spectral shift of the LPG

W-shaped filter is measured as -0.72 nm/°C.

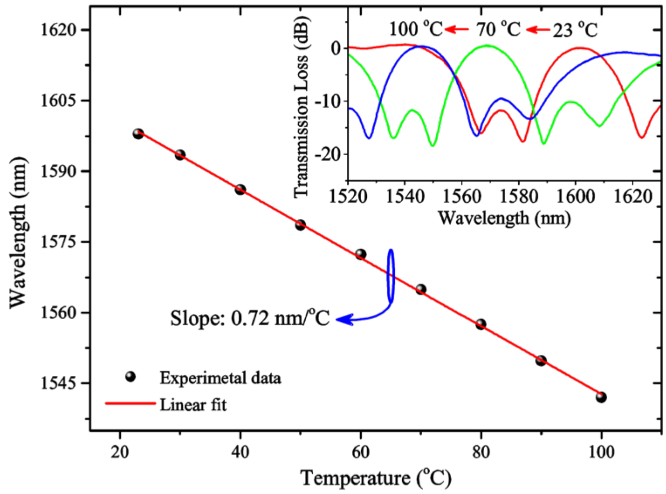

Figure 3.3 Measured central wavelength of the W-shaped filter against with temperature from 23 to 100°C. The corresponding transmission spectra at 23 (red curve), 70 (green curve) and 100°C (blue curve) are shown in the inset.

3.3 Fiber Laser Structure

To build a tunable mode-locked fiber laser, the W-shaped filter was then incorporated into a fiber oscillator together with the SWCNT absorber as shown in **Figure 3.5**. Two 980-nm laser diodes are used to bidirectionally pump a 7.8-m-long erbium-doped fiber (EDF) (Liekki Er30-4/125) for a broad gain spectrum. The peak core absorption of EDF at 1530 nm is typically 30 dB/m and the mode field diameter (MFD) at 1550 nm is 6.5 μm. **Figure 3.4** shows the measured small-signal gain profile of 1-m-long EDF under pump power of 100 mW at 980 nm. Unidirectional operation of the laser is realized with an optical isolator. Laser pulses are output from the 10% tap of a fused fiber coupler. To build a laser cavity with net anomalous dispersion, a 9-m-long SMF with the second-order dispersion of -22ps^2/km is incorporated A small piece of home-made SWCNT/PVA composite film is sanwiched between two FC/PC connectors and used as the mode locker. The linear loss of the SWCNT/PVA SA was measured to be 83.7% at 1560 nm. The nonlinear saturable absorption was measured by using a homemade ultrafast fiber laser equipped with a variable attenuator. The normalized non-saturable loss, modulation depth, and saturation intensity are 95%, 5% and 11 MW/cm^2, respectively.

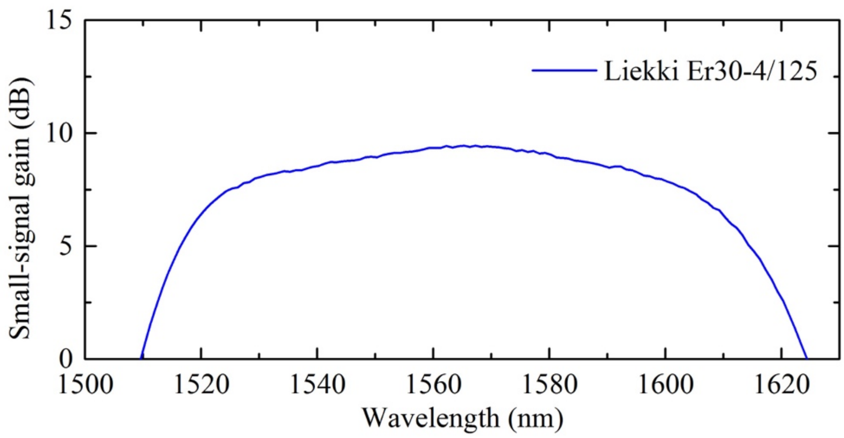

Figure 3.4 Measured small-signal gain profile of 1-m-long EDF.

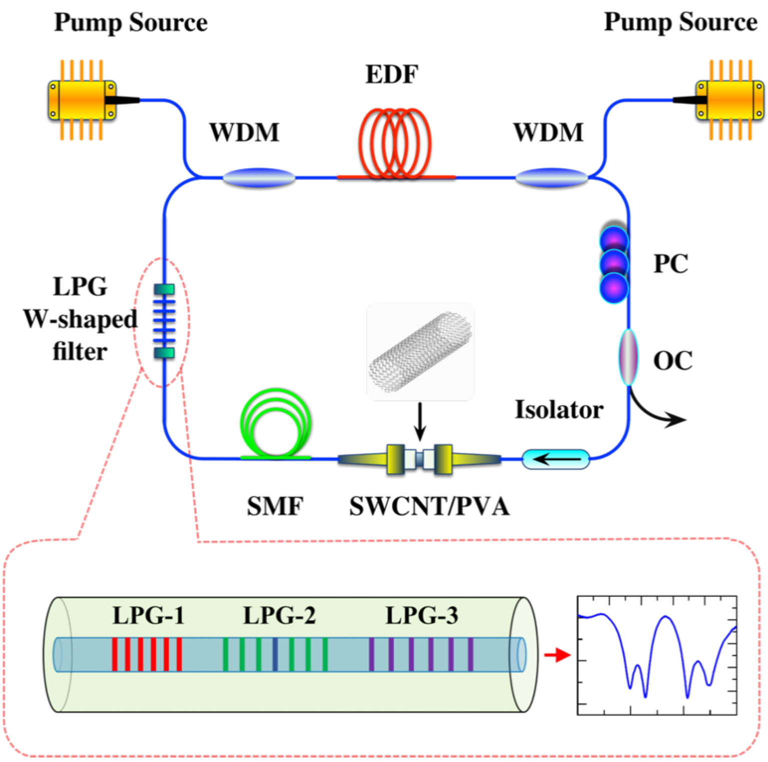

Figure 3.5 Configuration of the tunable mode-locked fiber laser with the W-shaped filter.

3.4 Experimental Results

3.4.1 Characteristics of Emitted Solitons

At room temperature (23°C) and under forward and backward pump powers of more than 51 and 10 mW, the fiber laser would change from continuous wave (CW) operation to mode-locking state. To optimize the mode locking, the PC was initially finely adjusted and then fixed during the entire wavelength-tuning process. The mode-locked laser is obtained at 1597 nm, which is consistent with the pass-band of the LPG W-shaped filter. And it is blue-shifted when the temperature of the filter is increased.

When the temperature of the LPG W-shaped filter is set at 50°C, a typical spectrum and temporal trace of the mode-locked laser are plotted in **Figure 3.6**. The output power of the laser is 820 μW, and the corresponding forward and backward pump powers were 70 and 33 mW, respectively. The low lasing efficiency is attributed to large insertion loss of the SWCNT/PVA SA. The apparent Kelly sidebands indicate that the mode locking operation in the anomalous dispersion regime. The central wavelength and bandwidth of the laser are 1572 nm and 3.04 nm, respectively. As shown in **Figure 3.6**(b), the autocorrelation (AC) trace of the mode-locked laser pulses was measured by an optical autocorrelator (Femtochrome, FR-103XL). If a $sech^2$ profile is assumed, the pulse duration is evaluated to be around 910 fs. As plotted in the inset, the pulse-to-pulse separation is measured as ~135 ns, corresponding to the laser cavity length of 28 m. The single-soliton mode locking operation state is verified by the regular pulse train and AC trace.

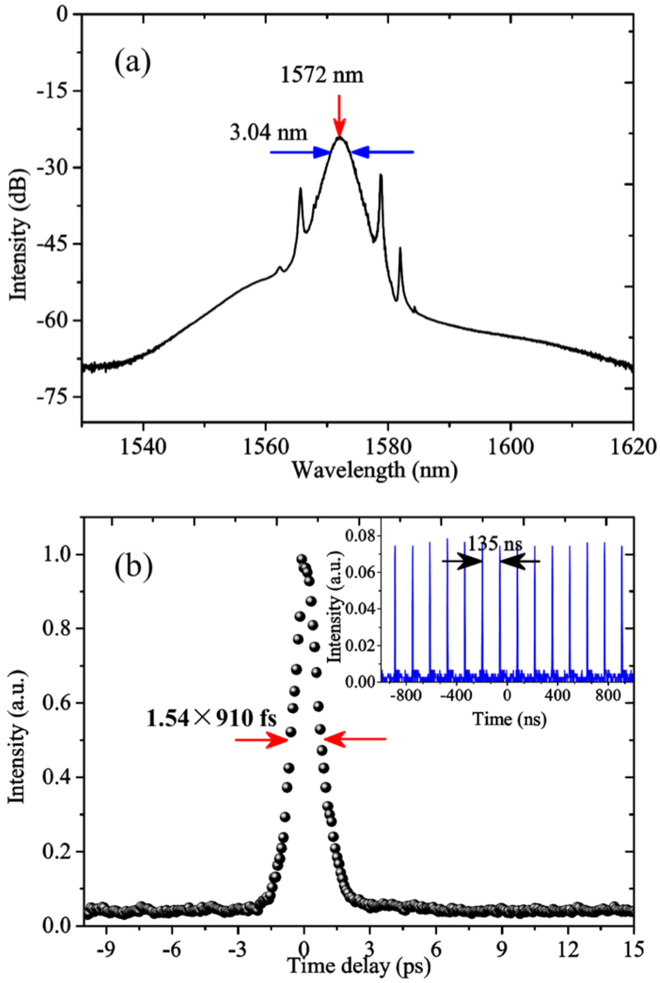

Figure 3.6 (a) Output spectrum and (b) autocorrelation trace of the mode-locked laser with the temperature of the LPG filter at 50°C.

3.4.2 Results of Wavelength Tuning

The spectral evolution of the mode-locked laser is shown in **Figure 3.7** when the temperature of the filter is increased from 23 to 100°C. In the experiment, the forward and backward pump powers were then adjusted to optimize the effective gain spectrum of the fiber oscillator. Since Er^{3+} ion operates at the three-level transition, the same net gain at shorter wavelength requires higher pump powers than that at longer wavelength in the fiber oscillator [133]. When the LPG W-shaped filter was at 23°C, the forward and backward pump powers were set as 51 and 10 mW resulting in mode locking at 1597 nm. With the temperature of the LPG filter at 100°C, the mode locking state was obtained at 1553 nm under forward and backward pump powers of 82 and 42 mW. The mode-locked laser is continuously shifted from 1597 to 1553 nm, while the Kelly sidebands are always-on during the entire wavelength-tuning process. As the PC is fixed, one can believe that the adjusting of LPG filter leads to wavelength tuning rather than the intra-cavity birefringence filtering effects.

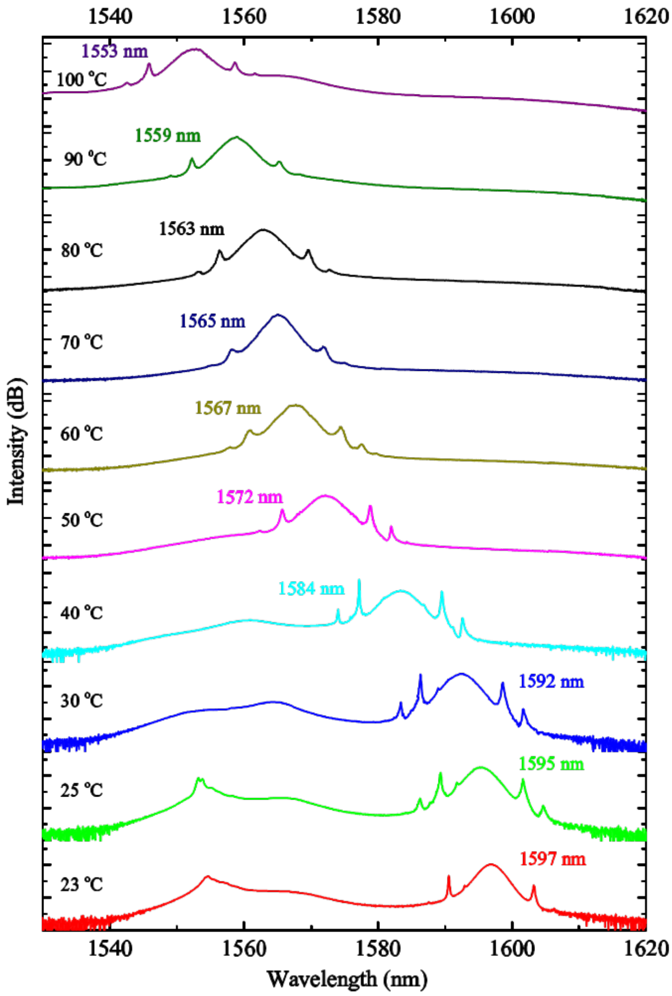

Figure 3.7 Wavelength tuning of the mode-locked laser with respect to the temperature of the filter from 23 to 100°C.

The change in the central wavelength of the tunable mode-locked laser against the temperature of the LPG filter is plotted in **Figure 3.8**(a). One can see that the laser wavelength monotonically decreases against with the temperature. The uneven gain profile of the fiber oscillator is attributed to the nonlinearity of the tuning curve. As shown in **Figure 3.8**(a), lower output power at wavelengths longer than ~1584 nm is attributed to the limited gain at long wavelengths.

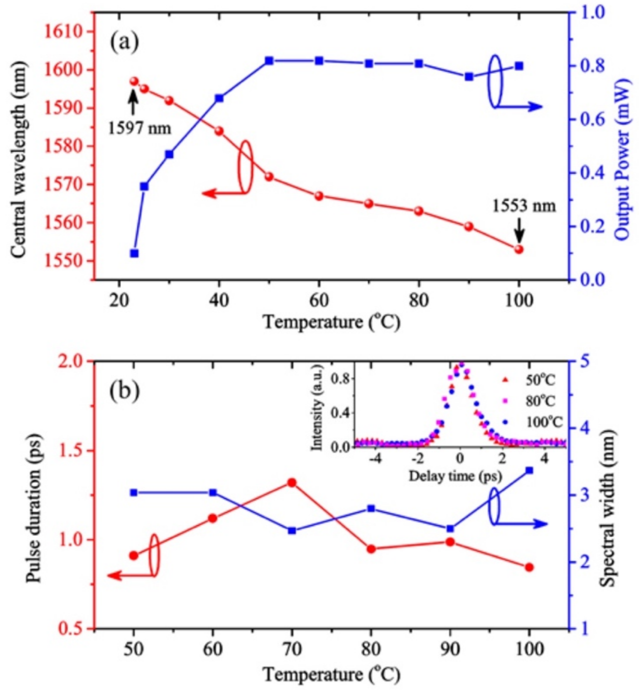

Figure 3.8 (a) Measured central wavelength and output power of the laser as a function of temperature of the LPG W-shaped filter and (b) measured pulse duration and spectral width of the laser at different temperatures. The AC traces of the laser pulses at 50, 80 and 100°C are depicted in the inset, respectively.

Figure 3.8(b) shows the pulse duration and spectral width of the mode-locked laser from 50 to 100°C. Owing to the limited sensitivity of the lower laser powers at longer wavelengths and used optical autocorrelator, the AC traces of the mode-locked pulses corresponding to the temperature from 23 to 40°C was not measured in the experiment. The spectral width varies from 2.5 to 3.4 nm, indicating the mode-locked pulses close to the transform limit. The pulse width changes between 0.85 and 1.32 ps and does not exhibit obvious dependence on the laser wavelength. The corresponding AC traces are plotted in the inset of **Figure 3.8**(b), when the temperature of the filter is 50, 80 and 100°C, respectively.

In order to demonstrate that the proposed LPG W-shaped filter can provide wider tunability, another experiment was conducted with a fiber oscillator with a shorter EDF. In addition to pumping condition, the gain spectrum of an EDF is determined by the length and doping concentration of erbium ion [133]. The length of the EDF was shortened from 7.8 to 1.9 m in the experiment. **Figure 3.9** shows the spectral evolution of the output mode-locked pulses, when the temperature of the filter was tuned from 70 to 110°C. One can see that the central wavelength of the mode-locked laser can be tuned from 1558 to 1531.6 nm continuously. However, the upper limit of the tuning range decreases from 1597 to 1558 nm owing to the limited gain at long wavelengths. The measured pulse durations change from 0.6 to 1.2 ps. The corresponding AC traces are shown in **Figure 3.9(b)**, indicating that the time-bandwidth products (TBPs) of tunable pulses are kept around 0.35.

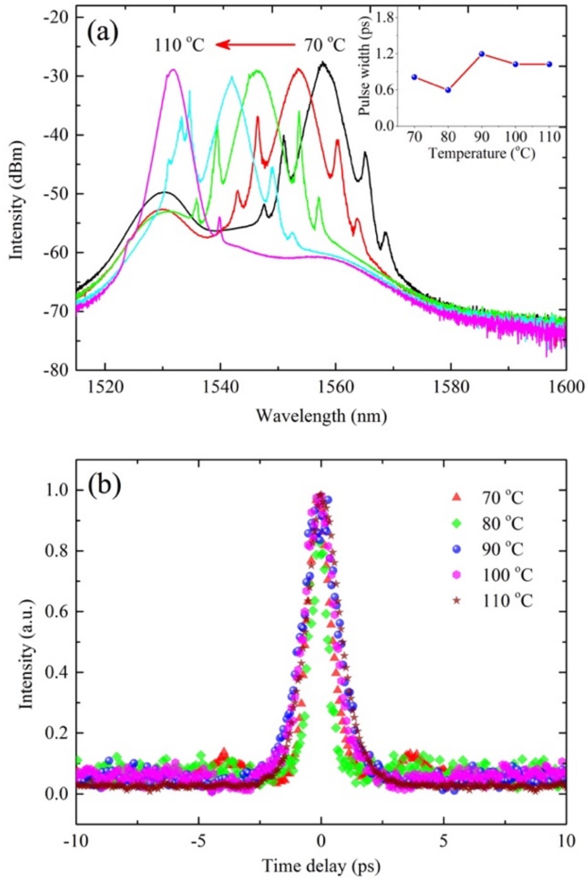

Figure 3.9 Output spectra and AC traces of the mode-locked laser with a 1.9-m-long EDF.

3.4.3 Theoretical Analysis of Wavelength Tuning

To examine the thermal tuning of the mode-locked fiber laser wavelength, a numerical simulation was conducted based on the split-step Fourier method (SSFM). **Figure 3.10** shows the simplified laser model for the simulation study. In general, the nonlinear propagation of an optical pulse in the optical fibers is described by [32],

$$\frac{\partial A}{\partial z} + \mathrm{i}\frac{\beta_2}{2}\frac{\partial^2 A}{\partial t^2} = \frac{g}{2}A + \mathrm{i}\gamma|A|^2 A + \frac{g}{2\Omega_g^2}\frac{\partial^2 A}{\partial t^2}, \qquad (3.4.1)$$

where A is the slowly varying envelope of an optical pulse, t and z are the propagation time and distance, respectively, β_2 and γ are the second-order dispersion and Kerr nonlinearity of optical fibers, Ω_g is the effective gain bandwidth, $g = g_0\exp(-E_p/E_s)$ relates to the gain saturation of EDF, where g_0, E_p, and E_s are the small-signal gain, pulse energy and gain saturation energy, respectively.

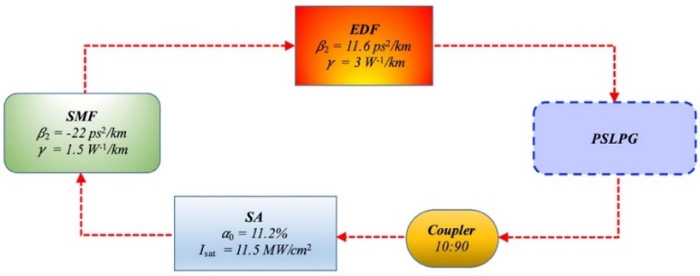

Figure 3.10 Simplified model of the mode-locked fiber laser.

The SWCNT/PVA SA is mathematically described based on a two-level saturable absorption model as,

$$\alpha(I) = \alpha_{ns} + \alpha_0/(1 + I/I_{sat}), \qquad (3.4.2)$$

where α_0, α_{ns} and I_{sat} are the modulation depth, nonsaturable loss and saturable absorption intensity, respectively. To approximate the experimental parameters, g_0 = 4.5 dB/m, Ω_g = 25 nm, γ = 3 $W^{-1}km^{-1}$, β_2 = 11.6 ps^2/km for the EDF, and γ = 1.3 $W^{-1}km^{-1}$, β_2 = -22 ps^2/km for other passive SMFs.

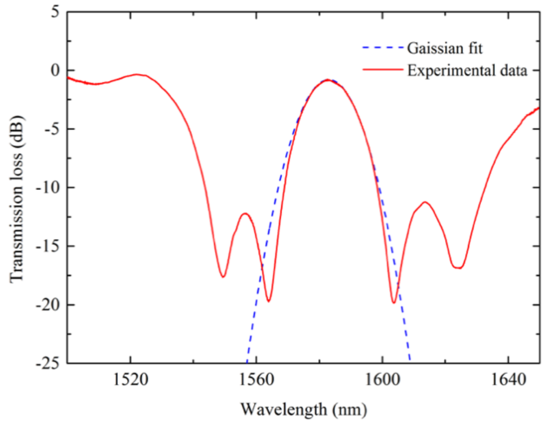

Figure 3.11 Measured (red curve) and Gaussian fitted (blue dash curve) spectra of the used LPG filter at 50°C.

As shown in **Figure 3.12**, the measured transmission spectrum of the LPG filter can be well fitted by a Gaussian function near the central wavelength. Thus, the used LPG filter is mathematically approximated in frequency domain as,

$$T(\omega) = T_l * exp(-0.5 * (\omega - \omega_c/\omega_p)^2)\,, \qquad (3.4.3)$$

where T_l is the insertion loss of the LPG filter, ω_p represents the 3-dB bandwidth of the pass-band, and ω_c corresponds to the central wavelength λ_c as determined by λ_c=λ_0-0.72*(T-25°C), where λ_0 is the central wavelength at room temperature and T is the temperature of the filter.

For each temperature from 25 to 115°C, a self-consistent solution was always obtained after thousands of computation roundtrips. The simulated mode-locked spectra at all temperatures are plotted in **Figure 3.12**. One can see that the relative peak intensities of spectra are correlated with the small-signal gain profile. The corresponding pulse duration is estimated as 0.8 ps. Note that the discrepancy between numerical simulations and experimental results is attributed to the non-ideal gain curve and the existence of extra birefringence interference filtering effects.

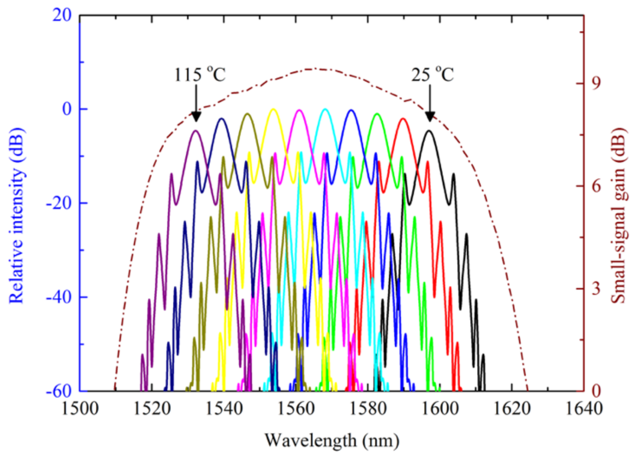

Figure 3.12 Simulated mode-locked spectra with thermal tuning from 25 to 100°C. The small-signal gain profile is plotted as a reference.

3.4.4 Spectral Shaping Effect

To investigate the filtering effect of PSLPG, two PSLPG filters with different bandwidths have been fabricated by using the aforementioned method. With grating period of 426 μm and length of 38 mm, the fabricated PSLPG (i.e. PSLPG-1) exhibits a spectral bandwidth of 18.2 nm as shown in **Figure 3.13**. By contrast, a longer PSLPG (i.e. PSLPG-2) with length of 42 mm shows a narrower bandwidth of 10.3 nm.

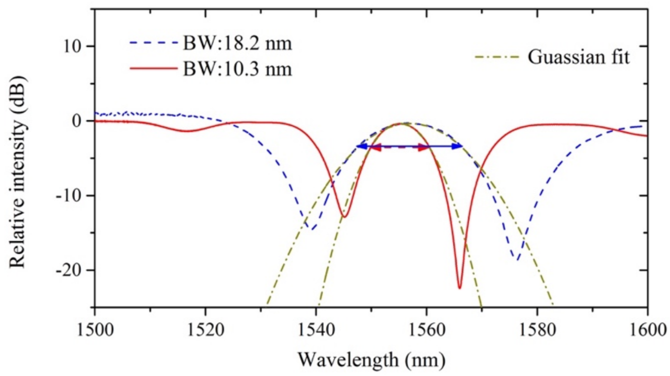

Figure 3.13 Transmission spectra of PSLPG-1 and PSLPG-2.

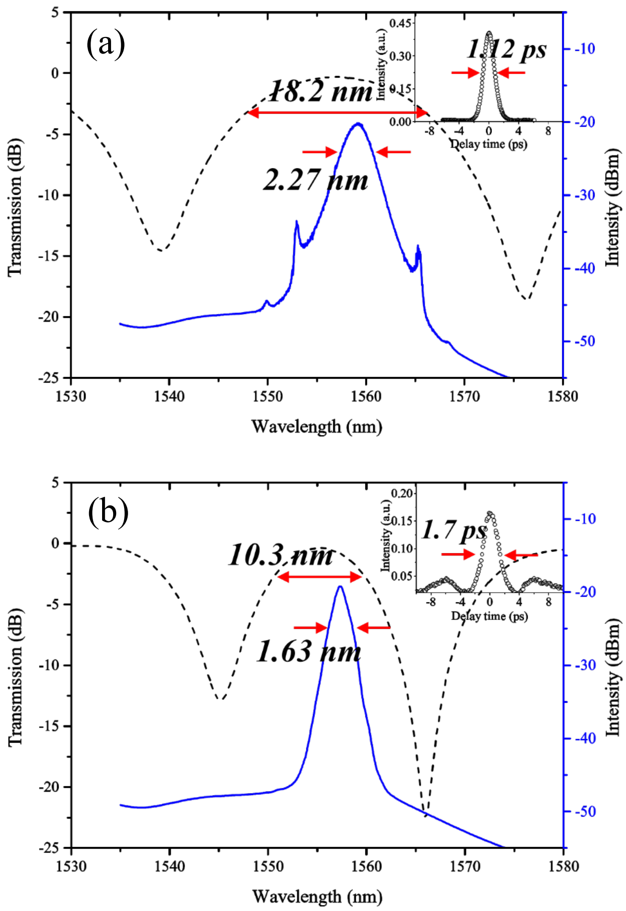

Figure 3.14 Measured spectra (blue curves) of the mode-locked laser with two different PSLPGs (black dash curves). The insets depict the corresponding AC traces.

Figure 3.14 shows output spectra and pulse traces of the mode-locked fiber laser with two PSLPG filters under pump power of 68 mW. When PSLPG-1 with 3-dB bandwidth of 18.2 nm is incorporated, the pulse duration and spectral width of the mode-locked laser are measured as 1.12 ps and 2.27 nm, respectively. By contrast, the spectral bandwidth of the laser is decreased to 1.63 nm by using PSLPG-2 with smaller bandwidth of 10.3 nm. We can observe that the Kelly sidebands are strongly suppressed by the narrow PSLPG-2 filter. Correspondingly, the pulse duration is broadened to 1.7 ps.

To examine the filtering effect of PSLPG in detail, the experimentally built mode-locked fiber laser was also theoretically simulated based on the SSFM. The calculated spectra and pulse traces of the mode-locked laser are plotted in **Figure 3.15**. By using PSLPG-1 as the spectral filter, the spectral width and pulse duration are calculated as 2.12 nm and 1.2 ps, respectively. While with PSLPG-2, they change to 1.54 nm and 1.65 ps, respectively. Moreover, one can see that the spectral Kelly sidebands are remarkably suppressed when PSLPG-2 is incorporated. To show the filtering effect of PSLPG-2 on the mode-locked pulses explicitly, the soliton solution obtained with PSLPG-1 was used as the starting signal of numerical simulation on the laser with PSLPG-2. As shown in **Figure 3.16**, the Kelly sidebands disappeared after 10 roundtrips and the spectral profile converged to a constant solution, which is the same as the that shown in **Figure 3.15**.

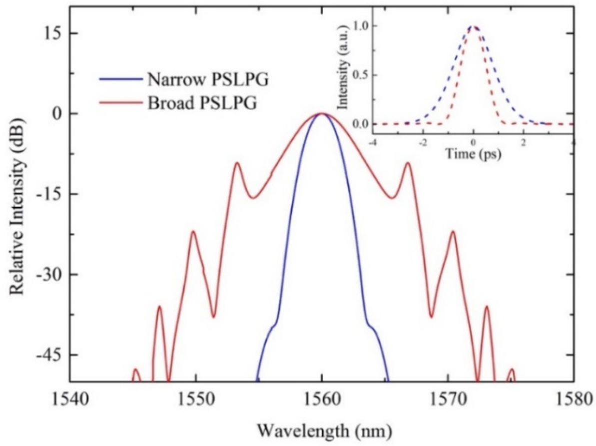

Figure 3.15 Simulated spectra and pulse profiles of the mode-locked lasers with PSLPG-1 and PSLPG-2.

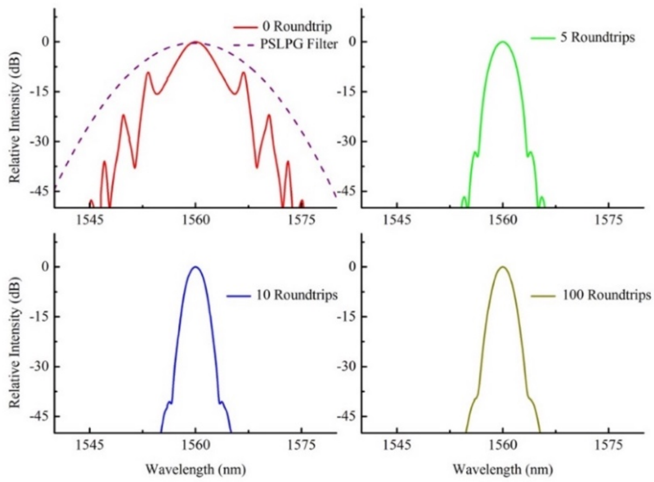

Figure 3.16 Simulated laser spectra after 0, 5, 10 and 100 roundtrips.

3.5 Summary

In summary, a widely tunable mode-locked fiber laser has been built based on a special LPG W-shaped filter. The central wavelength of the laser can be tuned from 1553 to 1597 nm continuously with the corresponding pulse duration varying between 0.85 and 1.32 ps. Wavelength extended to 1531.6 nm to cover both C and L bands has also been realized with a shorter EDF. Moreover, the spectral shaping effect of the PSLPG on the mode-locked pulses has been studied. Such an all-fiber widely tunable mode-locked fiber laser offers a compact and cost-effective ultrafast pulse source for various practical applications.

Chapter 4.

Optofluidic Tunable Mode-Locked Fiber Lasers

Ultrafine tunable mode locking offers an essential way to investigate the underlying phenomena of mode-locked fiber lasers, such as pulse bunching and bound solitions. In this chapter, an optofluidic tunable mode-locked fiber laser based on an LPG-integrated microfluidic chip is presented. By adjusting the flow rate ratio of two different solutions, the homemade microfluidic chip facilitates ultrafine tuning of the liquid's RI value and thus LPG's spectrum. Using such an optofluidic tunable filter, the central wavelength of the mode-locked laser can be tuned continuously. Stable mode-locked pulses are measured with pulse duration of 0.9 ps and repetition rate of 12.14 MHz, respectively. Furthermore, bound solitons with different pulse separations are demonstrated in the experiment.

4.1 Introduction

Tunable mode-locked fiber laser is of much interest because of its capability of flexible wavelength tuning, which provides a compact and cost-effective ultrafast source for various applications. One of efficient approaches to obtain tunable mode-locking is to insert a TBF in the laser cavity [62], [128], [110]. Particularly, optical fiber grating filters have received much attention in tunable ultrafast fiber lasers owing to their compactness, low insertion loss and potential low cost [129], [117]. As presented in the previous chapter, we have demonstrated a widely tunable all-fiber mode-locked laser by using a specially designed LPG W-shaped filter [134].

Tunable mode-locking also offers an efficient approach to study the underlying phenomena of mode-locked fiber lasers, such as pulse bunching [135], harmonic mode locking [136], bound solitons [137] and soliton rains [138]. Among them, bound solitons have received great attention owing to the meaningful multi-soliton interaction mechanisms and their applications in high-capacity fiber-optic telecommunications. Bounded as a stable unit due to the balance of repulsive and attractive effects, however, bound solitons are vulnerable to the change of laser parameters, e.g. dispersion, nonlinearity, gain and loss [139]. Therefore, there is a demand for ultrafine TBF device to precisely tune the overall laser gain but not disturb other parameters.

One of promising approaches to achieve such ultrafine spectral tuning is to utilize the optofluidic technology, which exhibits numerous intrinsic advantages such as high sensitivity, reconfigurability and compactness. With the versatile microchannel networks, photonic components like optical fiber gratings can be integrated into a microfluidic chip to develop new functional devices and applications [140]–[143].

In our study, an optofluidic tunable mode-locked fiber laser is presented based on a microfluidic chip integrated with a PSLPG. As shown in **Figure 4.1**, the fluidic flows in the microfluidic chip can be sufficiently mixed in a spiral mixer for ultrafinely tuning the liquid's RI and thus the PSLPG's spectrum. Such an optofluidic spectrum-tunable filter has been demonstrated for ultrafine tuning of the mode-locking status in the fiber oscillator.

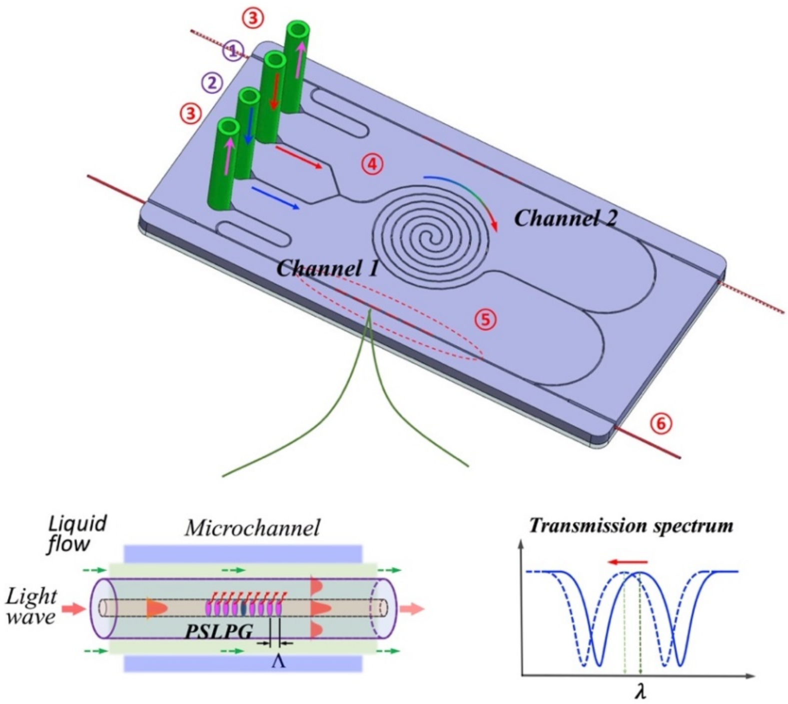

Figure 4.1 Schematic diagrams of (Top) the LPG-integrated microfluidic chip (① and ② are the inlets, ③ is the outlet, ④ is a spiral mixer, ⑤ is the PSLPG and ⑥ is the fiber pigtail), and (Bottom) the PSLPG filter.

4.2 Preparation of the LPG Integrated Optofluidic Device

The schematic diagram of the optofluidic device is illustrated in **Figure 4.1**, consisting of two inlets, two outlets, a spiral mixer and two throughout fiber-grating devices. When a high-precision motorized pump was used to adjust the flow rate ratio *v* between the calcium chloride ($CaCl_2$) aqueous solution (RI ~1.39) and DI water (RI ~1.333), the RI of aqueous solution surrounding LPG filter can be tuned as [144],

$$R_{mc} = \frac{R_1 + R_2 v_2 (1 \pm \varepsilon_2)/v_1(1 \pm \varepsilon_1)}{1 + v_2(1 \pm \varepsilon_2)/v_1(1 \pm \varepsilon_1)}, \tag{4.2.1}$$

where R_1 and R_2 are the RI values of the injected $CaCl_2$ solution and DI water, v_1 and v_2 are the corresponding flow rates, and ε_1 and ε_2 are the flow accuracies of the used two syringe pumps, respectively.

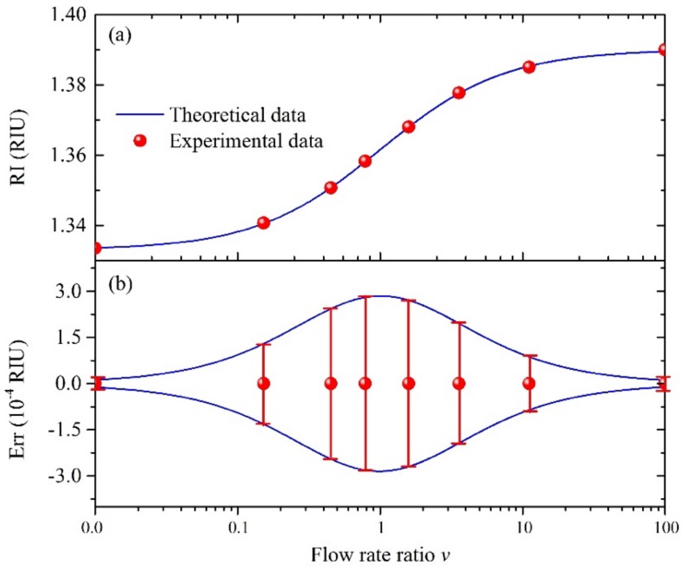

Figure 4.2 (a) Calculated RI and (b) deviation of the mixed liquid as a function of the flow rate ratio *v*.

Figure 4.2 depicts the RI and deviation of the mixed liquid as a function of the flow rate ratio *v*. By increasing the ratio *v* from 0 to 100, the RI of aqueous solution near LPG filter can be adjusted from 1.333 to 1.39. Based on the Eq.(4.2.1), when an ordinary microfluidic pump with the flow rate accuracy of 1% (NE-4000 Double Syringe Pump, New Era Pump Systems Inc.) is used, the resolvable RI change of the mixed aqueous solution can be calculated to be 2.85×10^{-4}.

As shown in the bottom of **Figure 4.1**, the RI change of surrounding medium will induce a change of the coupling wavelength of the PSLPG via the evanescent interaction between core and cladding mode:

$$\lambda = \left[n_{eff}(\lambda) - n_{clad}^{i}(\lambda)\right]\Lambda \,, \tag{4.2.2}$$

where $n_{eff}(\lambda)$ and $n_{clad}^{i}(\lambda)$ are the effective RIs of core mode and LP_{0i} cladding mode at the wavelength λ, respectively, and Λ is the period of the PSLPG. Since $n_{clad}^{i}(\lambda)$ depends on the RI value of surrounding fluids, i.e. R_{mc}, the resonant wavelength λ of the LPG is blue-shifted when the flow rate ratio *v* is increased.

4.2.1 Fabrication of the Microfluidic Chip

The microfluidic chip used in our research was fabricated in poly-dimethylsiloxane (PDMS) based on the replica moulding and thermal crosslinking method. With an own-established optical maskless lithography platform, the replication master was made in epoxy resin SU-8 [143].

Figure 4.3(b)-(c) depict the spiral mixer and Y-shaped branch of the SU-8 master, which were characterized with a laser scanning confocal microscope (VK- X200, Keyence, Japan). One can see that the surface of SU-8 master is very uniform and smooth. To integrate fiber gratings, the channel of the SU-8 mater is higher than 150 μm. The width of Y-shaped branch is 153 μm for interposition of optical fibers, while the width of the microchannel inside the spiral mixer is 120 μm.

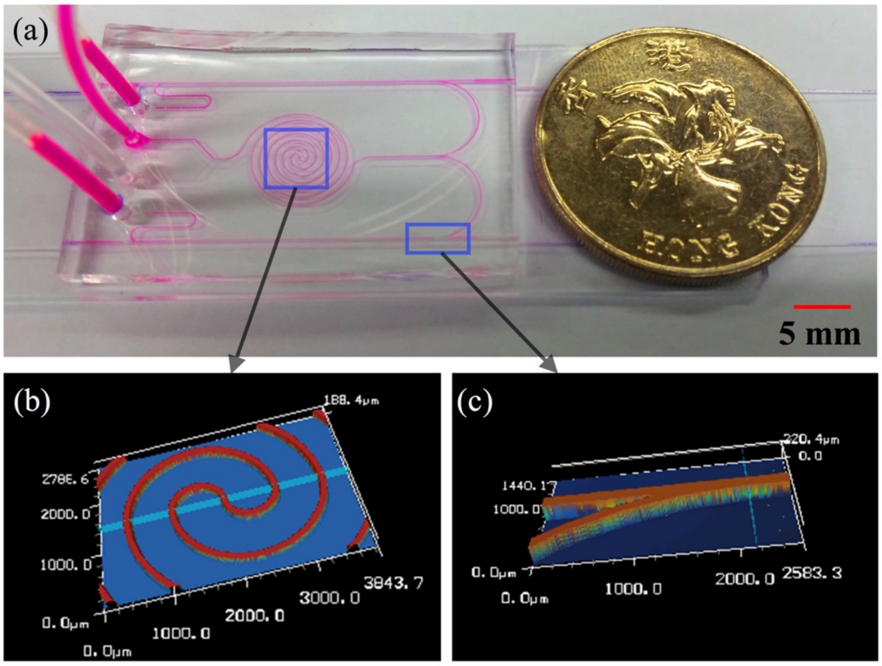

Figure 4.3 (a) Photo of the LPG-integrated microfluidic chip, and 3D topographic images of (b) the spiral mixer and (c) Y-shaped branch of the SU-8 master.

Later, a mixture of PDMS and crosslinker with a volume ratio of 10:1 was poured onto the SU-8 master and then thermally cured in an oven at

75°C for 1 hour. A solid PDMS slice was imprinted with a designed microchannel structure and then gently peeled off from the mould master. The inlets and outlets were drilled by using a hole puncher. Eventually, the PDMS slice was tightly bonded upon a clean glass substrate after treated with oxygen plasma for 3 minutes. As illustrated in **Figure 4.3**(a), the fabricated optofluidic chip consists of two inlets, two outlets, a spiral mixer and two throughout fiber gratings. Its miniature size can reduce the liquid consumption greatly, and the soft PDMS material can effectively protect LPGs from mechanical damage. To clearly show its micorfluidic networks, the chip was injected with solution of fluorescent dye Rhodamine 6G before taking the photo.

4.2.2 Characterization of the LPG Integrated Optofluidic Device

Based on a point-by-point fabrication technology, the used PSLPG (i.e. PSLPG-1) was fabricated in photosensitive SMF (PS1250/1500, Fibercore Ltd.) [132]. Its grating length and period are 30 mm and 427 μm, respectively. The optical spectrum of the PSLPG-1 immersed in DI water at 23°C is shown in **Figure 4.4**. The extinction ratio between the pass-band and the sideband dips is estimated to be around 17 dB. The corresponding central wavelength and 3-dB spectral width of its pass-band are measured as 1569.1 and 19.4 nm, respectively. The central wavelength of the pass-band decreases linearly proportionally with respect to the RI with the slope of 93.6 nm/RIU. Under the injection rate of 50 μL/s, the spectral response time of this optofluidic tunable device is estimated to be 0.1s, which is mainly determined by the time of fluids flowing from the microfluidic mixing point to the PSLPG filter. Note that the maximum injection rate is 53 μL/s limited by the syringe size and the maximum pressure endured by the sealed inlets.

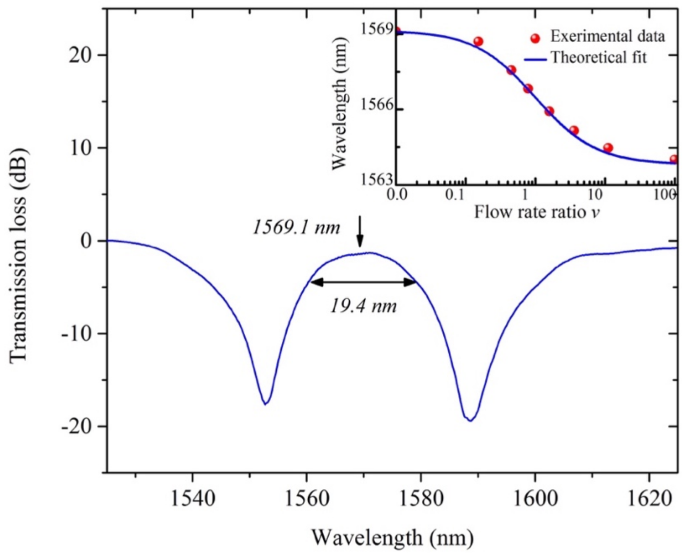

Figure 4.4 Measured optical spectrum of the PSLPG-1 filter. The inset depicts its central wavelengths as a function with the flow rate ratio.

4.3 Configuration of the Mode-Locked Fiber Laser

As illustrated in **Figure 4.5**, a tunable mode-locked fiber laser was then built by inserting the LPG-integrated microfluidic chip into the fiber oscillator. The insertion loss of the microfluidic LPG filter is around 0.5 dB.

A broadband gain was achieved by forward pumping a 1-m long EDF (Liekki Er80-4/125) with a 974-nm laser diode through a WDM. The peak absorption of EDF at 1530 nm is typically 80 dB/m and the MFD at 1550 nm is 6.5 μm. The small-signal gain of the EDFA is about 25 dB. Unidirectional operation of the laser is enabled by using an optical isolator, which is output from the 10% tap of a fiber coupler. To form a laser cavity with net anomalous dispersion, SMFs with length of 5 m is incorporated. A PC is used to adjust the cavity polarization state. An SA made in SWCNT/PVA film between two FC/APC fiber connectors is used as the mode locker. The non-staturable loss, modulation depth and saturation intensity of the SA are 95%, 5% and 11 MW/cm^2, respectively. The absorption loss of the incorporated SWCNT/PVA SA is 7 dB. The splicing losses between different fibers are negligible.

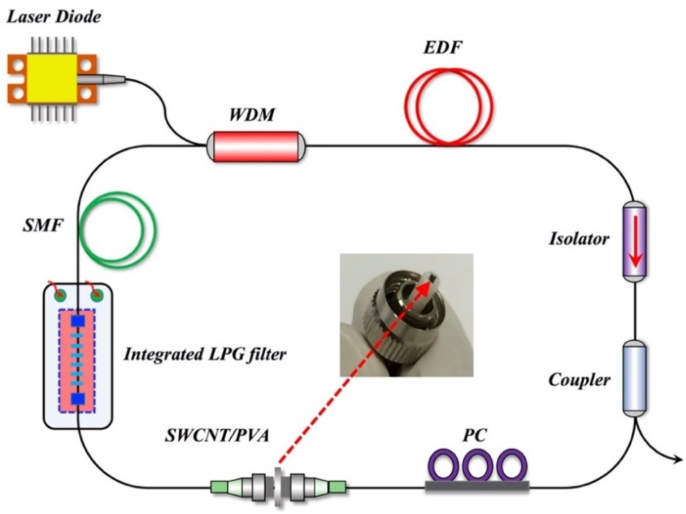

Figure 4.5 Experimental setup of the optofluidic tunable mode-locked fiber laser.

4.4 Experimental Results

4.4.1 Characterization of Emitted Solitons

Experimentally, the microfluidic chip was filled with DI water with injection rate of 50 μL/s. The PSLPG-1 was incorporated as an in-cavity tunable filter, stop bands at both sides of which prohibit lasing at undesirable wavelengths. Self-started mode locking was obtained under pump power higher than 43 mW. As plotted in **Figure 4.6**(a), typical emission spectrum of the mode-locked laser is obtained under pump power of 50 mW. Obvious Kelly sidebands indicate that the mode locking is working in the anomalous dispersion regime. As determined by the pass-band of PSLPG-1 and gain profile of the laser, the central wavelength is 1568.6 nm with 3-dB spectral width of 3.5 nm.

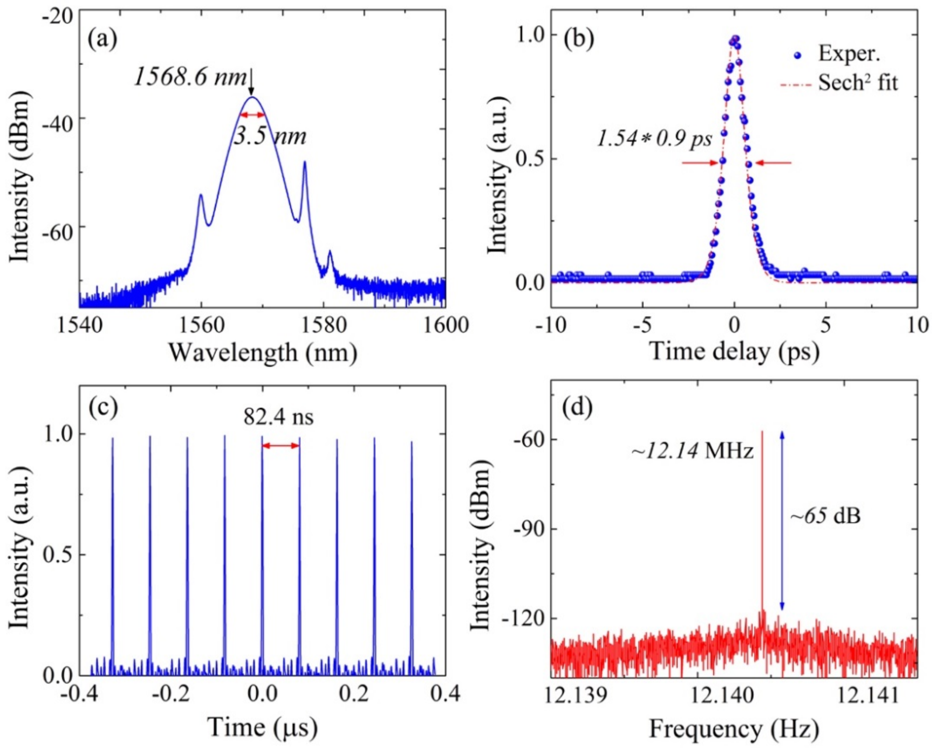

Figure 4.6 (a) Typical optical spectrum, (b) AC trace, (c) pulse train, and (d) RF spectrum of the tunable mode-locked fiber laser.

The mode-locked pulses are measured with an optical autocorrelator (Femtochrome, FR-103XL), a photodetector and an oscilloscope. When the $sech^2$ profile is assumed, the pulse duration is estimated as 0.9 ps, as shown in **Figure 4.6**(b). Thus, the calculated time-bandwidth product (TBP) of 0.38, indicating a slight chirp of the mode-locked pulses. As shown in **Figure 4.6**(c), the pulse-to-pulse separation is 82.4 ns, which is consistent with the pulse repetition rate of 12.14 MHz. The radio-frequency (RF) spectrum peak with an SNR of ~65 dB shows a stable mode locking operation state. The temperature of solutions was not significantly influenced by laser pulses.

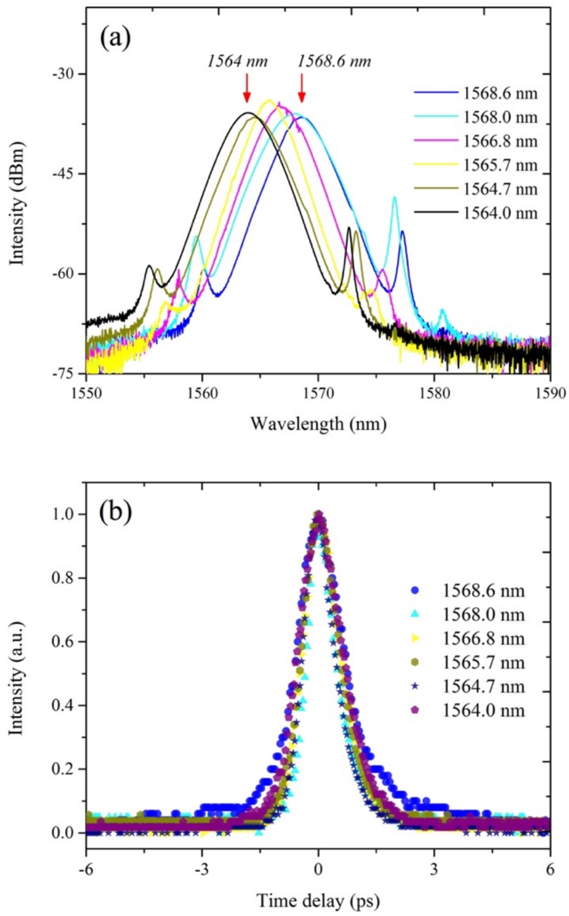

Figure 4.7 (a) Optical spectra and (b) AC traces of the tunable mode-locked fiber laser at different wavelengths.

4.4.2 Results of Wavelength Tuning

Under pump power of 50 mW and with PC fixed, the central wavelength of the mode-locked fiber laser was tuned continuously from 1568.6 to 1564 nm when the RI was adjusted from 1.333 to 1.39. The corresponding couples of flow rate ratio and RI are measured as (0, 1.333), (0.24, 1.344), (0.68, 1.356), (1.48, 1.367), (4.18, 1.379), and (100, 1.39), respectively. As shown in **Figure 4.7**(a), the sustained Kelly sidebands indicates that the mode locking state is maintained during the wavelength tuning. The spectral width of the mode-locked laser varies from 3.5 to 3.75 nm. **Figure 4.7**(b) shows the corresponding AC traces. The pulse duration changes between 0.74 and 1 ps, meaning the TBP of the emitted solitons always close to the transform limit. Owing to the unflatten gain spectrum of the fiber laser, both the lasing threshold and the peak intensity slightly changed at different wavelengths.

4.4.3 Observations of Bound Solitons

Moreover, stable bound solitons were observed when the state of PC was appropriately optimized. Typical optical spectrum of a tightly bounded soliton pair is depicted in **Figure 4.8**(a) Different from the normal spectrum of **Figure 4.6**(a), a modulation fringe occurs on the spectrum, modulation period (i.e. separation between two adjacent peaks) of which is measured as ~2.5 nm. A π phase difference between the two bounded solitons is verified by the symmetrical spectral profile [137]. As plotted in **Figure 4.8**(c), three peaks of the AC trace with intensity ratio of 1:2:1 reveal that the two bounded solitons share the same intensity and pulse duration. Consistent with the spectral modulation period, the soliton-to-soliton separation is measured as 2.92 ps. Under RI of 1.34, another loosely bounded soliton pair was established, as shown in **Figure 4.8**(b) and (d). Since the soliton separation is extended to 11.2 ps, the corresponding spectral modulation period is decreased to ~0.71 nm. Because a bound state results from a balance between various kinds of repulsive and attractive forces induced by nonlinear and dispersion effects, it is natural that a variation of these forces caused by a change of intra-cavity gain and loss will force a new balance. In a net-anomalous-dispersion cavity, XPM between two bounded solitons is a main factor causing an attraction force, which is balanced by the repulsive force induced by the dispersion effect [145]. As the cavity loss at the RI of 1.34 is higher than that at 1.333, the smaller attraction force caused by the weaker XPM effect results in a larger pulse separation as shown in **Figure 4.8**(c) and (d).

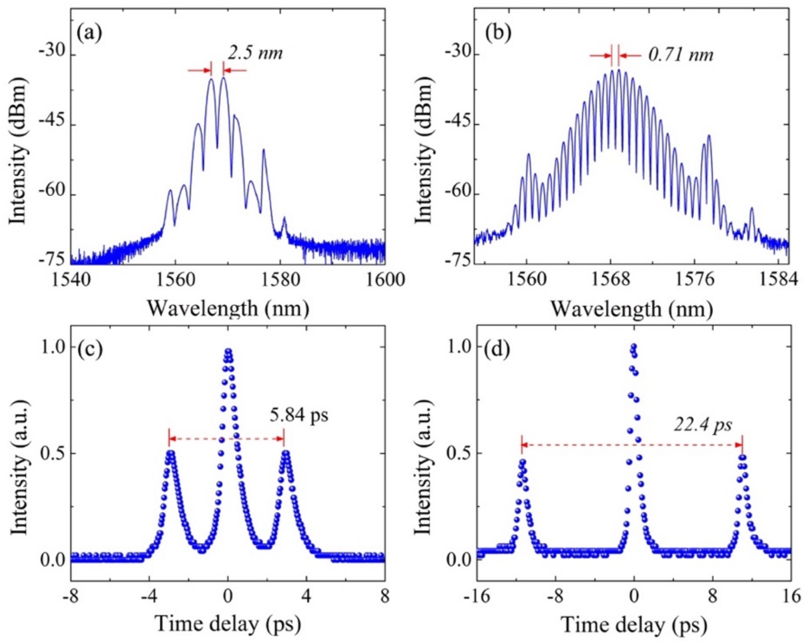

Figure 4.8 Measured optical spectra and AC traces of bound solitons with the RI of ~1.333 ((a) and (c)) and ~1.34 ((b) and (d)).

4.4.4 Extension of Tuning Range

To demonstrate the broad tunability of the proposed optofluidic technology, another PSLPG filter (i.e. PSLPG-2) with different central wavelength was used in the fiber oscillator. The grating period and length are measured as 428 μm and 34 mm for PSLPG-2, respectively. As shown in **Figure 4.9**, the pass-band of PSLPG-2 has a different central wavelength and spectral width of 1576.2 and 12.6 nm, respectively, and its RI sensitivity is measured to be 93.4 nm/RIU.

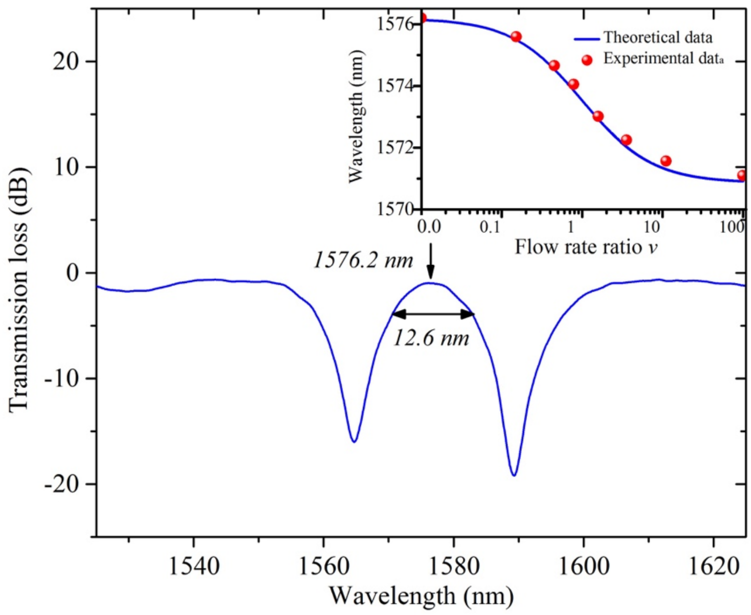

Figure 4.9 Measured optical spectrum of the PSLPG-2 filter. Its central wavelengths as a function of the flow rate ratio are plotted in the inset.

When the same pump power of 50 mW was used, self-started mode locking was obtained with the PSLPG-2 filter. With the flow rate ratio *v* increased from 0 to 100, the central wavelength of the mode-locked fiber laser is continuously tuned from 1576 nm to 1570 nm as shown in **Figure 4.10**(a). The Kelly sidebands was observed to disappear owing to the narrow pass-band of the PSLPG-2 filter. It is noteworthy that the leftmost spectral humps are induced by the unsuppressed ASE of the laser.

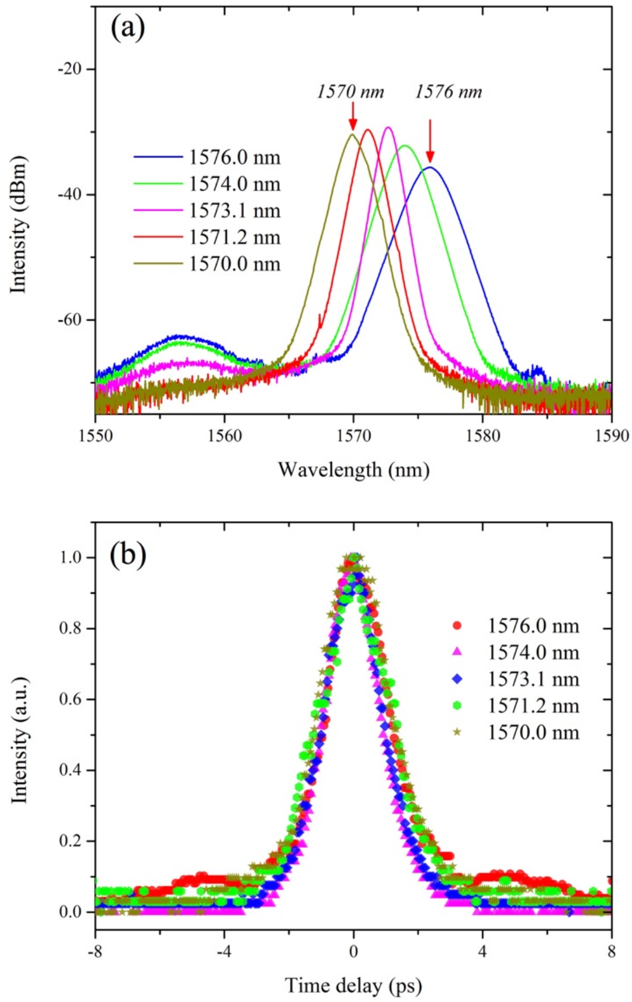

Figure 4.10 (a) Measured spectra and (b) AC traces of the mode-locked fiber laser at different wavelengths with the PSLPG-2 filter.

The corresponding AC traces at different wavelengths are also depicted in **Figure 4.10**(b). The pedestals of the AC trace at 1576 nm are attributed to the unsuppressed CW noise of the pulses. The pulse duration varies between 1 and 2.32 ps, which on average is broader than that of the mode-locked laser with PSLPG-1. In principle, a potential broader range of wavelength tuning can be obtained if multiple PSLPG filters are integrated into the microfluidic chip.

4.5 Discussions

Compared with the thermal tuning method in the previous chapter [134], this proposed optofluidic tuning technology shows an even higher wavelength-tuning accuracy. The possible RI change of the mixed aqueous solution even reaches to 2.14×10^{-5}, when a finer microfluidic pump with a high flow rate accuracy of 0.15% (e.g. using ELVEFLOW OB1-MK3, Elvesys Company) is utilized for controlling the microfludic flows. Under the measured RI sensitivity of the LPG filter of 93.6 nm/RIU, the potential wavelength-tuning accuracy of the optofluidic technology is estimated as high as 2.0 pm, which is significantly higher than the previous result with a commercial TBF. In comparison, the temperature-tuning accuracy of the packaged bulky LPG filter is assumed as 0.1°C, the typical wavelength-tuning accuracy of the thermally-tuned LPG filter is 72 pm.

Furthermore, the optofluidic tunable filter exhibits more advantages including high configurability. For instance, three or more solutions can be mixed with more microchannels for extending the tuning range or augmenting tunable parameters of the filter; absorptive solutions can also be applied to adjust its absorptance and thus the pass-band simultaneously.

4.6 Summary

In summary, a novel tunable mode-locking technology based on an LPG-integrated microfluidic chip has been demonstrated. The proposed optofluidic tunable filter facilitates ultrafine tuning of its central wavelength through precisely adjusting the microfluidic flows, resulting in tunable mode-locked fiber lasers from 1568.6 to 1564 nm and 1576 to 1570 nm, respectively. In the experiment, bound solitons with different pulse separations have also been demonstrated. Such an optofluidic tunable mode-locking technique with both ultrafine wavelength tuning capability and flexible configurability provides a promising way for advancing ultrafast fiber laser technology for both scientific and industrial applications.

Chapter 5.

High-Energy Soliton Fiber Lasers Using a CFBG Pair

In this chapter, a high-energy soliton mode-locked fiber laser with a CFBG pair is presented. To increase the net-cavity anomalous dispersion greatly, the CFBG pair with central wavelength of ~1560 nm is inserted into the fiber oscillator. An SWCNT/PVA SA is used and serves as an efficient mode locker. Stable mode-locked pulses are achieved with typical pulse duration of 8.05 ps. The soliton energy of 0.21 nJ is obtained and no soliton splitting is observed. Additionally, numerical simulations are conducted to study the formation of high-energy solitons in the mode-locked fiber laser.

5.1 Introduction

Without additional dispersion compensation, mode-locked erbium fiber lasers normally operate in the anomalous dispersion regime. In this regime, optical solitons can be formed owing to the balanced interplay between dispersion and nonlinearity in SMFs [146]. Consequently, the pulse energy of soliton is limited to less than 0.1 nJ because of the soliton area theorem. In order to break the limitation, various dispersion management methods have been proposed, including in-cavity dispersion stretching [147], similariton [23] and all-normal dispersion (ANDi) [148]. Owing to the balanced interaction among dispersion and nonlinearity, and gain and loss, large-energy dissipative solitons can be obtained in these new regimes. However, critical dispersion management and suitable spectral filtering are required in such laser cavities.

By contrast with dissipative soliton, conventional soliton can be easily established, whose pulse energy scales with the net-cavity dispersion of the mode-locked laser. To increase the net-cavity dispersion largely, long cavity mode-locked fiber lasers have been demonstrated by inserting kilometers of SMFs [149], [150]. However, the repetition rate of the mode-locked pulses was decreased greatly owing to long cavity lengths. One of promising solutions is to use the CFBG technology. By optimizing the parameters of chirp and apodization, CFBG enables to provide flexible and ripples-free GVD [151]. In addition, CFBG can be used for in-cavity spectral filtering. For instance, multi-wavelength and wavelength-tunable mode-locked fiber lasers have been demonstrated by incorporating CFBGs [117], [129], [152].

In this chapter, a high-energy mode-locked fiber laser is obtained by using a specially-designed CFBG pair. By using a Talbot interferometer, the CFBGs used in our research show large GVD and broadband reflection band. High-energy conventional solitons are demonstrated with typical pulse duration of 8.05 ps and pulse energy of 0.21 nJ, respectively. Additionally, the formation of high-energy solitons in the fiber oscillator is theoretically investigated.

5.2 Fabrication and Characterization of CFBG

5.2.1 Fabrication of CFBG

Normally, CFBG can be fabricated by using the phase mask technique and an excimer laser. However, the wavelength of CFBG is fixed by the phase mask. To provide CFBG with versatile wavelength, a Talbot interferometer together with a pulsed 213-nm solid state laser were used in our research. Particularly, the 213-nm pulsed laser exhibits excellent spatial coherence and grating inscription efficiency.

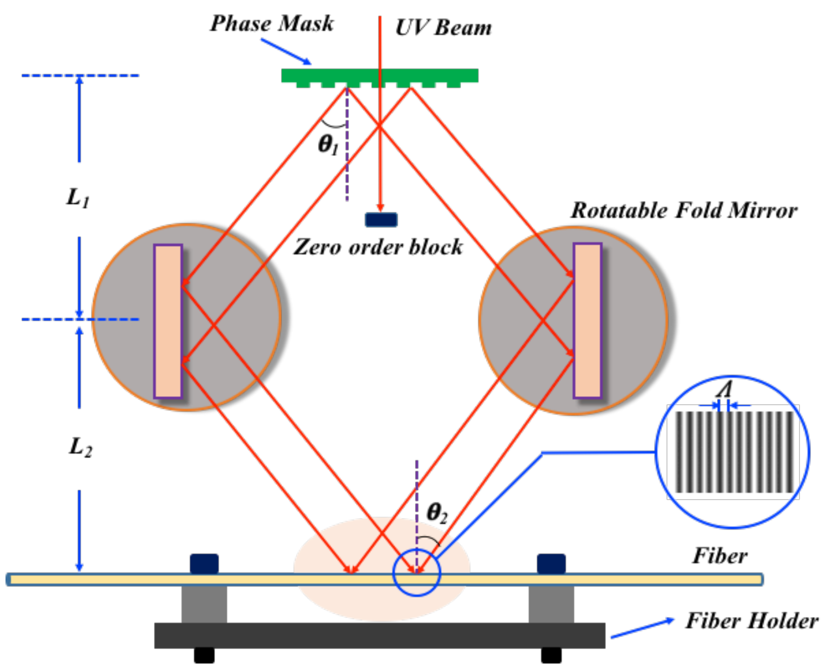

Figure 5.1 Schematic diagram of the Talbot interferometer.

Figure 5.1 shows the schematic diagram of the Talbot interferometer.

A circular UV beam (λ_{uv}~213 nm) with diameter of ~1 mm is normally incident on the phase mask and splits into two ±1 order diffractive beams, which intersect and interfere at the well-aligned optical fiber. A metal block is inserted to block the zero-order beam from the optical fiber. Based on the optical path condition, the Bragg wavelength of CFBG is expressed as,

$$\lambda_B = \frac{n_{eff}\lambda_{uv}}{2sin\left(\frac{\theta_2}{2}\right)}, \tag{5.2.1}$$

Where λ_B is the Bragg wavelength, n_{eff} is the effective RI of optical fiber and θ_2 is convergent angle of the two intersected beams. Thus, the Bragg wavelength of CFBG can be flexibly selected by precisely tuning the angle θ_2 with only one common phase mask.

In our research, the used phase mask is with central period and chirp rate of 730 nm and 2.8 nm/cm, respectively. Furthermore, CFBG was apodized in a Gaussian profile by scanning the UV beam spot. In order to obtain high reflectivity, the CFBG was inscribed in a photosensitive fiber preciously loaded in H_2 gas with pressure of 15 bar for two weeks.

5.2.2 Characterization of CFBG

As shown in **Figure 5.2**, the fabricated CFBG is centered at ~1560 nm with a high reflectivity of ~99%. The 3-dB bandwidth of its reflection band is measured to be ~4 nm. Additionally, the time delay curve was numerically calculated based on the transfer matrix method (TMM). It can be observed that interference ripples in the time delay curve are effectively suppressed with the Gaussian apodization. The GVD parameter is then calculated to be ~5 ps/nm.

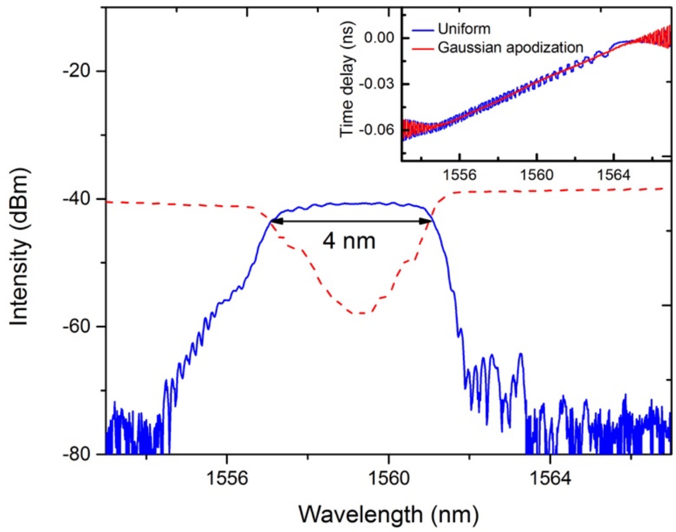

Figure 5.2 Measured reflection (blue curve) and transmission (red dash curve) spectrum of the fabricated CFBG. The inset shows the time delay characteristics of uniform and Gaussian apodized CFBG.

5.3 High-Energy Soliton Mode-Locked Fiber Lasers

5.3.1 Configuration of Laser

Figure 5.3 illustrates the configuration of the mode-locked erbium fiber laser incorporating a CFBG pair. A 1-m-long high-concentration EDF (Liekki Er80-4/125) is forward pumped by using a 974-nm laser diode. Laser emission is tapped from the 10% port of a fused fiber coupler. A piece of PC is used to adjust the cavity polarization state. A small piece of home-made SWCNT/PVA film is sandwiched between two FC/APC fiber connectors and used as an in-fiber mode locker.

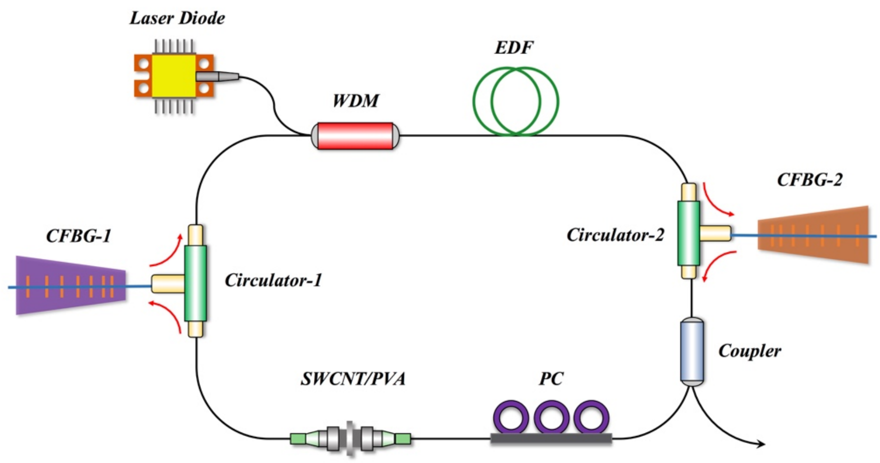

Figure 5.3 Schematic diagram of the mode-locked fiber laser.

5.3.2 Experimental Results

1) Laser without the CFBG pair

In the first stage, No CFBG was used in the laser cavity. Under pump power of higher than 40 mW, self-starting mode locking state was observed. With pump power of 65 mW, typical mode-locked spectrum and pulse trace were measured as shown in **Figure 5.4**. The central wavelength of the mode-locked pulse is 1565 nm and the 3-dB spectral width is ~5.39 nm. Spectral Kelly sidebands indicate that mode locking operation is in the anomalous dispersion regime. The mode-locked pulses were measured by using an optical autocorrelator (FR-103XL, Femtochrome Inc.) together with an oscilloscope. When a sech^2 profile is assumed, the pulse duration is

~220 fs. The corresponding pulse-to-pulse separation is measured to be 62 ns and the repetition rate is 16.1 MHz.

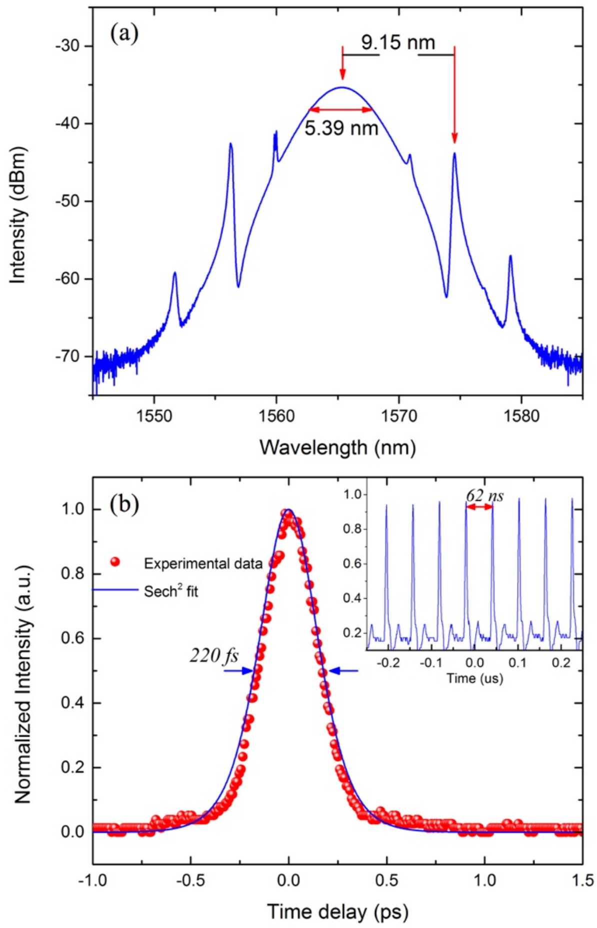

Figure 5.4 (a) Optical spectrum and (b) temporal traces of the mode-locked fiber laser.

2) Laser incorporating the CFBG pair

In the second stage, CFBG-1 was incorporated into the laser cavity (i.e. cavity-1) via a circulator. The net-cavity dispersion was then significantly increased to ~-8 ps^2. Under pump power of higher than ~46 mW, the mode locking was self-started. Under pump power of 88 mW, the mode-locked pulses are characterized as shown in **Figure 5.5**. Distinct Kelly sidebands of the laser spectrum prove mode locking in the anomalous dispersion regime. The reflection spectrum of CFBG-1 is also plotted as a reference. One can see that the reflection band of CFBG-1 wholly cover the laser spectrum, showing a weak spectral filtering effect on the mode-locked pulses. The 3-dB bandwidth of the laser spectrum is ~0.5 nm.

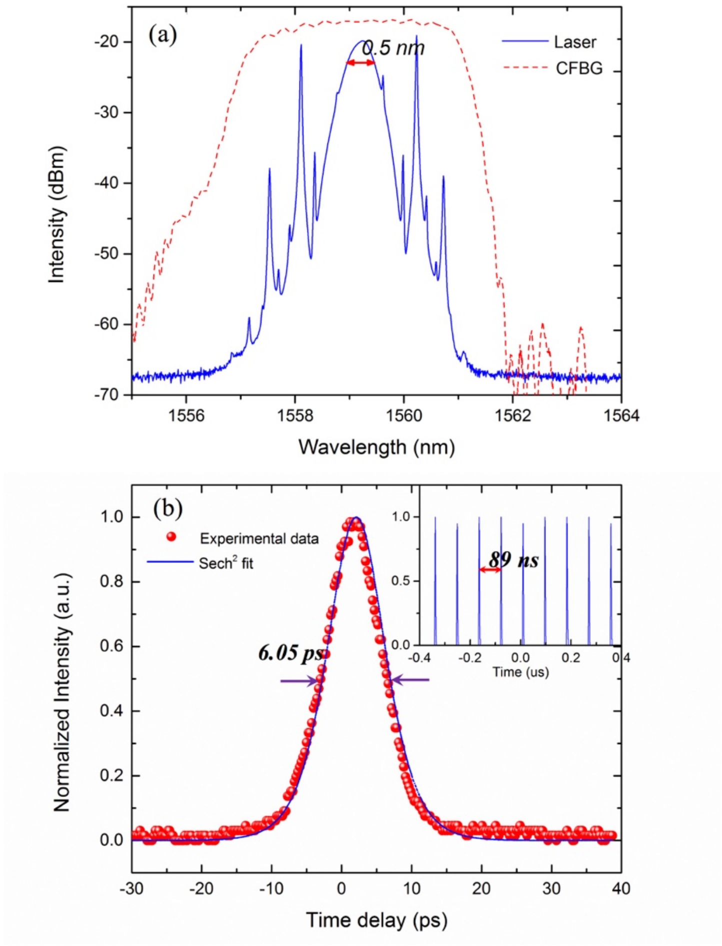

Figure 5.5 (a) Measured spectra and (b) temporal traces of the mode-locked laser with CFBG-1.

The emitted pulses were then measured with an optical autocorrelator together with an oscilloscope. When a $sech^2$ profile is assumed, the pulse duration is estimated as 6.05 ps. The TBP of the mode-locked pulses is calculated to be ~0.37, slightly larger than the transform limit (i.e. 0.315 for a $sech^2$ profile). The pulse-to-pulse separation is 89 ns, consistent with the repetition rate of 11.2 MHz. By increasing pump power, high-energy pulses are obtained with maximum pulse energy of 0.17 nJ.

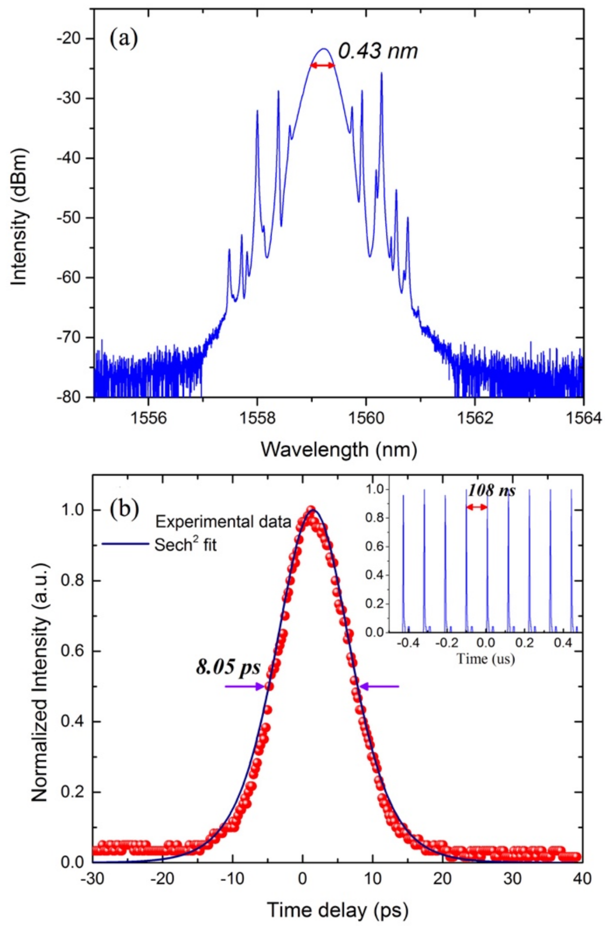

Figure 5.6 (a) Measured optical spectrum and (b) temporal traces of the mode-locked laser with a CFBG pair.

Eventually, the net-cavity dispersion was increase further to ~-16 ps^2

by using a CFBG pair. The threshold pump power of mode locking was increased slightly due to the additional insertion loss of two CFBGs. Under pump power of ~113 mW, the mode-locked pulses are characterized with 3-dB spectral width of ~0.43 nm and pulse duration of 8.05 ps, respectively, as shown in **Figure 5.6**. The TBP is calculated to be 0.47. Owing to the larger net-cavity dispersion, broader mode-locked pulses are formed in the fiber oscillator with the CFBG pair. The pulse-to-pulse separation is ~108 ns consistent with a longer cavity length. The maximum pulse energy is obtained at ~0.21 nJ. Clearly, the higher pulse energy can be obtained with a larger net-cavity dispersion. Additionally, AC traces of the mode-locked pulses under different pump powers are plotted in **Figure 5.7**. The pulse duration is increased with respect to pump power. The pulse duration is measured to be 6.36, 6.83 and 8.05 ps with pump power of 83, 89 and 113 mW, respectively.

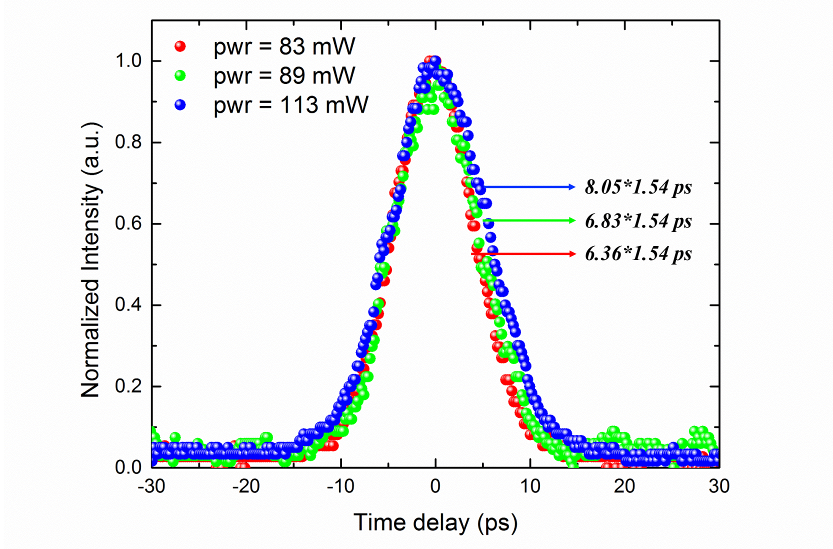

Figure 5.7 AC traces of the mode-locked laser at different pump powers.

5.4 Numerical Simulations

Moreover, the formation of high-energy conventional solitons in the fiber oscillator was theoretically studied based on the split-step Fourier method (SSFM). **Figure 5.8** shows the propagating process of the mode-locked pulse in the laser cavity. In general, the nonlinear propagation of an optical pulse in the optical fibers is described by,

$$\frac{\partial A}{\partial z} + \mathrm{i}\frac{\beta_2}{2}\frac{\partial^2 A}{\partial t^2} = \frac{g}{2}A + \mathrm{i}\gamma|A|^2 A + \frac{g}{2\Omega_g^2}\frac{\partial^2 A}{\partial t^2}, \qquad (5.4.1)$$

where A is the slowly varying envelope of an optical pulse, t and z are the propagation time and distance, respectively, β_2 and γ are the second-order dispersion and Kerr nonlinearity of optical fibers, Ω_g is the effective gain bandwidth, $g = g_0\exp(-E_p/E_s)$ relates to the gain saturation of EDF, where g_0,

E_p, and E_s are the small-signal gain, pulse energy and gain saturation energy, respectively. The above equation was numerically calculated based on the symmetric SSFM. The SWCNT/PVA SA is mathematically described based on a two-level saturable absorption model as,

$$\alpha(I) = \alpha_{ns} + \alpha_0/(1 + I/I_{sat}), \tag{5.4.2}$$

where α_0, α_{ns} and I_{sat} are the modulation depth, nonsaturable loss and saturable absorption intensity, respectively. To approximate the experimental parameters, g_0 = 30 dB/m, Ω_g = 25 nm, γ = 2.69 $W^{-1}km^{-1}$, β_2 = 33.65 ps^2/km for the EDF, and γ = 1.06 $W^{-1}km^{-1}$, β_2 = -22 ps^2/km for other passive SMFs. The effect of CFBG on the mode-locked pulse is expressed in frequency domain as,

$$A_{out}(\omega) = A_{in}(\omega) * R(\omega) * exp(i\beta_2\omega^2/2), \tag{5.4.3}$$

where $R(\omega)$ is the amplitude function of reflective spectrum, and β_2 = -8ps^2 for each CFBG.

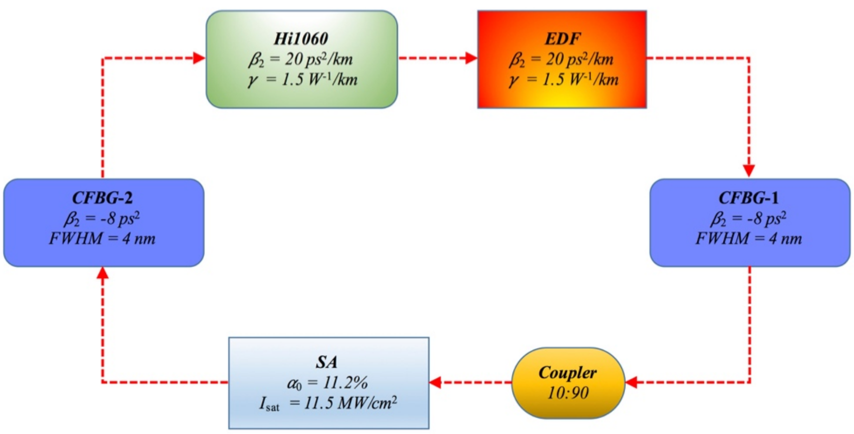

Figure 5.8 Flow chart of numerical simulation in the cavity-2.

A self-consistent solution was obtained after thousands of computation roundtrips for each fiber laser cavity. The calculated spectra and AC traces of the soliton solutions are plotted in **Figure 5.9**. In the mode-locked laser with CFBG-1, the spectral width and pulse duration are 0.51 nm and 6.15 ps, respectively. By contrast, they change to 0.38 nm and 8.1 ps in the fiber oscillator with a CFBG pair, respectively. The calculated instantaneous frequency curves more chirped pulses are obtained with a larger net-cavity dispersion. Clearly, the simulation results are well consistent with the experimental observations.

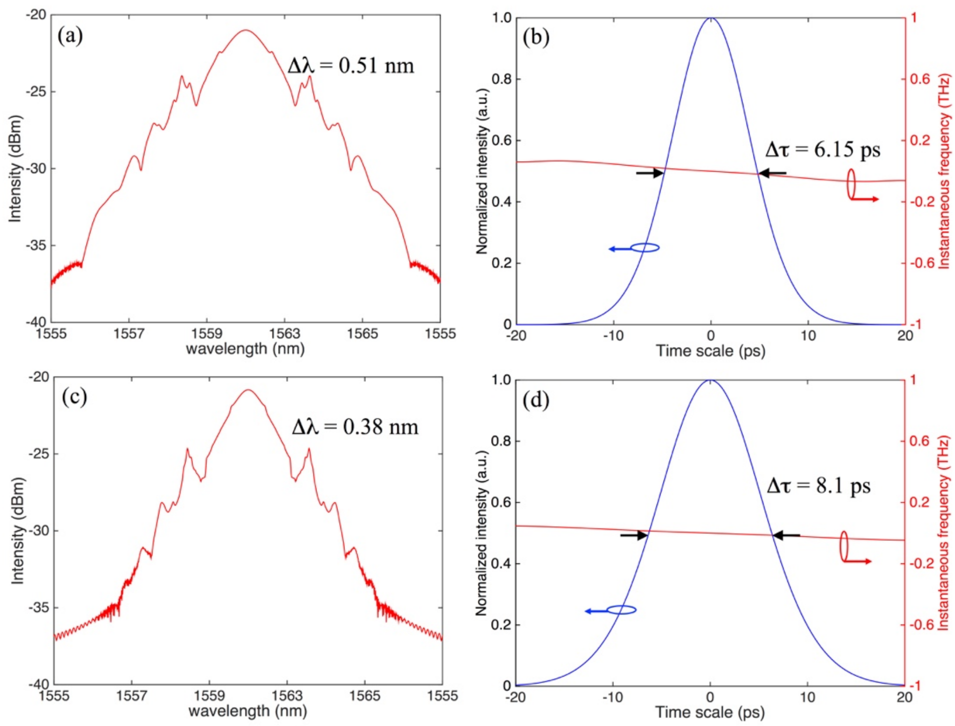

Figure 5.9 Calculated spectra, pulse profiles and instantaneous frequency curves of the mode-locked laser with ((a) and (b)) CFBG-1 and ((c) and (d)) a CFBG pair.

Moreover, the in-cavity propagating evolutions of the mode-locked pulses are illustrated in **Figure 5.10**. One can see that the large insertion loss of the SA is balanced with the high gain of the EDF. As shown in **Figure 5.10**(a), the dispersion effect and SPM experienced by solitons in SMFs are balanced. Moreover, the nonlinear pulse compression caused by the SWCNT SA is cancelled by the dispersion effect induced by the CFBG. As shown in **Figure 5.10**(c) and (d), the mode-locked pulse evolves as like “breathe” in the fiber oscillator. After stretched by the CFBG pair, the broad pulse varies very slightly in the subsequent SMFs, avoiding over accumulation of nonlinear phase and thus soliton splitting. However, the spectral width of the mode-locked pulse remains unchanged, indicating weak filtering effect of the CFBG pair.

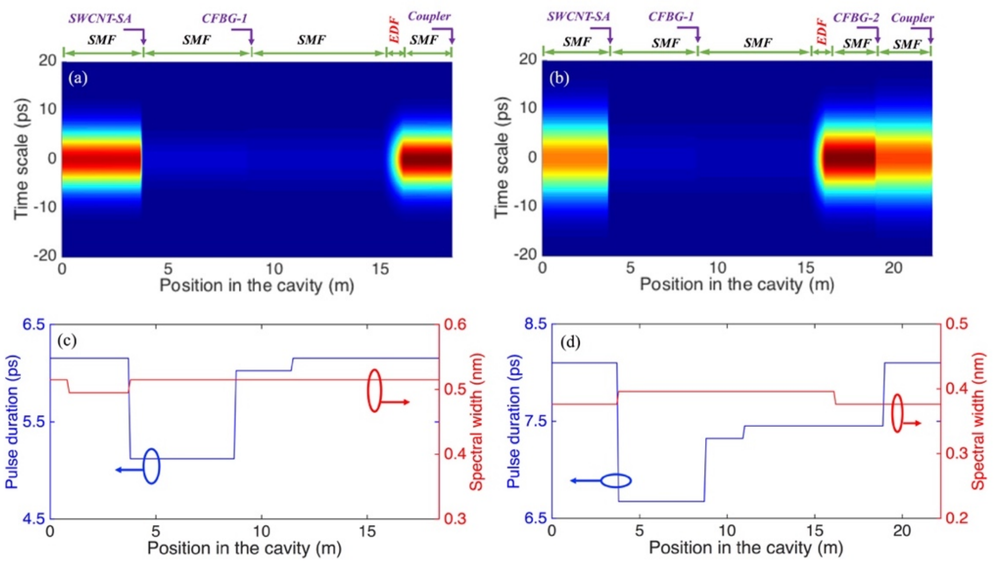

Figure 5.10 In-cavity propagating evolutions of the mode-locked laser with ((a) and (c)) CFBG-1 and ((b) and (d)) the CFBG pair.

5.5 Summary

In summary, a high-energy soliton mode-locked fiber laser incorporating with a CFBG pair has been demonstrated. The net-cavity dispersion is increased greatly by incorporating the CFBG pair. Stable mode-locked conventional solitons have been achieved with typical pulse duration of ~8.05 ps. The maximum pulse energy is 0.2 nJ without soliton splitting, which is higher than the pulse energy obtained in standard SMFs (that is limited by the soliton area theorem). Moreover, the formation of the high-energy solitons free of breaking has been numerically investigated. Such a high-energy soliton fiber laser provides a promising pulsed laser seed for high-power fiber amplifiers and industrial applications.

Chapter 6.

Tunable Vector and Scalar Solitons Based on CFBGs

In this chapter, tunable vector and scalar soliton fiber lasers using CFBG filters are presented. On one hand, polarization-locked vector solitons are obtained from a non-PM mode-locked fiber laser, where a CFBG centered at 1610 nm is incorporated to serve as an all-fiber tunable spectral filter. By adjusting the CFBG, the central wavelength of vector solitons is tuned from 1606.8 to 1613.3 nm continuously. Additionally, the polarization-resolved spectra of the vector solitons are investigated by numerical simulations. On the other hand, linearly polarized scalar solitons are achieved in a PM mode-locked fiber laser. By adjusting the CFBGs at 1530 and 1560 nm, the central wavelength of scalar solitons can be continuously tuned from 1530 to 1537.7 nm and 1556 to 1561 nm, respectively.

6.1 Introduction

With the balanced interaction between the dispersion and nonlinearity of optical fibers, and the in-cavity gain and loss, solitons can be formed in a mode-locked fiber laser. In general, the complex GLE is used to describe the nonlinear propagation of soliton in a fiber laser. Furthermore, vector solitons consisting of two orthogonal polarization components can be established owing to fiber birefringence. For instance, various types of vector solitons have been reported, such as group-velocity-locked solitons [153], polarization-rotating solitons [43], [154] and polarization-locked solitons [40], [155].

To obtain stable vector solitons, a laser cavity without polarization discrimination is required [28]. Otherwise, the coherence between two orthogonal polarization parts could be broken. Normally, an SWCNT/PVA absorber is with polarization-insensitive absorption, which has been widely used to generate vector solitons. To the best of our knowledge, however, there exist few reports on wavelength-tunable vector solitons, which find important applications in soliton telecommunications.

On the other hand, linearly polarized scalar solitons are formed instead in a PM mode-locked fiber laser, which show excellent polarization and environmental stabilities [91], [156]. However, the emission wavelengths of reported scalar solitons are not tunable for some practical applications. In order to realize wavelength tuning, a TBF is always incorporated into a PM mode-locked fiber laser. However, large insertion loss would be introduced by the used free-space coupled PM-TBF [157]. A promising all-fiber solution to intra-cavity filtering is based on fiber grating technique. Among various fiber gratings, CFBG is of much interest because of its inherent advantages, including all-fiber format, low insertion loss and potentially low cost. For instance, wavelength-tunable and multi-wavelength mode-locked fiber lasers have been demonstrated based on CFBG filters [117], [129]. A PM-CFBG has also been used as a non-tunable spectral reflector in a linear-cavity ytterbium fiber laser [158]. Nevertheless, there exist few reported works on using CFBGs in all-fiber tunable PM mode-locked lasers till now, which are valuable for various polarization-sensitive applications.

In our study, we comprehensively investigate tunable vector and scalar solitons based on CFBGs. An all-fiber tunable spectral filter is constructed by mounting the CFBG onto a plastic cantilever. By mechanically adjusting the cantilever, the CFBG's reflection spectrum can be continuously tuned. In a non-PM mode-locked fiber laser, a Bismuth-based EDF (Bi-EDF) is used to provide gain at 1610 nm, emitting tunable L-band vector solitons. While in a PM mode-locked fiber laser, CFBGs centered at 1530 and 1560 nm are incorporated to obtain tunable linearly-polarized scalar solitons at C band, respectively.

6.2 Tunable Vector Solitons

6.2.1 Configuration of the Laser for Vector Solitons

Figure 6.1 shows the experimental setup of the tunable mode-locked fiber laser generating vector solitons. A 101.3-cm-long Bi-EDF with Er^{3+} doping concentration of 6500 ppm/wt is forward pumped with a Raman laser at 1475 nm. Laser output is tapped from the 10% port of a fiber coupler, which is then resolved in polarization by using a PC together with an inline PBS. Another PC is used to adjust the cavity polarization state. A fiber isolator is inserted to force unidirectional operation of laser. An SWCNT/PVA film is sandwiched between two FC/APC fiber connectors and serves as the in-fiber mode locker. The normalized non-saturable loss, modulation depth, and saturable intensity of the SA are 95%, 5% and 11MW/cm^2, respectively.

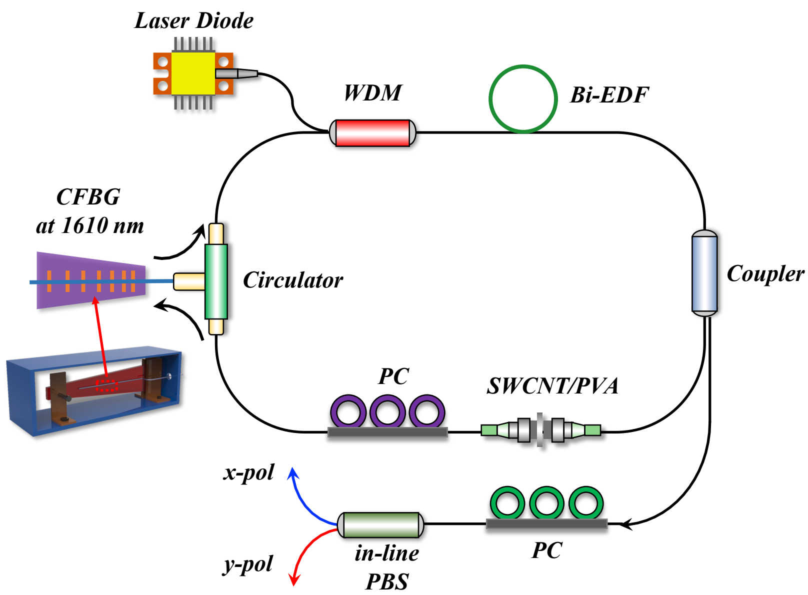

Figure 6.1 Setup of the tunable mode-locked fiber laser generating L-band vector solitons.

In order to obtain wavelength tuning, a home-made CFBG centered at ~1610 nm is inserted into the laser cavity through a non-PM fiber circulator.

The CFBG was fabricated by using the same method described in the previous chapter. As shown in **Figure 6.2**(a), the CFBG is fixed onto one surface of a left-angled triangle cantilever beam with length L = 20 cm, width w = 3 cm, and thickness of 0.5 cm, respectively. Based on the elongation and photoelastic effects, the central wavelength of the CFBG is shifted by translating the screw is along the direction of x-axis. Because the lateral stress on the CFBG is so weak, the induced relatively low birefringence does not significantly change the laser polarization, which is favorable for tunable vector solitons. Note that the chirp of CFBG keeps unchanged during the tuning of the plastic cantilever.

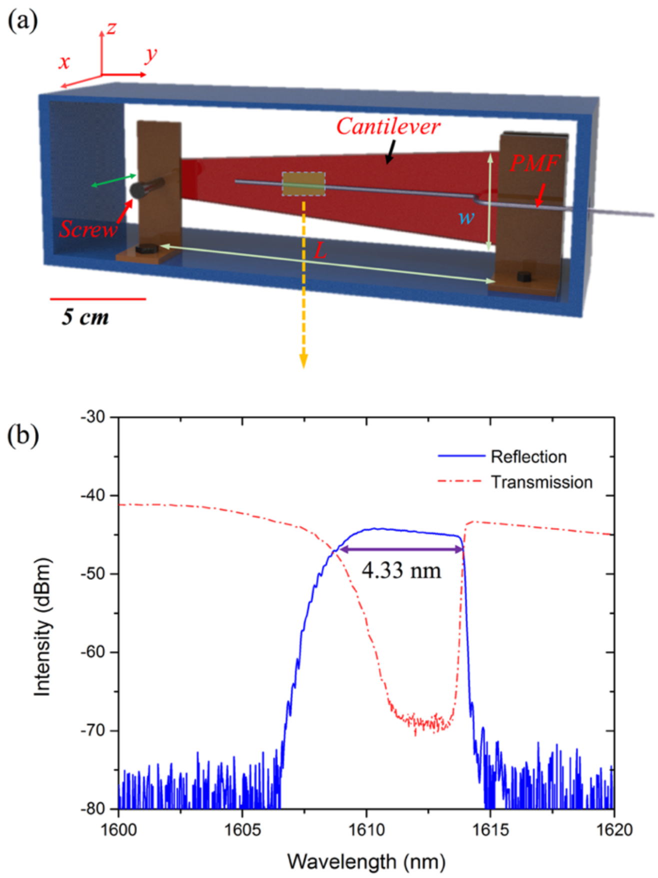

Figure 6.2 (a) Configuration of the cantilever beam and (b) measured optical spectra of the CFBG.

Measured optical spectra of the CFBG are shown in **Figure 6.2**(b), where one can see that the top of reflection band is flat and smooth without apparent interference ripples. The central wavelength and 3-dB spectral width are measured ~1612 and ~4.33 nm, respectively. In addition, its reflectivity is estimated as high as ~99.7%. Based on the chirp rate and length of the CFBG, its GVD is also calculated to be ~5 ps/nm.

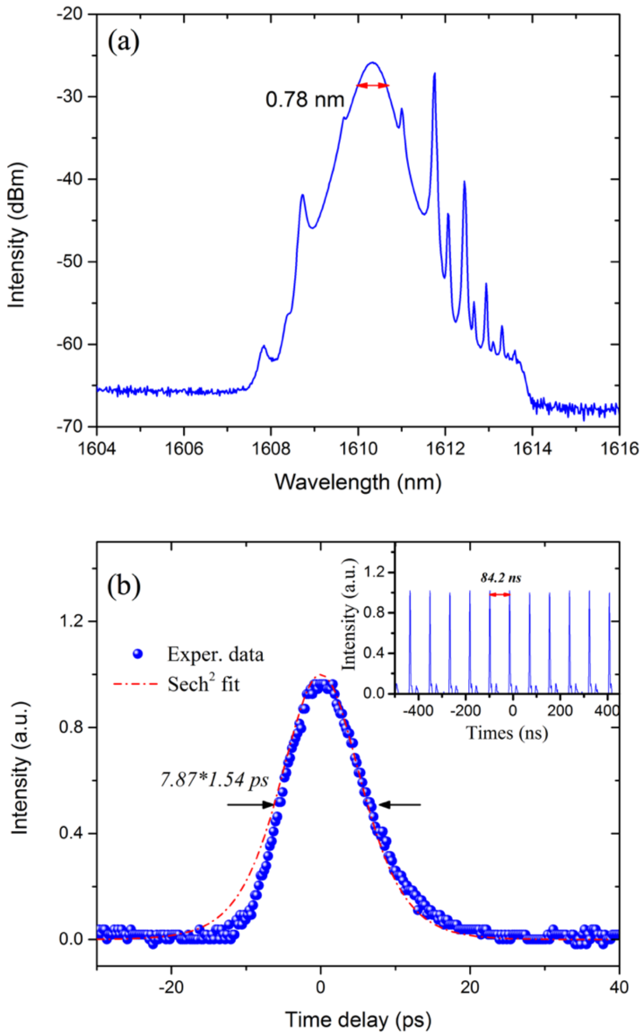

Figure 6.3 (a) Optical spectrum and (b) AC and oscilloscope traces of the L-band vector solitons.

6.2.2 Characterization of Tunable Vector Solitons

The laser transited from continuous wave operation to mode locking state under pump power of higher than 165 mW. With pump power of 197 mW, the mode-locked laser was characterized as shown in **Figure 6.3**. The central wavelength and 3-dB bandwidth of the laser spectrum are ~1610 nm and 0.78 nm, respectively. The pulse-to-pulse separation is measured to be 84.2 ns, corresponding to a repetition rate of 11.87 MHz. With the assumption of a sech^2 profile, the pulse duration is estimated to be 7.87 ps.

To investigate the polarization property of the emitted solitons, a PC together with an in-line PBS are utilized as shown in **Figure 6.1**. The extra-cavity PC was carefully adjusted till the long axis of the polarization ellipse was aligned with *x*-polarization axis (i.e. 0° axis) of the PBS. The polarization-resolved spectrum and pulse train of solitons are examined as shown in **Figure 6.4**. Clearly, the soliton spectra along the 0° and 90° axes show different profiles. Apart from the Kelly sidebands, there exist other spectral sidebands, which are attributed to the FWM interaction between the two orthogonal polarization modes. The oscilloscope traces along the 0° and 90° axes are plotted in **Figure 6.4**(b). The equal intensity of the polarization-resolved oscilloscope trace indicates the polarization phase at two exes is locked at every roundtrip. In addition, the pulse intensity on 90° axis is ~0.15 time lower than that on 0° axis, confirming that the obtained vector solitons are elliptically polarized.

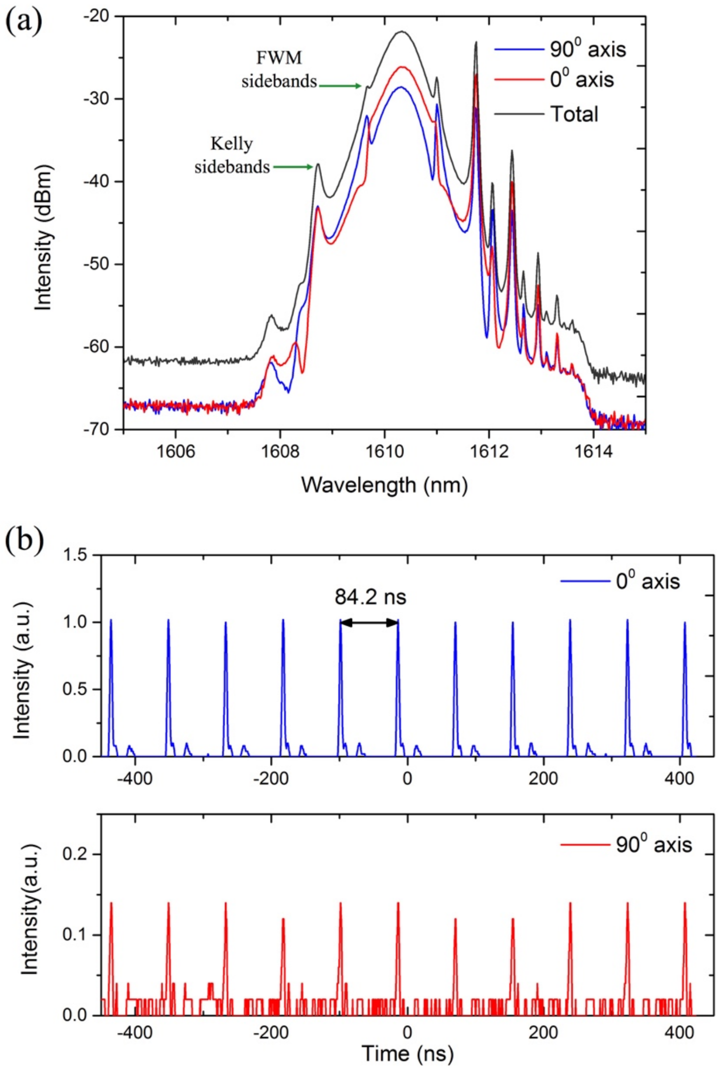

Figure 6.4 (a) Optical spectra and (b) oscilloscope traces of vector solitons on the on the 0° and 90° axes.

Moreover, these FWM sidebands of vector solitons can be shifted by adjusting the in-cavity PC. As shown in **Figure 6.5**, the FWM sidebands are shifted further from the spectrum peak. It could be supposed that the "out of phase" wavelengths of vector solitons are correlated with the cavity birefringence.

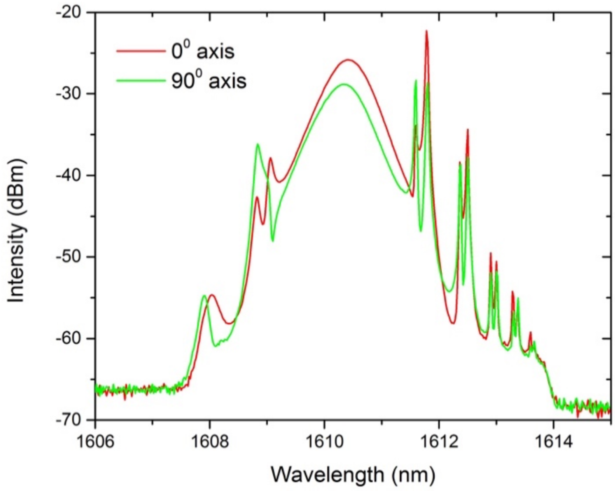

Figure 6.5 Optical spectra of the vector solitons on the 0° and 90° axes after the in-cavity PC was adjusted.

With pump power unchanged and in-cavity PC fixed, the spectrum of vector solitons can be continuously tuned by mechanically tilting the cantilever. As shown in **Figure 6.6**, the central wavelength of vector solitons is tuned from 1606.8 to 1613.3 nm continuously. However, the FWM sidebands stay at the same spectral positions, indicating that the "polarization-locked" state sustains with wavelength tuning. It could be supposed that the cavity birefringence remains unchanged with adjusting of CFBG. It is noteworthy that the spectrum peak fluctuates slightly due to the inhomogeneous gain at ~1610 nm.

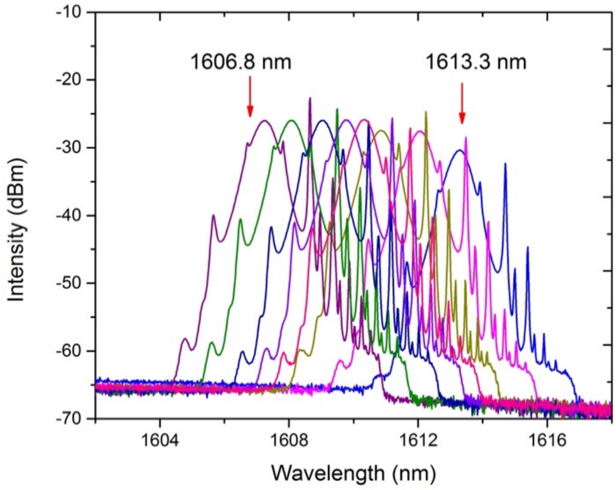

Figure 6.6 Spectral evolution of the tunable vector solitons.

6.2.3 Numerical Analysis

Furthermore, the formation of FWM spectral sidebands of vector solitons was numerically investigated based on SSFM. Two coupled GLE equations that govern the nonlinear propagation of pulse in a weakly birefringent fiber laser are expressed as,

$$\frac{\partial u}{\partial z} - i\beta u + \delta\frac{\partial u}{\partial t} + \frac{i}{2}\beta_2\frac{\partial^2 u}{\partial t^2} + \frac{\alpha_l}{2}u = i\gamma\left(|u|^2 + \frac{2}{3}|v|^2\right)u + i\frac{\gamma}{3}u^*v^2 + \frac{g}{2}u + \frac{g}{2{\Omega_g}^2}\frac{\partial^2 u}{\partial t^2}, \tag{6.2.1}$$

$$\frac{\partial v}{\partial z} + i\beta v - \delta\frac{\partial v}{\partial t} + \frac{i}{2}\beta_2\frac{\partial^2 v}{\partial t^2} + \frac{\alpha_l}{2}v = i\gamma\left(|v|^2 + \frac{2}{3}|u|^2\right)v + i\frac{\gamma}{3}v^*u^2 + \frac{g}{2}v + \frac{g}{2{\Omega_g}^2}\frac{\partial^2 v}{\partial t^2}, \tag{6.2.2}$$

where u and v represent the normalized envelopes of the two orthogonally-polarized components, $2\beta = 2\pi\Delta n/\lambda$ is the propagation constant difference between the two polarization components and $L_b = \lambda/\Delta n$ is the beat length of the cavity, $2\delta = 2\beta\lambda/2\pi c$ is the inverse group velocity difference, β_2 is the second-order dispersion coefficient and γ represents the nonlinearity of the optical fiber, g is the saturable gain coefficient of the laser and Ω_g is the gain bandwidth. For an erbium fiber laser, the gain saturation is described as,

$$g = g_0 \, exp\left[-\frac{1}{E_s}\int_{-\infty}^{t}(|u|^2 + |v|^2)dt\right], \qquad (6.2.3)$$

where g_0 is the small-signal gain coefficient and E_s is the gain saturation energy. To approximate the experiments, the following parameters are used: γ_{EDF} = 1 W^{-}1/km, γ_{EDF} = 64 W^{-}1/km, Ω_g = 25 nm, E_s = 50 pJ, β_{SMF} = –23 ps^2/km, β_{EDF} = 168 ps^2/km, Cavity length L = 20.4 m.

Based on the numerical computation method described in the previous chapter, the above GLE equations are numerically solved here. **Figure 6.7** shows the spectra of simulated vector solitons on the 0° and 90° axes when the beat length $L_b = 5L$. FWM spectral sidebands can be observed clearly, which vary out-of-phase between the 0° and 90° axes and are consistent with the experimental observations. These extra sidebands disappeared in case that the FWM terms in Eq.(6.2.1)-(6.2.2) were omitted, which indicates that those extra sidebands are induced by the FWM-based coherent interaction [39], [40], [84]. When the beat length is significantly decreased to $L_b = 0.1L$, the FWM sidebands disappear as shown in **Figure**

6.8. And the two orthogonally-polarized spectra exhibit the same profile. It could be supposed that the large cavity birefringence supports generation of scalar solitons.

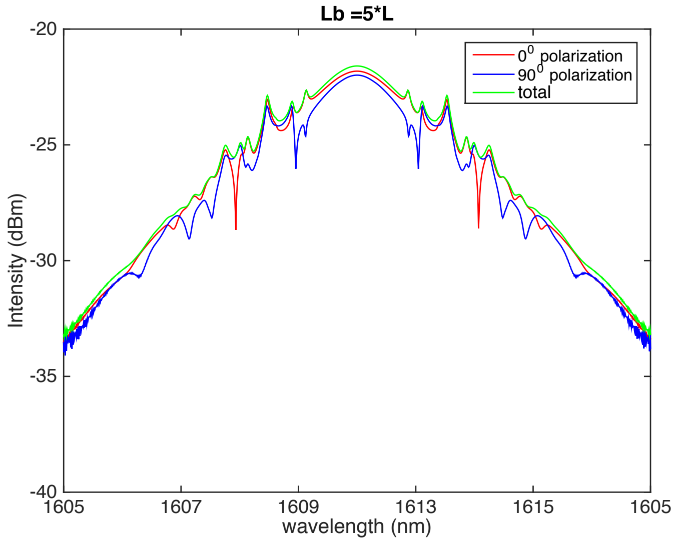

Figure 6.7 Simulated spectra of vector solitons on the 0° and 90° axes when $L_b = 5L$.

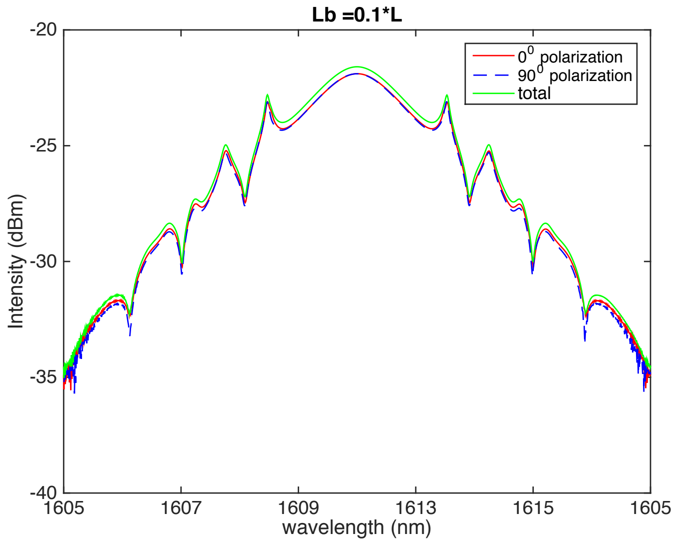

Figure 6.8 Simulated spectra of vector solitons on the 0° and 90° axes when $L_b = 0.1L$.

6.3 Tunable Scalar Solitons

6.3.1 Configuration of the Laser for Scalar Solitons

Figure 6.9 shows the experimental setup of the tunable mode-locked fiber laser generating scalar solitons. A 2.7-m-long PM-EDF (Coractive Er35-7-PM) is forward pumped with a 974-nm laser diode through a PM-WDM. Laser output is tapped from the 10% port of a PM fiber coupler. A small piece of home-made SWCNT/PVA film was sandwiched between two PM fiber connectors and acts as an in-fiber mode locker, of which the normalized non-saturable loss, modulation depth and saturable intensity are measured to be 95%, 5% and 11MW/cm^2, respectively.

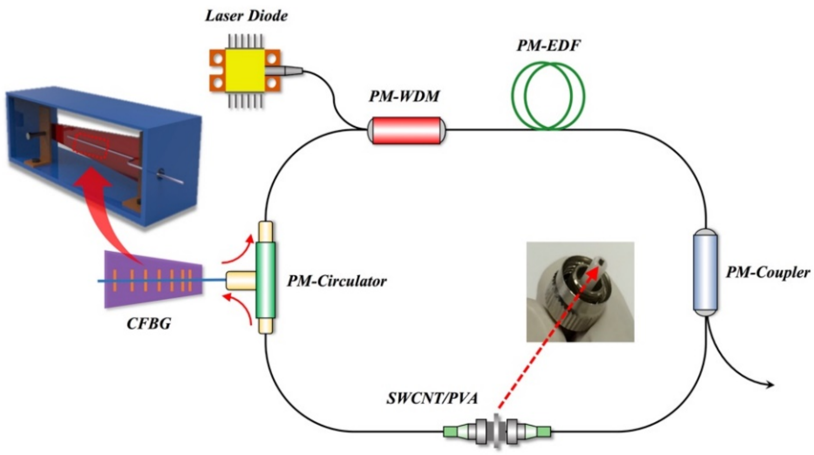

Figure 6.9 Experimental setup of the tunable mode-locked fiber laser generating C-band scalar solitons.

To implement wavelength tuning, a home-made CFBG at ~1530 nm is incorporated into the laser cavity via a PM fiber circulator. As shown in

Figure 6.10(a), the CFBG is mounted onto one surface of a left-angled triangle cantilever beam that was previously used for vector solitons. The spectral shape of CFBG remains unchanged along with wavelength tuning. Note that the induced relatively low birefringence does not affect the laser polarization.

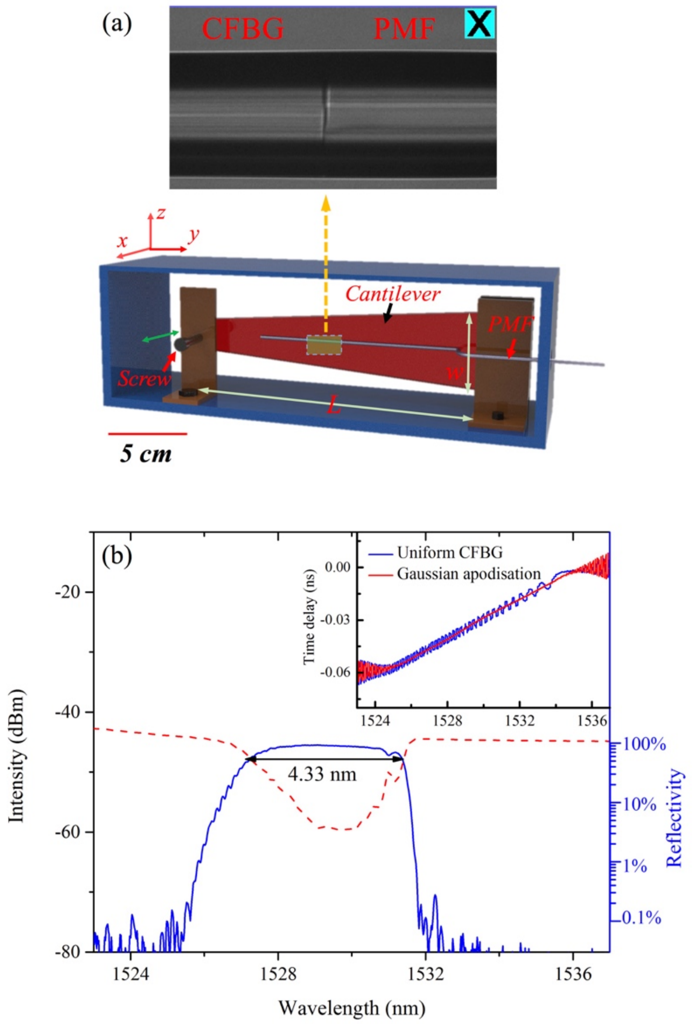

Figure 6.10 (a) Microscope image of splicing section between CFBG and PMF (top) and configuration of cantilever beam (bottom) and (b) measured optical spectra of the CFBG.

To weaken the polarization cross-coupling in the non-PM fibers, the CFBG is closely spliced to the PM fiber (PMF) as shown in **Figure 6.10**(a). The splice loss is estimated to be ~0.05 dB. Measured optical spectra of the CFBG are shown in **Figure 6.10**(b), where it can be observed that the reflection top is flat and smooth without interference ripples. The central wavelength and 3-dB bandwidth of reflection spectrum are ~1530 nm and ~4.33 nm, respectively. And the CFBG reflectivity is estimated as high as ~97%. Based on the TMM, the time delay of the CFBG is also numerically calculated as plotted in the inset of **Figure 6.10**(b). The ripples of the delay curve are efficiently suppressed with the Gaussian apodization. And the GVD parameter of the CFBG is calculated to be ~5 ps/nm.

6.3.2 Characterization of Tunable Scalar Solitons

1) Tunable scalar solitons around 1530 nm

In the experiment, the laser changed from continuous wave state to mode locking state under pump power of higher than 46 mW. Different from the laser cavity for vector solitons, no PCs are used here. Under pump power of 88 mW, measured spectrum of the scalar solitons is shown in **Figure 6.11**. The central wavelength is ~1530 nm as determined by the CFBG. Distinct Kelly sidebands of the spectrum indicate that the operation of mode locking in the anomalous dispersion regime. The 3-dB spectral width is measured to be ~0.48 nm. To investigate the dispersion effect of grating, the CFBG together with the PM circulator were removed and replaced by a PM isolator. Stable mode locking was observed again but at the wavelength of ~1555 nm as shown in the inset of **Figure 6.11**. The 3-dB spectral width changes to be ~8.76 nm. Successful mode locking at the two wavelengths verifies a broadband operation range of the SWCNT SA.

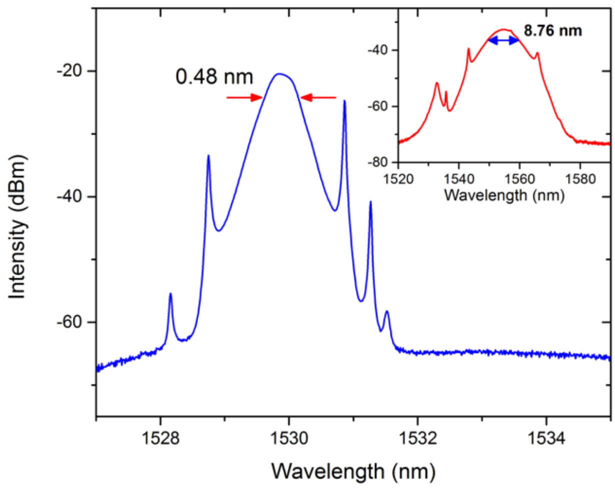

Figure 6.11 Measured spectra of the PM mode-locked fiber laser with and without (inset) the CFBG.

The mode-locked pulses were then measured with an optical autocorrelator, a photodetector and an oscilloscope. **Figure 6.12** shows the AC traces of the emitted scalar solitons. With the assumption of a sech^2 profile, the pulse duration of the CFBG-incorporated laser is evaluated to be 6.94 ps. The TBP is thus calculated as ~0.43, indicating that the mode-locked pulses are slightly chirped. In comparison, the CFBG-omitted laser produces much narrower pulses with duration of ~370 fs as shown in the inset of **Figure 6.12**. It can be supposed that the large anomalous dispersion of CFBG broadens the mode-locked pulses. As shown in **Figure 6.13**(a), the pulse-to-pulse separation is 34.55 ns, corresponding to a repetition rate of 28.94 MHz. The RF spectrum peak owns a moderate signal-to-noise ratio (SNR) of ~60 dB, which could be attributed to the small modulation depth of the used SWCNT/PVA film. Average output power increases proportionally to pump power as shown in **Figure 6.13**(b). The maximum average output power and pulse energy are 2.17 mW and ~63 pJ, respectively. Under higher pump powers, unstable mode locking state was induced by the heat accumulation on the SA.

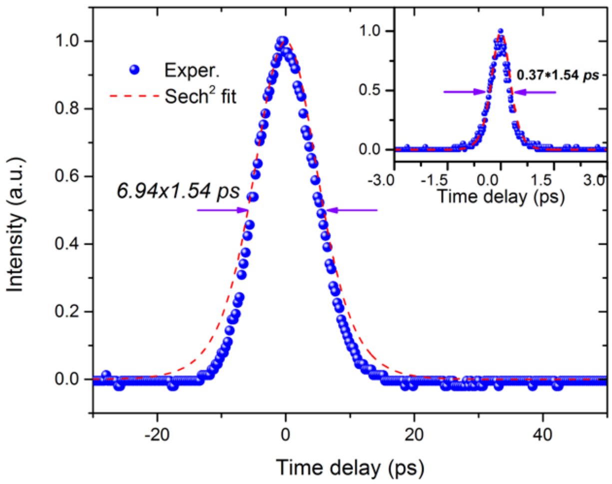

Figure 6.12 Measured AC traces of the PM mode-locked fiber laser with and without (inset) the CFBG.

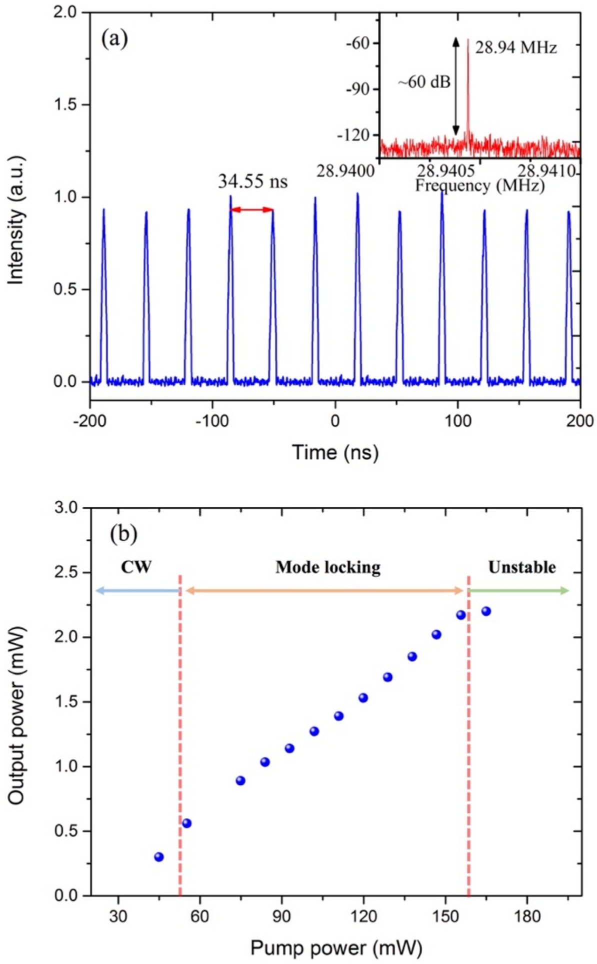

Figure 6.13 (a) Measured pulse train and RF spectrum (inset) and (b) output average power against with pump power of the PM mode-locked fiber laser using the CFBG.

Additionally, a polarimeter (Profile PAT9000) was used to measure the polarization property of the PM laser emission. As shown in **Figure 6.14**, the degree of polarization (DOP) is measured to be ~99.5% and well maintained over a long period of time with relatively little variation, confirming the exsistence of scalar solitons. The corresponding polarization ellipticity varies between -1.5° and -1° over a period of 100 seconds.

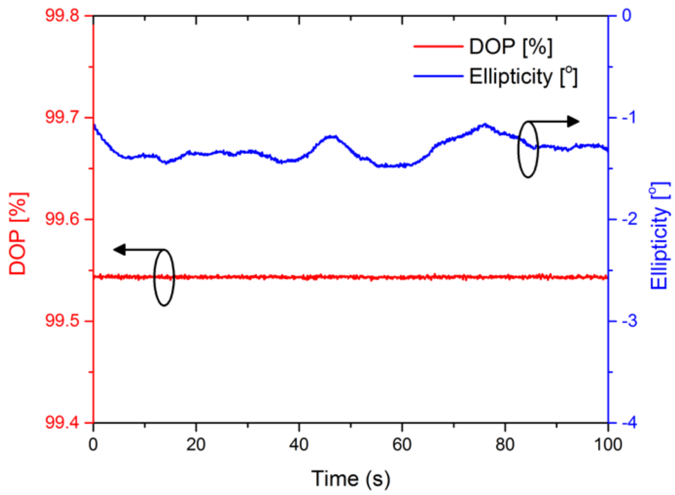

Figure 6.14 Measured DOP and polarization ellipticity of the scalar solitons over 100-second period.

When pump power is 93 mW, the wavelength of the scalar solitons was continuously tuned from 1530 to 1537.7 nm by tilting the cantilever as shown in **Figure 6.15**(a). The limited tuning range is attributed to the insufficient gain at wavelengths shorter than 1530 nm. The always-on Kelly sidebands proves the sustained mode locking state during the wavelength tuning process. Owing to the inhomogeneous gain profile around 1530 nm, the spectrum peak fluctuates a little. The corresponding pulse duration and spectral width of the scalar solitons are plotted with respect to wavelength in **Figure 6.15**(b). The pulse duration changes from 6.5 to 8.8 ps and does not show obvious dependence on the laser wavelength. Additionally, the corresponding spectral width changes from 0.34 to 0.63 nm, indicating that the pulses are close to the transform limit.

Corresponding AC traces of the scalar solitons are also plotted in the inset of **Figure 6.15**(b).

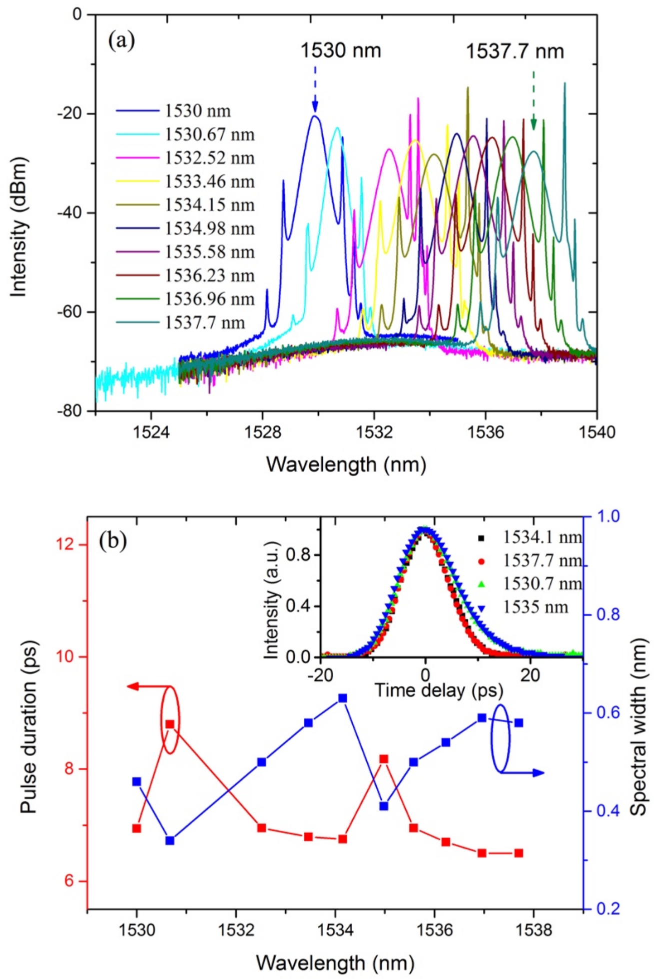

Figure 6.15 (a) Optical spectra and (b) pulse durations and spectral widths of the tunable scalar solitons at different wavelengths.

2) Tunable scalar solitons around 1560 nm

To show the broad tunability of the proposed grating technique, another CFBG centered at ~1560 nm was used instead, whose spectra are plotted in **Figure 6.16**. The central wavelength and 3-dB spectral width are ~1558 nm and ~4 nm, respectively. In addition, the CFBG reflectivity is evaluated to be ~97%.

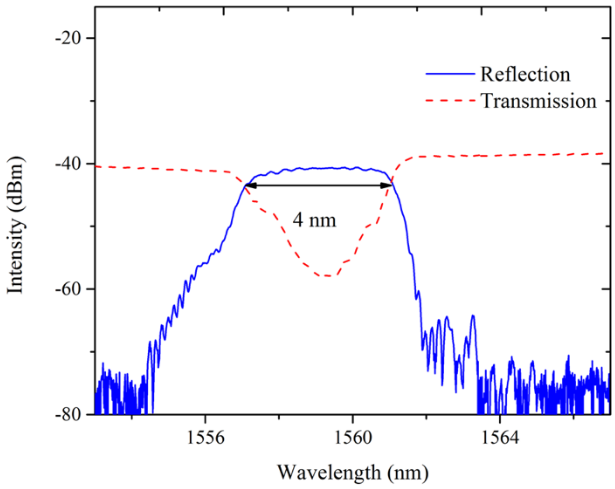

Figure 6.16 Measured reflection and transmission spectra of the CFBG centered at 1560 nm.

In this experiment, a 4.7-m-long PM-EDF (Coractive Er35-7-PM) was bi-directionally pumped with two 974-nm laser diodes via two PM-WDMs. The laser then transited from continuous wave operation to mode locking state when forward and backward pump powers were increased to higher than 56 and 10 mW, respectively. Under pump powers of 88 mW (forward) and 49 mW (backward), optical spectrum of the obtained scalar solitons is plotted in **Figure 6.17**(a). The central wavelength is 1558.5 nm as determined by the CFBG. The Kelly sidebands mean the mode locking in the anomalous dispersion regime. And the 3-dB spectral width is measured as ~0.45 nm.

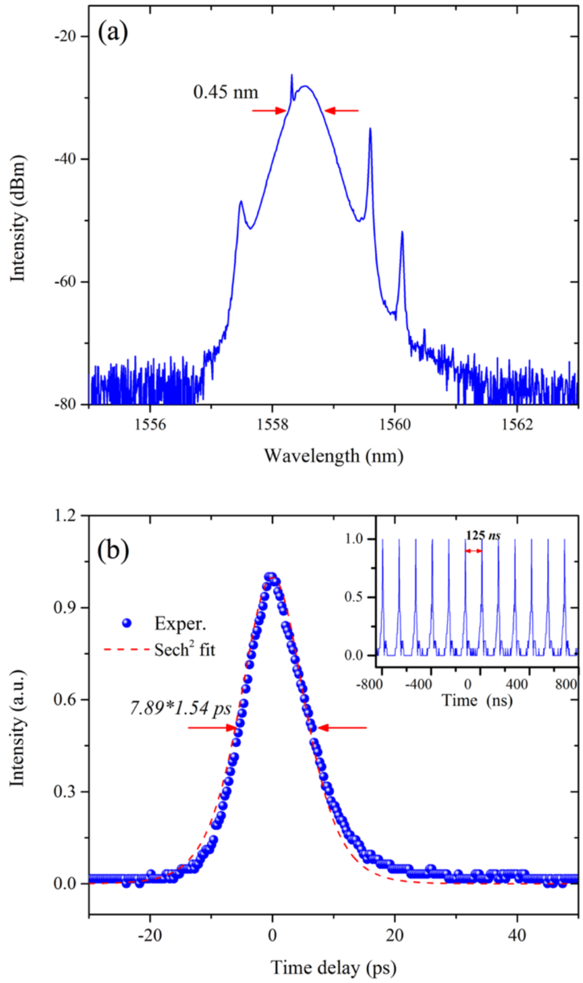

Figure 6.17 (a) Optical spectra and (b) AC traces of the PM mode-locked fiber laser with and without (inset) the 1560-nm CFBG.

When a sech^2 profile is assumed, the pulse duration of the CFBG-used laser is 7.89 ps as shown in **Figure 6.17**(b). The TBP is calculated as ~0.44, showing a slight chirping of the mode-locked pulse. The pulse-to-pulse separation is 125 ns, consistent with a repetition rate of 7.9 MHz. The maximum output average power and pulse energy are 2.17 mW and ~0.27 nJ, respectively.

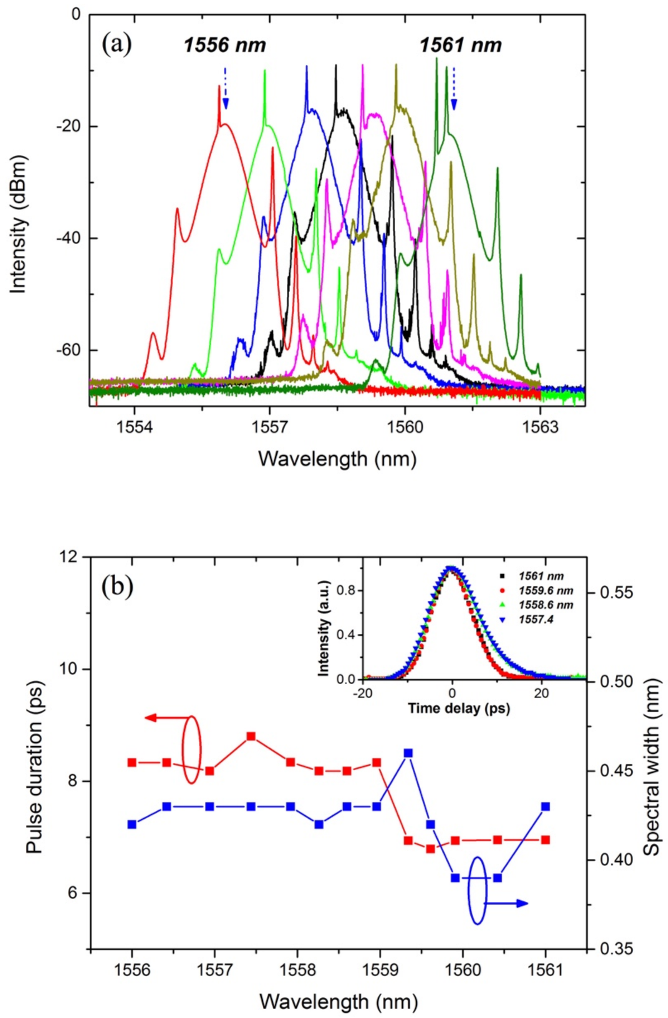

Figure 6.18 (a) Optical spectra and (b) pulse durations and spectral widths of the tunable scalar solitons at different wavelengths.

Under pump power of 88 mW (forward) and 49 mW (backward), the central wavelength of the scalar solitons can be continuously tuned from 1556 to 1561 nm by tuning the cantilever as shown in **Figure 6.18**(a). The Kelly sidebands sustain when the CFBG is adjusted, indicating that the mode locking state is always on. The CW spectral spikes are resulted from the high insertion loss of SA. **Figure 6.18**(b) plots the pulse duration and spectral width with respect to wavelength of the scalar solitons. The pulse duration changes from 6.79 to 8.8 ps and the spectral width varies between 0.39 and 0.46 nm, indicating that the scalar solitons exhibit somewhat chirping. The typical AC traces are plotted in the inset of **Figure 6.18**(b).

6.4 Summary

In summary, we have demonstrated tunable vector and scalar solitons based on CFBGs. The home-made CFBGs are mounted on a plastic cantilever to serve as all-fiber tunable spectral filters. Firstly, tunable vector solitons at L-band have been obtained in a non-PM mode-locked fiber laser using a Bi-EDF. By adjusting the CFBG at 1610 nm, the wavelength of the vector solitons can be tuned from 1606.8 to 1613.3 nm continuously. Moreover, the formation of extra spectral sidebands due to FWM coherent interaction has been numerically confirmed. Later, tunable scalar solitons at C-band have been realized in a PM mode-locked fiber laser. Linearly polarized scalar solitons are measured with the DOP of 99.5%. By adjusting the CFBGs, the wavelength of scalar solitons can be continuously tuned in C band. The presented technique of tuning wavelength with a CFBG and utilizing a broadband SA can be readily adopted for various fiber lasers ranging from 1 to 2 μm.

Chapter 7.

Conclusions and Future Outlook

7.1 Conclusions

In this dissertation, fiber gratings, i.e. LPG and CFBG, have been used to develop important all-fiber tunable mode-locked lasers. To provide all-fiber spectrum-tunable filters, specially-designed fiber gratings have been fabricated based on the own-established grating fabrication platforms. To offer a broadband mode locker, a home-made SWCNT/PVA film has been inserted between two fiber connectors. The presented technique of tuning wavelength by fiber gratings and using a broadband SA can be readily adopted to various fiber lasers from 1 to 2 μm.

By using the flexible point-by-point method and a 248-nm excimer laser, PSLPGs at different wavelengths have been fabricated and act as all-fiber spectrum-tunable filters. Among them, a W-shaped filter has been proposed by using a three-LPG concatenated structure. Through adjusting the temperature of the W-shaped filter from 23 to 110°C, a widely tunable mode-locked fiber laser has been demonstrated covering C and L bands. Moreover, an optofluidic tunable mode-locked fiber laser has been obtained by integrating the PSLPG into a microfluidic chip. By adjusting the flow rate ratio of the microfluidic flows accurately, the central wavelength of the mode-locked laser has been ultrafinely tuned. Furthermore, bound solitons with variable soliton separations have been experimentally observed. With ultrafine wavelength-tuning capability and flexible configurability, such a grating-integrated optofluidic chip offers a promising platform to develop valuable ultrafast lasers for scientific and industrial applications.

Based on a Talbot interferometer and a 213-nm pulsed UV laser, CFBGs centered at the wavelength of 1530, 1560 and 1610 nm have been fabricated, respectively. The interference ripples of the time delay of these CFBGs have been suppressed with Gaussian apodization. Firstly, a CFBG pair has been used to increase the net-cavity dispersion of a mode-locked fiber laser significantly, emitting high-energy conventional solitons free of splitting. As an efficient dispersion compensation device, CFBG offers a promising approach to improve pulse energy of solitons higher than the limit of soliton area theorem. Later, the CFBGs have been mounted on a plastic cantilever to serve as all-fiber tunable spectral filters. On one hand, tunable vector solitons at L band have been obtained for the first time by using a Bi-EDF and a CFBG at 1610 nm. The central wavelength of the polarization-locked solitons can be tuned from 1606.8 to 1613.3 nm. On the other hand, tunable scalar solitons have also been demonstrated from a PM mode-locked fiber laser using CFBGs. By adjusting the CFBGs at

1530 and 1560 nm, the wavelength of the scalar solitons has been tuned continuously in C band. Such tunable linearly polarized scalar solitons are valuable for various polarization sensitive applications, including but not limited to nonlinear frequency conversion.

7.2 Future Outlook

By using fiber gratings together with the SWCNT absorber, various tunable mode-locked fiber lasers have been demonstrated in this dissertation. As the EDFs are used as active media, the emission wavelengths are located in the optical communication window (i.e. 1.5–1.6 μm). Actually, apart from the EDF, other rare-earth-ion doped fibers (e.g. Yb- and Tm-doped fibers) have been extensively used in fiber lasers, and are commercially available nowadays. Thus, it will be of interest to adopt the presented technique in Yb and Tm fiber lasers, extending the wavelengths of tunable mode-locked fiber lasers to 1 and 2 μm. In particular, tunable mode-locked fiber lasers at 2 μm are valuable owing to their important applications, such as medical surgery, LiDAR systems and gas spectroscopy.

In addition, all mode-locked fiber lasers built in our research operate in the anomalous dispersion regime and emit conventional solitons. Except these, other kinds of solitons, e.g. dissipative solitons and similaritons, could also be formed in mode-locked fiber lasers. In particular, dissipative solitons can achieve relatively high pulse energies without wave-breaking, which are valuable for material processing and frequency conversion (e.g. supercontinuum and THz-wave generation). Thus, it will be interesting to exploit fiber gratings for tunable dissipative solitons.

In our study, the temperature and RI responses of LPG have been exploited in tunable mode-locked fiber lasers. In general, these responses depend on the orders of corresponding cladding modes and properties of optical fibers. By optimizing the cladding-mode orders and fiber structures, the wavelength tunability of LPG can be improved. For instance, it is meaningful to exploit the microstructured optical fiber grating as a tunable spectral filter, whose structural flexibility provides a possibility to engineer fiber dispersion, nonlinearity and modal properties.

Eventually, an optofluidic tunable mode-locked fiber laser has been demonstrated by using an LPG-integrated microfluidic chip, the spectrum of which can be ultrafinely tuned. From a broad point of view, the versatile optofluidic chip can be readily used to manipulate other fiber properties, such as dispersion, nonlinearity and birefringence, and thus optimize the performance of the mode-locked fiber lasers in other terms. Conversely, the evanescent field of mode-locked pulses can be used to actively detect or modify the fluidic matters in the optofluidic chip, which is promising in bio-chemical detection and optical tweezers.

References

[1] U. Keller, “Recent developments in compact ultrafast lasers,” *Nature*, vol. 424, no. 6950, pp. 831–838, 2003.

[2] A. H. Zewail, “Femtochemistry: recent progress in studies of dynamics and control of reactions and their transition states,” *J. Phys. Chem.*, vol. 100, no. 31, pp. 12701–12724, 1996.

[3] L. F. Mollenauer, P. V Mamyshev, J. Gripp, M. J. Neubelt, N. Mamysheva, L. Grüner-Nielsen, and T. Veng, “Demonstration of massive wavelength-division multiplexing over transoceanic distances by use of dispersion-managed solitons.,” *Opt. Lett.*, vol. 25, no. 10, pp. 704–706, 2000.

[4] R. Holzwarth, T. Udem, T. W. Hänsch, J. C. Knight, W. J. Wadsworth, and P. S. J. Russell, “Optical frequency synthesizer for precision spectroscopy,” *Phys. Rev. Lett.*, vol. 85, no. 11, pp. 2264–2267, 2000.

[5] R. Holzwarth, M. Zimmermann, T. Udem, and T. W. Hänsch, “Optical clockworks and the measurement of laser frequencies with a mode-locked frequency comb,” *IEEE J. Quantum Electron.*, vol. 37, no. 12, pp. 1493–1501, 2001.

[6] M. Ferray, A. L’Huillier, X. F. Li, L. A. Lompre, G. Mainfray, and C.

Manus, “Multiple-harmonic conversion of 1064 nm radiation in rare gases,” *J. Phys. B At. Mol. Opt. Phys.*, vol. 21, no. 3, pp. L31–L35, 1999.

[7] A. J. Demaria, D. A. Stetser, and H. Heynau, “Self mode-locking of lasers with saturable absorbers,” *Appl. Phys. Lett.*, vol. 8, no. 7, pp. 174–176, 1966.

[8] U. Keller, D. A. B. Miller, G. D. Boyd, T. H. Chiu, J. F. Ferguson, and M. T. Asom, “Solid-state low-loss intracavity saturable absorber for Nd:YLF lasers: an antiresonant semiconductor Fabry–Perot saturable absorber,” *Opt. Lett.*, vol. 17, no. 7, p. 505, 1992.

[9] U. Keller, K. J. Weingarten, F. X. Kärtner, D. Kopf, B. Braun, I. D. Jung, R. Fluck, C. Hönninger, N. Matuschek, and J. Aus Der Au, “Semiconductor saturable absorber mirrors (SESAM’s) for femtosecond to nanosecond pulse generation in solid-state lasers,” *IEEE J. Sel. Top. Quantum Electron.*, vol. 2, no. 3, pp. 435–451, 1996.

[10] D. E. Spence, P. N. Kean, and W. Sibbett, “60-fsec pulse generation from a self-mode-locked Ti:sapphire laser.,” *Opt. Lett.*, vol. 16, no. 1, pp. 42–44, 1991.

[11] E. Innerhofer, T. Südmeyer, F. Brunner, R. Häring, A. Aschwanden, R. Paschotta, C. Hönninger, M. Kumkar, and U. Keller, “60-W average

power in 810-fs pulses from a thin-disk Yb:YAG laser," *Opt. Lett.*, vol. 28, no. 5, p. 367, 2003.

[12] L. Krainer, R. Paschotta, S. Lecomte, M. Moser, K. J. Weingarten, and U. Keller, "Compact Nd: YVO4 lasers with pulse repetition rates up to 160 GHz," *IEEE J. Quantum Electron.*, vol. 38, no. 10, pp. 1331–1338, 2002.

[13] D. H. Sutter, G. Steinmeyer, L. Gallmann, N. Matuschek, F. Morier-Genoud, U. Keller, V. Scheuer, G. Angelow, and T. Tschudi, "Semiconductor saturable-absorber mirror-assisted Kerr-lens mode-locked Ti : sapphire laser producing pulses in the two- cycle regime," *Opt. Lett.*, vol. 24, no. 9, pp. 631–633, 1999.

[14] R. Ell, U. Morgner, F. X. Kärtner, J. G. Fujimoto, E. P. Ippen, V. Scheuer, G. Angelow, T. Tschudi, M. J. Lederer, A. Boiko, and B. Luther-Davies, "Generation of 5-fs pulses and octave-spanning spectra directly from a Ti:sapphire laser," *Opt. Lett.*, vol. 26, no. 6, p. 373, 2001.

[15] M. E. Fermann and I. Hartl, "Ultrafast fibre lasers," *Nat. Photonics*, vol. 7, no. 11, pp. 868–874, 2013.

[16] M. E. Fermann and I. Hartl, "Ultrafast fiber laser technology," *IEEE J. Sel. Top. Quantum Electron.*, vol. 15, no. 1, pp. 191–206, 2009.

[17] A. Tünnermann, T. Schreiber, and J. Limpert, “Fiber lasers and amplifiers: an ultrafast performance evolution.,” *Appl. Opt.*, vol. 49, no. 25, pp. F71–F78, 2010.

[18] I. N. Duling III, “All-fiber ring soliton laser mode locked with a nonlinear mirror.,” *Opt. Lett.*, vol. 16, no. 8, pp. 539–541, 1991.

[19] S. Gray and A. B. Grudinin, “Soliton fiber laser with a hybrid saturable absorber.,” *Opt. Lett.*, vol. 21, no. 3, pp. 207–209, 1996.

[20] P. Grelu and N. Akhmediev, “Dissipative solitons for mode-locked lasers,” *Nat. Photonics Phot.*, vol. 6, no. 2, pp. 84–92, 2012.

[21] J. M. Dudley, S. Coen, and G. Genty, “Supercontinuum generation in photonic crystal fiber,” *Rev. Mod. Phys.*, vol. 78, no. 4, pp. 1135–1184, 2006.

[22] G. Genty, S. Coen, and J. M. Dudley, “Fiber supercontinuum sources (Invited),” *J. Opt. Soc. Am. B*, vol. 24, no. 8, p. 1771, 2007.

[23] F. Ö. Ilday, J. R. Buckley, W. G. Clark, and F. W. Wise, “Self-similar evolution of parabolic pulses in a laser,” *Phys. Rev. Lett.*, vol. 92, no. 21, p. 213902, 2004.

[24] B. Oktem, C. Ulgudur, and F. O. Ilday, “Soliton-similariton fibre laser,” *Nat Phot.*, vol. 4, no. 5, pp. 307–311, 2010.

[25] W. H. Renninger, A. Chong, and F. W. Wise, “Self-similar pulse

evolution in an all-normal-dispersion laser," *Phys. Rev. A*, vol. 82, no. 2, p. 21805, 2010.

[26] A. Hasegawa and F. Tappert, "Transmission of stationary nonlinear optical pulses in dispersive dielectric fibers. II. Normal dispersion," *Appl. Phys. Lett.*, vol. 23, no. 4, pp. 171–172, 1973.

[27] L. F. Mollenauer, R. H. Stolen, and J. P. Gordon, "Experimental observation of picosecond pulse narrowing and solitons in optical fibers," *Phys. Rev. Lett.*, vol. 45, no. 13, pp. 1095–1098, 1980.

[28] L. F. Mollenauer and K. Smith, "Demonstration of soliton transmission over more than 4000 km in fiber with loss periodically compensated by Raman gain," *Opt. Lett.*, vol. 13, no. 8, pp. 675–677, 1988.

[29] L. F. Mollenauer, S. G. Evangelides, and J. P. Gordon, "Wavelength division multiplexing with solitons in ultra-long distance transmission using lumped amplifiers," *IEEE J. Light. Technol.*, vol. 9, no. 3, pp. 362–367, 1991.

[30] W. H. Renninger, A. Chong, and F. W. Wise, "Dissipative solitons in normal-dispersion fiber lasers," *Phys. Rev. A*, vol. 77, no. 2, p. 23814, 2008.

[31] A. Cabasse, B. Ortaç, G. Martel, A. Hideur, and J. Limpert, "Dissipative solitons in a passively mode-locked Er-doped fiber with

strong normal dispersion," *Opt. Express*, vol. 16, no. 23, p. 19322, 2008.

[32] D. Mao, X. Liu, D. Han, and H. Lu, "Compact all-fiber laser delivering conventional and dissipative solitons.," *Opt. Lett.*, vol. 38, no. 16, pp. 3190–3193, 2013.

[33] S. A. Babin, E. V. Podivilov, D. S. Kharenko, A. E. Bednyakova, M. P. Fedoruk, V. L. Kalashnikov, and A. Apolonski, "Multicolour nonlinearly bound chirped dissipative solitons," *Nat. Commun.*, vol. 5, p. 4653, 2014.

[34] Y. D. Cui, X. M. Liu, and C. Zeng, "Conventional and dissipative solitons in a CFBG-based fiber laser mode-locked with a graphene – nanotube mixture," *Laser Phys. Lett.*, vol. 11, no. 5, p. 55106, 2014.

[35] C. Finot and G. Millot, "Synthesis of optical pulses by use of similaritons," *Opt. Express*, vol. 12, no. 21, pp. 5104–5109, 2004.

[36] M. Olivier, M. Gagnon, S. Duval, M. Bernier, and M. Piche, "All-fiber amplifier similariton laser based on a fiber Bragg grating filter," *Opt. Lett.*, vol. 40, no. 23, pp. 5650–5653, 2015.

[37] E. A. Zlobina, D. S. Kharenko, S. I. Kablukov, and S. A. Babin, "Four wave mixing of conventional and Raman dissipative solitons from single fiber laser," *Opt. Express*, vol. 23, no. 13, p. 16589, 2015.

[38] D. S. Kharenko, A. E. Bednyakova, E. V. Podivilov, M. P. Fedoruk, A. Apolonski, and S. a. Babin, "Feedback-controlled Raman dissipative solitons in a fiber laser," *Opt. Express*, vol. 23, no. 2, p. 1857, 2015.

[39] L. M. Zhao, D. Y. Tang, H. Zhang, and X. Wu, "Polarization rotation locking of vector solitons in a fiber ring laser.," *Opt. Express*, vol. 16, no. 14, pp. 10053–10058, 2008.

[40] D. Y. Tang, H. Zhang, L. M. Zhao, and X. Wu, "Observation of high-order polarization-locked vector solitons in a fiber laser," *Phys. Rev. Lett.*, vol. 101, no. 15, pp. 1–4, 2008.

[41] J. B. Schroeder, S. Coen, T. Sylvestre, and B. J. Eggleton, "Dark and bright pulse passive mode-locked laser with in-cavity pulse-shaper," *Opt. Express*, vol. 18, no. 22, pp. 22715–22721, 2010.

[42] J. Sotor, G. Sobon, and K. M. Abramski, "Scalar soliton generation in all-polarization-maintaining, graphene mode-locked fiber laser.," *Opt. Lett.*, vol. 37, no. 11, pp. 2166–8, 2012.

[43] M. Han, S. Zhang, X. Li, H. Zhang, H. Yang, and T. Yuan, "Polarization dynamic patterns of vector solitons in a graphene mode-locked fiber laser," *Opt. Express*, vol. 23, no. 3, pp. 2424–2435, 2015.

[44] X. Li, S. Zhang, H. Han, M. Han, H. Zhang, L. Zhao, F. Wen, and Z.

Yang, “Different polarization dynamic states in a vector Yb-doped fiber laser,” *Opt. Express*, vol. 23, no. 8, pp. 10747–10755, 2015.

[45] M. E. Fermann, F. Haberl, M. Hofer, and H. Hochreiter, “Nonlinear amplifying loop mirror,” *Opt. Lett.*, vol. 15, no. 13, p. 752, 1990.

[46] J. Szczepanek, T. M. Kardas, M. Michalska, C. Radzewicz, and Y. Stepanenko, “Simple all-PM-fiber laser mode-locked with a nonlinear loop mirror,” *Opitcs Lett.*, vol. 40, no. 15, pp. 3500–3503, 2015.

[47] M. Hofer, M. E. Fermann, F. Haberl, M. H. Ober, and A. J. Schmidt, “Mode locking with cross-phase and self-phase modulation.,” *Opt. Lett.*, vol. 16, no. 7, pp. 502–504, 1991.

[48] K. Tamura, E. P. Ippen, H. A. Haus, and L. E. Nelson, “77-fs pulse generation from a stretched-pulse mode-locked all-fiberring laser,” *Opt. Lett.*, vol. 18, no. 13, pp. 1080–1082, 1993.

[49] K. Tamura, J. Jacobson, E. P. Ippen, H. A. Haus, and J. G. Fujimoto, “Unidirectional ring resonators for self-starting passively mode-locked lasers,” *Opt. Lett.*, vol. 18, no. 3, pp. 220–222, 1993.

[50] O. Okhotnikov, A. Grudinin, M. Pessa, O. Oleg, G. Anatoly, and P. Markus, “Ultra-fast fibre laser systems based on SESAM technology: New horizons and applications,” *New J. Phys.*, vol. 6, no. 1, p. 177, 2004.

[51] P. Avouris, M. Freitag, and V. Perebeinos, “Carbon-nanotube photonics and optoelectronics,” *Nat. Photonics*, vol. 2, no. 6, pp. 341–350, 2008.

[52] A. Martinez and Z. Sun, “Nanotube and graphene saturable absorbers for fibre lasers,” *Nat. Photonics*, vol. 7, no. 11, pp. 842–845, 2013.

[53] T. Hasan, Z. Sun, F. Wang, F. Bonaccorso, P. H. Tan, A. G. Rozhin, and A. C. Ferrari, “Nanotube-polymer composites for ultrafast photonics,” *Adv. Mater.*, vol. 21, no. 38, pp. 3874–3899, 2009.

[54] Q. Bao, H. Zhang, Y. Wang, Z. Ni, Y. Yan, Z. X. Shen, K. P. Loh, and D. Y. Tang, “Atomic-layer graphene as a saturable absorber for ultrafast pulsed lasers,” *Adv. Funct. Mater.*, vol. 19, no. 19, pp. 3077–3083, 2009.

[55] S. Wang, H. Yu, H. Zhang, A. Wang, M. Zhao, Y. Chen, L. Mei, and J. Wang, “Broadband few-layer MoS2 saturable absorbers,” *Adv. Mater.*, vol. 26, no. 21, pp. 3538–3544, 2014.

[56] P. Yan, A. Liu, Y. Chen, J. Wang, S. Ruan, H. Chen, and J. Ding, “Passively mode-locked fiber laser by a cell-type WS2 nanosheets saturable absorber,” *Sci. Rep.*, vol. 5, p. 12587, 2015.

[57] S. Y. Set, H. Yaguchi, Y. Tanaka, M. Jablonski, Y. Sakakibara, a. Rozhin, M. Tokumoto, H. Kataura, Y. Achiba, and K. Kikuchi,

"Mode-locked fiber lasers based on a saturable absorber incorporating carbon nanotubes," *OFC 2003 Opt. Fiber Commun. Conf. 2003.*, pp. 2–4, 2003.

[58] Y.-W. Song, S. Yamashita, C. S. Goh, and S. Y. Set, "Carbon nanotube mode lockers with enhanced nonlinearity via evanescent field interaction in D-shaped fibers.," *Opt. Lett.*, vol. 32, no. 2, pp. 148–150, 2007.

[59] Q. Fang, K. Kieu, and N. Peyghambarian, "An all-fiber 2-m wavelength-tunable mode-locked laser," *IEEE Photonics Technol. Lett.*, vol. 22, no. 22, pp. 1656–1658, 2010.

[60] S. Y. Choi, F. Rotermund, H. Jung, K. Oh, and D.-I. Yeom, "Femtosecond mode-locked fiber laser employing a hollow optical fiber filled with carbon nanotube dispersion as saturable absorber.," *Opt. Express*, vol. 17, no. 24, pp. 21788–21793, 2009.

[61] A. Martinez, K. Zhou, I. Bennion, and S. Yamashita, "In-fiber microchannel device filled with a carbon nanotube dispersion for passive mode-lock lasing," *Opt. Express*, vol. 16, no. 20, pp. 15425–15430, 2008.

[62] F. Wang, A. G. Rozhin, V. Scardaci, Z. Sun, F. Hennrich, I. H. White, W. I. Milne, and A. C. Ferrari, "Wideband-tuneable, nanotube

mode-locked, fibre laser," *Nat. Nanotechnol.*, vol. 3, no. 12, pp. 738–742, Dec. 2008.

[63] E. J. R. Kelleher, J. C. Travers, Z. Sun, A. G. Rozhin, A. C. Ferrari, S. V. Popov, and J. R. Taylor, "Nanosecond-pulse fiber lasers mode-locked with nanotubes," *Appl. Phys. Lett.*, vol. 95, no. 11, pp. 1–4, 2009.

[64] T. Noronen, S. Firstov, E. Dianov, and O. G. Okhotnikov, "1700 nm dispersion managed mode-locked bismuth fiber laser," *Sci. Rep.*, vol. 6, p. 24876, 2016.

[65] M. A. Solodyankin, E. D. Obraztsova, A. S. Lobach, A. I. Chernov, A. V Tausenev, V. I. Konov, and E. M. Dianov, "Mode-locked 1.93 µm thulium fiber laser with a carbon nanotube absorber," *Opt. Lett.*, vol. 33, no. 12, pp. 1336–1338, 2008.

[66] H. Zhang, D. Tang, R. J. Knize, L. Zhao, Q. Bao, and K. P. Loh, "Graphene mode locked, wavelength-tunable, dissipative soliton fiber laser," *Appl. Phys. Lett.*, vol. 96, no. 11, p. 111112, 2010.

[67] Z. X. Zhang, Z. W. Xu, and L. Zhang, "Tunable and switchable dual-wavelength dissipative soliton generation in an all-normal-dispersion Yb-doped fiber laser with birefringence fiber filter.," *Opt. Express*, vol. 20, no. 24, pp. 26736–42, 2012.

[68] S. Huang, Y. Wang, P. Yan, J. Zhao, H. Li, and R. Lin, "Tunable and switchable multi-wavelength dissipative soliton generation in a graphene oxide mode-locked Yb-doped fiber laser," *Opt. Express*, vol. 22, no. 10, pp. 11417–11426, 2014.

[69] X. H. Li, Y. S. Y. G. Wang, Y. S. Y. G. Wang, X. H. Hu, W. Zhao, X. L. Liu, J. Yu, C. X. Gao, W. Zhang, Z. Yang, C. Li, and D. Y. Shen, "Wavelength-switchable and wavelength-tunable all-normal-dispersion mode-locked yb-doped fiber laser based on single-walled carbon nanotube wall paper absorber," *IEEE Photonics J.*, vol. 4, no. 1, pp. 234–241, 2012.

[70] J. Sotor, G. Sobon, I. Pasternak, A. Krajewska, W. Strupinski, and K. M. Abramski, "Simultaneous mode-locking at 1565 nm and 1944 nm in fiber laser based on common graphene saturable absorber," *Opt. Express*, vol. 21, no. 16, pp. 18994–19002, 2013.

[71] Z. B. Liu, X. He, and D. N. Wang, "Passively mode-locked fiber laser based on a hollow-core photonic crystal fiber filled with few-layered graphene oxide solution," *Opt. Lett.*, vol. 36, no. 16, pp. 3024–3026, 2011.

[72] G. Sobon, J. Sotor, J. Jagiello, R. Kozinski, M. Zdrojek, M. Holdynski, P. Paletko, J. Boguslawski, L. Lipinska, and K. M. Abramski,

"Graphene Oxide vs. Reduced Graphene Oxide as saturable absorbers for Er-doped passively mode-locked fiber laser," *Opt. Express*, vol. 20, no. 17, pp. 19463–19473, 2012.

[73] M. Zhang, R. C. T. Howe, R. I. Woodward, E. J. R. Kelleher, F. Torrisi, G. Hu, S. V. Popov, J. R. Taylor, and T. Hasan, "Solution processed MoS2-PVA composite for sub-bandgap mode-locking of a wideband tunable ultrafast Er:fiber laser," *Nano Res.*, vol. 8, no. 5, pp. 1522–1534, 2015.

[74] J. Du, Q. Wang, G. Jiang, C. Xu, C. Zhao, Y. Xiang, Y. Chen, S. Wen, and H. Zhang, "Ytterbium-doped fiber laser passively mode locked by few-layer Molybdenum Disulfide (MoS2) saturable absorber functioned with evanescent field interaction," *Sci. Rep.*, vol. 4, p. 6346, 2014.

[75] D. Mao, Y. Wang, C. Ma, L. Han, B. Jiang, X. Gan, S. Hua, W. Zhang, T. Mei, and J. Zhao, "WS2 mode-locked ultrafast fiber laser," *Sci. Rep.*, vol. 5, p. 7965, 2015.

[76] H. Liu, X.-W. Zheng, M. Liu, N. Zhao, A.-P. Luo, Z.-C. Luo, W.-C. Xu, H. Zhang, C.-J. Zhao, and S.-C. Wen, "Femtosecond pulse generation from a topological insulator mode-locked fiber laser," *Opt. Express*, vol. 22, no. 6, pp. 6868–6873, 2014.

[77] M. Liu, Z. R. Cai, S. Hu, A. P. Luo, C. J. Zhao, H. Zhang, W. C. Xu, and Z. C. Luo, "Dissipative rogue waves induced by long-range chaotic multi-pulse interactions in a fiber laser with a topological insulator-deposited microfiber photonic device," *Opitcs Lett.*, vol. 40, no. 20, pp. 4767–4770, 2015.

[78] X. Li, X. Liu, X. Hu, L. Wang, H. Lu, Y. Wang, and W. Zhao, "Long-cavity passively mode-locked fiber ring laser with high-energy rectangular-shape pulses in anomalous dispersion regime.," *Opt. Lett.*, vol. 35, no. 19, pp. 3249–3251, 2010.

[79] X. Liu, "Numerical and experimental investigation of dissipative solitons in passively mode-locked fiber lasers with large net-normal-dispersion and high nonlinearity.," *Opt. Express*, vol. 17, no. 25, pp. 22401–16, 2009.

[80] O. Pottiez and A. Kuzin, "High energy noise-like pulsing in a double-clad Er / Yb figure-of-eight fiber laser," *Opt. Express*, vol. 24, no. 13, pp. 1549–1551, 2016.

[81] A. P. Luo, Z. C. Luo, H. Liu, X. W. Zheng, Q. Y. Ning, N. Zhao, W. C. Chen, and W. C. Xu, "Noise-like pulse trapping in a figure-eight fiber laser," *Opt. Express*, vol. 23, no. 8, pp. 10421–10427, 2015.

[82] B. Sun, A. Wang, C. Gu, G. Chen, L. Xu, D. Chung, and Q. Zhan,

"Mode-locked all-fiber laser producing radially polarized rectangular pulses," *Opt. Lett.*, vol. 40, no. 8, pp. 1691–1694, 2015.

[83] J. Li, Z. Zhang, Z. Sun, H. Luo, Y. Liu, Z. Yan, C. Mou, L. Zhang, and S. K. Turitsyn, "All-fiber passively mode-locked Tm-doped NOLM-based oscillator operating at 2-µm in both soliton and noisy-pulse regimes.," *Opt. Express*, vol. 22, no. 7, pp. 7875–82, 2014.

[84] H. Zhang, D. Y. Tang, L. M. Zhao, and N. Xiang, "Coherent energy exchange between components of a vector soliton in fiber lasers," *Opt. Express*, vol. 16, no. 17, pp. 12618–12623, 2008.

[85] D. D. Han, X. M. Liu, Y. D. Cui, G. X. Wang, C. Zeng, and L. Yun, "Simultaneous picosecond and femtosecond solitons delivered from a nanotube-mode-locked all-fiber laser," *Opt. Lett.*, vol. 39, no. 6, pp. 1565–1568, 2014.

[86] C. Huang, C. Wang, W. Shang, N. Yang, Y. Tang, and J. Xu, "Developing high energy dissipative soliton fiber lasers at 2 micron," *Sci. Rep.*, vol. 5, p. 13680, 2015.

[87] K. Kieu, R. J. Jones, and N. Peyghambarian, "Generation of few-cycle pulses from an amplified carbon nanotube mode-locked fiber laser system," *IEEE Photonics Technol. Lett.*, vol. 22, no. 20, pp. 1521–1523, 2010.

[88] B. Xu, A. Martinez, S. Y. Set, C. S. Goh, and S. Yamashita, "Polarization maintaining, nanotube-based mode-locked lasing from figure of eight fiber laser," *IEEE Photonics Technol. Lett.*, vol. 26, no. 2, pp. 180–182, 2014.

[89] R. I. Woodward, E. J. R. Kelleher, D. Popa, T. Hasan, F. Bonaccorso, A. C. Ferrari, S. V. Popov, and J. R. Taylor, "Scalar nanosecond pulse generation in a nanotube mode-locked environmentally stable fiber laser," *IEEE Photonics Technol. Lett.*, vol. 26, no. 16, pp. 1672–1675, 2014.

[90] H. H. Liu and K. K. Chow, "High fundamental-repetition-rate bound solitons in carbon nanotube-based fiber lasers," *IEEE Photonics Technol. Lett.*, vol. 27, no. 8, pp. 867–870, 2015.

[91] N. Nishizawa, Y. Seno, K. Sumimura, Y. Sakakibara, E. Itoga, H. Kataura, and K. Itoh, "All-polarization-maintaining Er-doped ultrashort-pulse fiber laser using carbon nanotube saturable absorber," *Opt. Express*, vol. 16, no. 13, pp. 9429–9435, 2008.

[92] H. Zhang, D. Tang, R. J. Knize, L. Zhao, Q. Bao, and K. P. Loh, "Graphene mode locked, wavelength-tunable, dissipative soliton fiber laser," *Appl. Phys. Lett.*, vol. 96, no. 111112, pp. 1–6, 2010.

[93] H.-R. Chen, C.-Y. Tsai, H.-M. Cheng, K.-H. Lin, and W.-F. Hsieh,

"Passive mode locking of ytterbium- and erbium-doped all-fiber lasers using graphene oxide saturable absorbers.," *Opt. Express*, vol. 22, no. 11, pp. 12880–9, 2014.

[94] G. P. Agrawal, *Nonlinear Fiber Optics Fifth Edition Nonlinear Fiber Optics*. 2013.

[95] C. R. Giles and E. Desurvire, "Modeling erbium-doped fiber amplifiers," *IEEE J. Light. Technol.*, vol. 9, no. 2, pp. 271–283, 1991.

[96] K. O. Hill and G. Meltz, "Fiber Bragg grating technology fundamentals and overview," *IEEE J. Light. Technol.*, vol. 15, no. 8, pp. 1263–1276, 1997.

[97] K. O. Hill, K. Takiguchi, F. Bilodeau, B. Malo, T. Kitagawa, S. Thériault, D. C. Johnson, and J. Albert, "Chirped in-fiber Bragg gratings for compensation of optical-fiberdispersion," *Opt. Lett.*, vol. 19, no. 17, pp. 1314–1316, 1994.

[98] A. M. Vengsarkar, P. J. Lemaire, J. B. Judkins, V. Bhatia, T. Erdogan, and J. E. Sipe, "Long-period fiber gratings as band-rejection filters," *IEEE J. Light. Technol.*, vol. 14, no. 1, pp. 58–65, 1996.

[99] M. R. Fernández-Ruiz, M. Li, M. Dastmalchi, A. Carballar, S. LaRochelle, and J. Azaña, "Picosecond optical signal processing based on transmissive fiber Bragg gratings," *Opt. Lett.*, vol. 38, no. 8, pp.

1247–1249, 2013.

[100] A. Kersey, M. A. Davis, H. J. Patrick, M. Leblanc, K. P. Koo, C. G. Askins, M. A. Putnam, and E. J. Friebele, "Fiber grating sensors," *IEEE J. Light. Technol.*, vol. 15, no. 8, pp. 1442–1463, 1997.

[101] J. Albert, L.-Y. Shao, and C. Caucheteur, "Tilted fiber Bragg grating sensors," *Laser Photon. Rev.*, vol. 7, no. 1, pp. 83–108, 2013.

[102] A. P. Zhang, G. Yan, S. Gao, S. He, B. Kim, J. Im, and Y. Chung, "Microfluidic refractive-index sensors based on small-hole microstructured optical fiber Bragg gratings," *Appl. Phys. Lett.*, vol. 98, no. 22, p. 221109, 2011.

[103] J. Wang, Z. Liu, S. Gao, A. P. Zhang, Y. Shen, H. Tam, and S. Member, "Fiber-optic anemometer based on Bragg grating inscribed in metal-filled microstructured optical fiber," *IEEE J. Light. Technol.*, vol. 34, no. 21, pp. 4884–4889, 2016.

[104] A. M. Vengsarkar, N. S. Bergano, C. R. Davidson, J. R. Pedrazzani, J. B. Judkins, and P. J. Lemaire, "Long-period fiber-grating-based gain equalizers," *Opt. Lett.*, vol. 21, no. 5, pp. 336–338, 1996.

[105] D. S. Moon, U.-C. Paek, and Y. Chung, "Multi-wavelength lasing oscillations in an erbium-doped fiber laser using few-mode fiber Bragg grating.," *Opt. Express*, vol. 12, no. 25, pp. 6147–6152, 2004.

[106] J. Sun, D. Yitang, Z. Yejin, C. Xiangfei, and X. Shizhong, "Dual-wavelength DFB fiber laser based on unequalized phase shifts," *IEEE Photonics Technol. Lett.*, vol. 18, no. 23, pp. 2493–2495, 2006.

[107] M. Yan, S. Luo, L. Zhan, Z. Zhang, and Y. Xia, "Triple-wavelength switchable Erbium doped fiber laser with cascaded asymmetric exposure long-period fiber gratings.," *Opt. Express*, vol. 15, no. 7, pp. 3685–91, 2007.

[108] B. Sun, A. Wang, L. Xu, C. Gu, Z. Lin, H. Ming, and Q. Zhan, "Low-threshold single-wavelength all-fiber laser generating cylindrical vector beams using a few-mode fiber Bragg grating.," *Opt. Lett.*, vol. 37, no. 4, pp. 464–6, 2012.

[109] L. Wang, X. Dong, P. P. Shum, X. Liu, and H. Su, "Random laser with multiphase-shifted Bragg grating in Er/Yb-codoped fiber," *IEEE J. Light. Technol.*, vol. 33, no. 1, pp. 95–99, 2015.

[110] T. Erdogan, "Fiber grating spectra," *IEEE J. Light. Technol.*, vol. 15, no. 8, pp. 1277–1294, 1997.

[111] H. Ke, K. S. Chiang, and J. H. Peng, "Analysis of phase-shifted long-period fiber gratings," *Photonics Technol. Lett. IEEE*, vol. 10, no. 11, pp. 1596–1598, 1998.

[112] X. Shu, T. Allsop, B. Gwandu, L. Zhang, and I. Bennion,

"High-temperature sensitivity of long-period gratings in B-Ge codoped fiber," *IEEE Photonics Technol. Lett.*, vol. 13, no. 8, pp. 818–820, 2001.

[113] W. J. Stephen and P. T. Ralph, "Optical fibre long-period grating sensors: characteristics and application," *Meas. Sci. Technol.*, vol. 14, no. 5, p. R49, 2003.

[114] J. F. Ding, A. P. Zhang, L. Y. Shao, J. H. Yan, and S. He, "Fiber-taper seeded long-period grating pair as a highly sensitive refractive-index sensor," *IEEE Photonics Technol. Lett.*, vol. 17, no. 6, pp. 1247–1249, 2005.

[115] O. Deparis, R. Kiyan, O. Pottiez, M. Blondel, I. G. Korolev, S. a Vasiliev, and E. M. Dianov, "Bandpass filters based on pi-shifted long-period fiber gratings for actively mode-locked erbium fiber lasers.," *Opt. Lett.*, vol. 26, no. 16, pp. 1239–1241, 2001.

[116] X. Zhu, C. Wang, S. Liu, D. Hu, J. Wang, and C. Zhu, "Switchable dual-wavelength and passively mode-locked all-normal-dispersion Yb-doped fiber lasers," *IEEE Photonics Technol. Lett.*, vol. 23, no. 14, pp. 956–958, 2011.

[117] X. Liu, D. Han, Z. Sun, C. Zeng, H. Lu, D. Mao, Y. Cui, and F. Wang, "Versatile multi-wavelength ultrafast fiber laser mode-locked by

carbon nanotubes," *Sci. Rep.*, vol. 3, p. 2718, 2013.

[118] R. Gumenyuk, I. Vartiainen, H. Tuovinen, and O. G. Okhotnikov, "Dissipative dispersion-managed soliton 2 μm thulium/holmium fiber laser.," *Opt. Lett.*, vol. 36, no. 5, pp. 609–611, 2011.

[119] L. Zhang, Y. Feng, and X. Gu, "Experimental and numerical studies of mode-locked fiber laser with large normal and anomalous dispersion," *Opt. Express*, vol. 21, no. 10, pp. 790–794, 2013.

[120] S. Duval, M. Olivier, M. Bernier, R. Vallée, and M. Piché, "Ultrashort pulses from an all-fiber ring laser incorporating a pair of chirped fiber Bragg gratings," *Opt. Lett.*, vol. 39, no. 4, pp. 989–992, 2014.

[121] R. I. Woodward, E. J. R. Kelleher, T. H. Runcorn, S. Loranger, D. Popa, V. J. Wittwer, A. C. Ferrari, S. V Popov, R. Kashyap, and J. R. Taylor, "Fiber grating compression of giant-chirped nanosecond pulses from an ultra-long nanotube mode-locked fiber laser," *Opt. Lett.*, vol. 40, no. 3, pp. 387–390, 2015.

[122] Y. C. Chen, N. R. Raravikar, L. S. Schadler, P. M. Ajayan, Y. P. Zhao, T. M. Lu, G. C. Wang, and X. C. Zhang, "Ultrafast optical switching properties of single-wall carbon nanotube polymer composites at 1.55 μm," *Appl. Phys. Lett.*, vol. 81, no. 6, pp. 975–977, 2002.

[123] V. S. Letokhov, "Laser biology and medicine.," *Nature*, vol. 316, no.

6026, pp. 325–330, 1985.

[124] H. Zhang, D. Y. Tang, L. M. Zhao, Q. L. Bao, and K. P. Loh, "Large energy mode locking of an erbium-doped fiber laser with atomic layer graphene," *Opt. Express*, vol. 17, no. 20, pp. 17630–17635, 2009.

[125] "Passively mode-locked fiber laser based on a hollow-core photonic crystal fiber filled with few-layered graphene oxide solution," *Opt. Lett.*, vol. 36, no. 16, p. 3024, 2011.

[126] H. Xia, H. Li, C. Lan, C. Li, X. Zhang, S. Zhang, and Y. Liu, "Ultrafast erbium-doped fiber laser mode-locked by a CVD-grown molybdenum disulfide (MoS2) saturable absorber," *Opt. Express*, vol. 22, no. 14, pp. 17341–17348, 2014.

[127] S. Y. Set, H. Yaguchi, Y. Tanaka, and M. Jablonski, "Laser mode locking using a saturable absorber incorporating carbon nanotubes," *IEEE J. Light. Technol.*, vol. 22, no. 1, pp. 51–56, 2004.

[128] Z. Sun, D. Popa, T. Hasan, F. Torrisi, F. Wang, E. R. J. R. Kelleher, J. C. Travers, V. Nicolosi, and A. C. Ferrari, "A stable, wideband tunable, near transform-limited, graphene-mode-locked, ultrafast laser," *Nano Res.*, vol. 3, no. 9, p. 653, 2010.

[129] X. He, Z. Liu, and D. N. Wang, "Wavelength-tunable, passively mode-locked fiber laser based on graphene and chirped fiber Bragg

grating," *Opt. Lett.*, vol. 37, no. 12, p. 2394, 2012.

[130] O. Deparis, R. Kiyan, O. Pottiez, M. Blondel, I. G. Korolev, S. A. Vasiliev, and E. M. Dianov, "Bandpass filters based on π-shifted long-period fiber gratings for actively mode-locked erbium fiber lasers," *Opt. Lett.*, vol. 26, no. 16, pp. 1239–1241, 2001.

[131] X. Zhu, C. Wang, S. Liu, D. Hu, J. Wang, C. Zhu, Z. Xiaojun, W. Chinhua, L. Shixin, H. Danfeng, W. Jiajun, and Z. Canyan, "Switchable Dual-Wavelength and Passively Mode-Locked All-Normal-Dispersion Yb-Doped Fiber Lasers," *IEEE Photonics Technol. Lett.*, vol. 23, no. 14, pp. 956–958, 2011.

[132] A. P. Zhang, X. W. Chen, J. H. Yan, Z. G. Guan, S. He, and H. Y. Tam, "Optimization and fabrication of stitched long-period gratings for gain flattening of ultrawide-band EDFAs," *IEEE Photonics Technol. Lett.*, vol. 17, no. 12, pp. 2559–2561, 2005.

[133] X. Dong, P. Shum, N. Ngo, C. Chan, B.-O. Guan, and H.-Y. Tam, "Effects of active fiber length on the tunability of erbium-doped fiber ring lasers," *Opt. Express*, vol. 11, no. 26, pp. 3622–3627, 2003.

[134] J. Wang, A. P. Zhang, Y. Shen, H. Tam, and P. K. A. Wai, "Widely tunable mode-locked fiber laser using carbon nanotube and LPG W-shaped filter," *Opitcs Lett.*, vol. 40, no. 18, pp. 4329–4332, 2015.

[135] D. Y. Tang, B. Zhao, L. M. Zhao, and H. Y. Tam, “Soliton interaction in a fiber ring laser,” *Phys. Rev. E*, vol. 72, no. 1, pp. 1–10, 2005.

[136] A. B. Grudinin and S. Gray, “Passive harmonic mode locking in soliton fiber lasers,” *J. Opt. Soc. Am. B*, vol. 14, no. 1, p. 144, 1997.

[137] L. Gui, X. Xiao, and C. Yang, “Observation of various bound solitons in a carbon-nanotube-based erbium fiber laser,” *J. Opt. Soc. Am. B*, vol. 30, no. 1, p. 158, 2012.

[138] S. Chouli and P. Grelu, “Rains of solitons in a fiber laser,” *Opt. Express*, vol. 17, no. 14, pp. 11776–11781, 2009.

[139] N. N. Akhmediev and A. Ankiewicz, “Multisoliton solutions of the complex Ginzburg-Landau equation,” *Phys. Rev. Lett.*, vol. 79, no. 21, pp. 4047–4051, 1997.

[140] L. K. Chin, A. Q. Liu, J. B. Zhang, C. S. Lim, and Y. C. Soh, “An on-chip liquid tunable grating using multiphase droplet microfluidics,” *Appl. Phys. Lett.*, vol. 93, no. 16, p. 164107, 2008.

[141] K. Chao, M. Lin, and R. Yang, “An in-plane optofluidic microchip for focal point control,” *Lab Chip*, vol. 13, no. 19, pp. 3886–3892, 2013.

[142] M. I. Lapsley, S. C. S. Lin, X. Mao, and T. J. Huang, “An in-plane, variable optical attenuator using a fluid-based tunable reflective interface,” *Appl. Phys. Lett.*, vol. 95, no. 8, pp. 2007–2010, 2009.

[143] M. Yin, B. Huang, S. Gao, A. P. Zhang, and X. Ye, "Optical fiber LPG biosensor integrated microfluidic chip for ultrasensitive glucose detection," *Biomed. Opt. Express*, vol. 7, no. 5, p. 2067, 2016.

[144] C. Fang, B. Dai, R. Hong, C. Tao, Q. Wang, X. Wang, D. Zhang, and S. Zhuang, "Tunable optical limiting optofluidic device filled with graphene oxide dispersion in ethanol," *Sci. Rep.*, vol. 5, p. 15362, 2015.

[145] M. Olivier and M. Piché, "Origin of the bound states of pulses in the stretched-pulse fiber laser.," *Opt. Express*, vol. 17, no. 2, pp. 405–18, 2009.

[146] F. W. Wise, A. Chong, and W. H. Renninger, "High-energy femtosecond fiber lasers based on pulse propagation at normal dispersion," *Laser Photon. Rev.*, vol. 2, no. 1–2, pp. 58–73, 2008.

[147] M. H. Ober, M. Hofer, and M. E. Fermann, "42-fs pulse generation from a mode-locked fiber laser started with a moving mirror.," *Opt. Lett.*, vol. 18, no. 5, pp. 367–369, 1993.

[148] W. H. Renninger, A. Chong, and F. W. Wise, "Pulse shaping and evolution in normal-dispersion mode-locked fiber lasers," *IEEE J. Sel. Top. Quantum Electron.*, vol. 18, no. 1, pp. 389–398, 2012.

[149] Y. Senoo, N. Nishizawa, Y. Sakakibara, K. Sumimura, E. Itoga, H.

Kataura, and K. Itoh, “Ultralow-repetition-rate, high-energy, polarization-maintaining, Er-doped, ultrashort-pulse fiber laser using single-wall-carbon-nanotube saturable absorber.,” *Opt. Express*, vol. 18, no. 20, pp. 20673–20680, 2010.

[150] H. Sayinc, D. Mortag, D. Wandt, J. Neumann, and D. Kracht, “Sub-100 fs pulses from a low repetition rate Yb-doped fiber laser.,” *Opt. Express*, vol. 17, no. 7, pp. 5731–5735, 2009.

[151] K. Ennser, M. N. Zervas, and R. I. Laming, “Optimization of apodized linearly chirped fiber gratings for optical communications,” *IEEE J. Quantum Electron.*, vol. 34, no. 5, pp. 770–778, 1998.

[152] M. E. Fermann, K. Sugden, and I. Bennion, “High-power soliton fiber laser based on pulse width control with chirped fiber Bragg gratings.,” *Opt. Lett.*, vol. 20, no. 2, pp. 172–4, 1995.

[153] Z. C. Wu, L. Li, Q. Zhang, D. Y. Tang, and D. Y. Shen, “Manipulation of group-velocity-locked vector solitons from fiber lasers manipulation of group-velocity-locked vector solitons from fiber lasers,” *IEEE Photonics J.*, vol. 8, no. 2, p. 1501206, 2016.

[154] Y. F. Song, H. Zhang, D. Y. Tang, and D. Y. Shen, “Polarization rotation vector solitons in a graphene mode-locked fiber laser.,” *Opt. Express*, vol. 20, no. 24, pp. 27283–9, 2012.

[155] T. Chen, C. Liao, D. N. Wang, and Y. Wang, "Polarization-locked vector solitons in a mode-locked fiber laser using polarization-sensitive few-layer graphene deposited D-shaped fiber saturable absorber," *J. Opt. Soc. Am. B*, vol. 31, no. 6, p. 1377, 2014.

[156] G. Sobon, J. Sotor, I. Pasternak, A. Krajewska, W. Strupinski, and K. M. Abramski, "All-polarization maintaining, graphene-based femtosecond Tm-doped all-fiber laser," *Opt. Express*, vol. 23, no. 7, pp. 9339–9346, 2015.

[157] Y. Ozeki and D. Tashiro, "Fast wavelength-tunable picosecond pulses from a passively mode-locked Er fiber laser using a galvanometer-driven intracavity filter," *Opt. Express*, vol. 23, no. 12, pp. 15186–15194, 2015.

[158] B. Ortaš, J. Limpert, and A. TŘnnermann, "Self-starting passively mode-locked chirped-pulse fiber laser," *Opt. Express*, vol. 15, no. 25, pp. 16794–16799, 2007.